Leg 207 Preliminary Report

Demerara Rise: Equatorial Cretaceous and
Paleogene Paleoceanographic Transect, Western Atlantic

4 January–6 March 2003

Shipboard Scientific Party

Ocean Drilling Program
Texas A&M University
1000 Discovery Drive
College Station TX 77845-9547
USA

April 2003

PUBLISHER'S NOTES

This report was prepared from shipboard files by scientists who participated in the cruise. The report was assembled under time constraints and does not contain all works and findings that will appear in the *Initial Reports* of the ODP *Proceedings*. Reference to the whole or to part of this report should be made as follows:

Shipboard Scientific Party, 2002. Leg 207 Preliminary Report. *ODP Prelim. Rpt.,* 107 [Online]. Available from World Wide Web: <http://www-odp.tamu.edu/publications/prelim/207_prel/207PREL.PDF>. [Cited YYYY-MM-DD]

Distribution: Electronic copies of this series may be obtained from the Ocean Drilling Program's World Wide Web site at http://www-odp.tamu.edu/publications.

This publication was prepared by the Ocean Drilling Program, Texas A&M University, as an account of work performed under the international Ocean Drilling Program, which is managed by Joint Oceanographic Institutions, Inc., under contract with the National Science Foundation. Funding for the program is provided by the following agencies:

Australia/Canada/Chinese Taipei/Korea Consortium for Ocean Drilling
Deutsche Forschungsgemeinschaft (Federal Republic of Germany)
Institut National des Sciences de l'Univers–Centre National de la Recherche Scientifique (INSU-CNRS; France)
Ocean Research Institute of the University of Tokyo (Japan)
National Science Foundation (United States)
Natural Environment Research Council (United Kingdom)
European Science Foundation Consortium for Ocean Drilling (Belgium, Denmark, Finland, Iceland, Ireland, Italy, The Netherlands, Norway, Portugal, Spain, Sweden, and Switzerland)
Marine High-Technology Bureau of the State Science and Technology Commission of the People's Republic of China

DISCLAIMER

The following scientists and participants were aboard the *JOIDES Resolution* for Leg 207 of the Ocean Drilling Program:

SHIPBOARD SCIENTIFIC PARTY

Jochen Erbacher
Co-Chief Scientist
Bundesanstalt für Geowissenschaften und Rohstoffe
ODP-Koordination
Stilleweg 2
30655 Hannover
Germany
Work: (49) 511-643-2795
Fax: (49) 511-643-3663
j.erbacher@bgr.de

David C. Mosher
Co-Chief Scientist
Bedford Institute of Oceanography
Geological Survey of Canada
1 Challenger Drive
PO Box 1006
Dartmouth NS B2Y 4A2
Canada
Work: (902) 426-3149
Fax: (902) 426-4104
dmosher@nrcan.gc.ca

Mitchell J. Malone
Staff Scientist/Inorganic Geochemist
Ocean Drilling Program
Texas A&M University
1000 Discovery Drive
College Station TX 77845-9547
USA
Work: (979) 845-5218
Fax: (979) 845-0876
malone@odpemail.tamu.edu

Debora Berti
Physical Properties Specialist
Department of Oceanography
Texas A&M University
Mail Stop 3146
College Station TX 77843
USA
Work: (979) 845-9467
debora@ocean.tamu.edu

Karen L. Bice
Stratigraphic Correlator/MST Operator
Department of Geology and Geophysics
Woods Hole Oceanographic Institution
Mail Stop 23
Woods Hole MA 02543
USA
Work: (508) 289-3320
Fax: (508) 457-2187
kbice@whoi.edu

Helen Bostock
Sedimentologist
Department of Geology
Australian National University
ACT 0200 Canberra
Australia
Work: (61) 02 61254303
Fax: (61) 02 61255544
helenb@geology.anu.edu.au

Hans-Jürgen Brumsack
Inorganic Geochemist
Institut für Chemie und Biologie des Meeres (ICBM)
Carl von Ossietzky Universität Oldenburg
Postfach 2503
D-26111 Oldenburg, Lower Saxony
Germany
Work: (49) 441-798-3584
Fax: (49) 441-798-3404
brumsack@icbm.de

Taniel Danelian
Paleontologist (radiolarians)
Laboratoire de Micropaléontologie, C. 104
Université Pierre et Marie Curie
4 Place Jussieu
75252 Paris
France
Work: (33) 1 4427 4981
Fax: (33) 1 4427 3831
danelian@ccr.jussieu.fr

Astrid Forster
Organic Geochemist
Marine Biogeochemistry and Toxicology (MBT)
Nederlands Instituut voor Onderzoek der Zee (NIOZ)
PO Box 59
1790 AB Den Burg, Texel
The Netherlands
Work: (31) 222-369-568
Fax: (31) 222-319-674
forster@nioz.nl

Felix Heidersdorf
Logging Scientist
Department of Geosciences
University of Bremen
Marine Technology/Environmental Research
Klagenfurter Strasse
28359 Bremen
Germany
Work: (49) 421-218-7184
Fax: (49) 421-218-7179
felixh@uni-bremen.de

Jorijntje Henderiks
Sedimentologist
Department of Geology and Geochemistry
Stockholm Universitet
Svante Arrheniusväg 8C
106 91 Stockholm
Sweden
Work: (46) 8-6747832
Fax: (46) 8-6747897
jorijntje.henderiks@geo.su.se

Thomas R. Janecek
Stratigraphic Correlator/MST Operator
Antarctic Research Facility
Florida State University
108 Carraway Building
Tallahassee FL 32306-4100
USA
Work: (850) 644-2407
Fax: (850) 644-4214
janecek@gly.fsu.edu

Christopher Junium
Sedimentologist
543 Deike Building
Pennsylvania State University
University Park PA 16801
USA
Work: (814) 863-6793
Fax: (814) 867-6711
cjunium@geosc.psu.edu

Laurence Le Callonnec
Sedimentologist
Département de Géologie Sédimentaire
Université Pierre et Marie Curie
4 Place Jussieu, Case 116
Paris Cedex 05
France
Work: (33) 1 44 27 4790
Fax: (33) 1 44 27 4965
lecallon@ccr.jussieu.fr

Ken MacLeod
Sedimentologist
Department of Geological Sciences
University of Missouri, Columbia
Columbia MO 65211-1380
USA
Work: (573) 884-3118
Fax: (573) 882-5458
MacLeodK@missouri.edu

Philip A. Meyers
Organic Geochemist
Department of Geological Sciences
University of Michigan
2534 C.C. Little Building
Ann Arbor MI 48109-1063
USA
Work: (734) 764-0597
Fax: (734) 763-4690
pameyers@umich.edu

H. Jörg Mutterlose
Paleontologist (nannofossils)
Institut für Geologie, Mineralogie und Geophysik
Ruhr Universität Bochum
Univeristätsstrasse 150
44801 Bochum
Germany
Work: (49) 234-322-3249, ext. 3250
Fax: (49) 234-321-4571
joerg.mutterlose@ruhr-uni-bochum.de

Hiroshi Nishi
Paleontologist (foraminifers)
Graduate School of Social and Cultural Studies
Kyushu University
4-2-1 Ropponmatsu, Chuo-Ku
Fukuoka 810-8560
Japan
Work: (81) 92-726-4643
Fax: (81) 92-726-4843
hnishi@rc.kyushu-u.ac.jp

Richard D. Norris
Paleontologist (Foraminifers)
Scripps Institution of Oceanography
MS 0244
La Jolla CA 92093-0244
USA
Work: (858) 822-1868
Fax: (858)
rnorris@ucsd.edu

James G. Ogg
Paleomagnetist
Department of Earth and Atmospheric Sciences
Purdue University
1397 Civil Building
West Lafayette IN 47907-1397
USA
Work: (765) 494-8681
Fax: (765) 496-1210
jogg@purdue.edu

A. Matthew O'Regan
Physical Properties Specialist
Graduate School of Oceanography
University of Rhode Island
Narragansett Bay Campus
Narragansett RI 02882
USA
Work: (401) 874-6537
oregan@geo.uri.edu

Brice Rea
Logging Staff Scientist
Department of Geology
University of Leicester
Leicester LE1 7RH
United Kingdom
Work: (44) 116 252 3785
Fax: (44) 116 252 3918
brr2@le.ac.uk

Philip Sexton
Sedimentologist
School of Ocean and Earth Sciences
Southampton Oceanography Centre
European Way
Southampton SO14 3ZH
United Kingdom
Work: (44) 23-8059-6108
pfs@soc.soton.ac.uk

Helen Sturt
Microbiologist
Department of Geology and Geophysics
Woods Hole Oceanographic Institution
Mail Stop 22
Woods Hole MA 02543
USA
Work: (508) 289-3678
Fax: (508) 457-2187
hsturt@whoi.edu

Yusuke Suganuma
Paleomagnetist
Department of Ocean Floor Geoscience
University of Tokyo
1-15-1 Minamidai, Nakano-Ku
Tokyo 164-8639
Japan
Work: (81) 3-5351-6442
Fax: (81) 3-5351-6438
suga@ori.u-tokyo.ac.jp

Jürgen W. Thurow
Sedimentologist
Department of Earth Sciences
University College London
Gower Street
London WC1E 6BT
United Kingdom
Work: (44) 20-7679-2416
Fax: (44) 20-7388-7614
j.thurow@ucl.ac.uk

Paul A. Wilson
Inorganic Geochemist
School of Ocean and Earth Sciences
Southampton Oceanography Centre
European Way
Southampton SO14 3ZH
United Kingdom
Work: (44) 23-8059-6164
Fax: (44) 23-8059-3052
paw1@soc.soton.ac.uk

Sherwood W. Wise Jr.
Paleontologist (nannofossils)
Department of Geological Sciences, 4100
Florida State University
108 Carraway Building
Tallahassee FL 32306-4100
USA
Work: (850) 644-6265
Fax: (850) 644-4214
wise@gly.fsu.edu

Christine Glatz
Undergraduate Student Trainee/Sedimentologist
3703 Sandy Forks
Kingwood TX 77339
USA
Work: (281) 348-9585
Cell: (909) 515-4817
discodollydiva@yahoo.com

TRANSOCEAN OFFICIALS

Thomas Hardy
Master of the Drilling Vessel
Overseas Drilling Ltd.
707 Texas Avenue South, Suite 213D
College Station TX 77840-1917
USA

Wayne Malone
Drilling Superintendent
Overseas Drilling Ltd.
707 Texas Avenue South, Suite 213D
College Station TX 77840-1917
USA

ODP SHIPBOARD PERSONNEL

Lisa Brandt
Marine Laboratory Specialist (Chemistry)

Grace Castellini
Marine Laboratory Specialist (Core)

Lisa Crowder
Marine Laboratory Specialist (Underway Geophysics)

David Fackler
Programmer

Randy Gjesvold
Marine Electronics Specialist

Dennis Graham
Marine Laboratory Specialist (Chemistry)

Ted Gustafson
Marine Laboratory Specialist (Downhole Tools/
Thin Sections)

Margaret Hastedt
Marine Computer Specialist

Scott Herman
Marine Laboratory Specialist (Paleomagnetism)

Michiko Hitchcox
Marine Laboratory Specialist (Yeoperson)

Eric Jackson
Marine Laboratory Specialist (Core)

Tomomi Kondo
Marine Laboratory Specialist (Core)

Michael Meiring
Marine Electronics Specialist (X-Ray)

William Mills
Laboratory Officer

Erik Moortgat
Marine Computer Specialist

Chieh Peng
Assistant Laboratory Officer/Storekeeper

Thomas Pettigrew
Operations Manager

Cyndi Prince
Marine Laboratory Specialist (Photography)

Mads Radsted
Marine Laboratory Specialist (Physical Properties)

Kerry Swain
Schlumberger Logging Engineer

Paula Weiss
Marine Laboratory Specialist (Curation)

ABSTRACT

A principal objective of Leg 207 was to recover relatively expanded, shallowly buried Cretaceous and Paleogene sediments from Demerara Rise off Suriname, South America, that could be used for paleoceanographic study of the tropical Atlantic. This period of the Earth's history involved episodes of ocean anoxia, rapid climate change, mass extinction, and opening of the equatorial Atlantic gateway. Five sites were drilled in a depth transect from 3200 to 1900 meters below sea level (mbsl) (modern water depth), which resulted in recovery of multiple sequences of Cenomanian and Turonian black shales, Campanian–Maastrichtian chalk, and Paleocene, lower Eocene, and middle Eocene chalk. In aggregate, the recovered sections form a continuous record of tropical sedimentation from the late middle Eocene (~38 Ma) to the late Campanian (~76 Ma) and from the Santonian (~83.5 Ma) to the late early Cenomanian (~98 Ma). The oldest sedimentary rocks recovered during Leg 207 are lower and middle Albian claystones (Site 1258) and the youngest are Pliocene–Pleistocene clay-rich nannofossil oozes (Site 1261).

Critical intervals recovered include multiple copies of ocean anoxic events (OAEs) 2 and 3. In total, ~650 m of black shales has been recovered. OAEs result from major shifts in ocean circulation patterns and represent significant perturbations in the global carbon cycle, with massive deposition of organic carbon in marine environments. They are hypothesized to have played a major role in the evolution of Earth's climatic and biotic history. The entire sequence of black shale sediments has a cyclical overprint of organic matter–rich black shale alternating with laminated foraminiferal packstone and occasional glauconitic bioturbated intervals. These alternations reflect varying levels of bottom water dysoxia and surface water productivity and may show Milankovitch forcing periodicities.

Interstitial water chemical analyses show that ~100 m.y. after deposition of the black shales, these sediments continue to act as a bioreactor that dominates organic matter degradation via sulfate reduction and methanogenesis. The other prominent feature seen in the Leg 207 pore waters is the presence of a brine at three sites characterized by chloride concentrations >60% higher than standard seawater. Data suggests that the shales act as an aquifer for the brines.

Six copies of the Cretaceous/Tertiary (K/T) boundary were recovered from three sites. Each of these intervals contain a 1- to 2-cm-thick graded spherule ejecta layer, presumably resulting from fallout of the meteorite impact and representing the first occurrence of the ejecta layer on the South American craton. The interval is accompanied by the disappearance of many species of microfossils and a bloom in new species following the event. Strong sediment physical property contrasts around the K/T boundary make this event a prominent reflection horizon in seismic profile that is correlated from site to site and throughout the study area.

Leg 207 recovered the Paleocene/Eocene (P/E) boundary at all five sites, with 10 cores spanning the boundary interval. The P/E boundary was a period of significant and rapid global warming (5°–7° at the poles), mass extinction in oceanic microorganisms, and widespread shoaling of the carbonate compensation depth. The entire episode of global warming is estimated to have lasted ~84 k.y., whereas noticeably light $\delta^{13}C$ in marine carbonates persisted for ~220 k.y. A dark green clay-rich bed that is in sharp contact with underlying chalk represents the P/E boundary at all the sites. Site 1260 has distinct lamination from just below to ~100 cm above the boundary. Magnetic susceptibility measurements suggest that the clay-rich part of the boundary sequence ranges from 1 to 2 m thick.

All sites display pronounced cyclicity in physical property measurements and sediment color. The pervasive cyclicity in physical property records offers the possibility not only of refining the chronology

around critical intervals but also crosschecking results between sites and understanding past climate forcing mechanisms.

INTRODUCTION

Overview of Scientific Objectives

The best examples in the geologic record of rapid (1 k.y. to 1 m.y.) wholesale extinctions linked to massive perturbations of the global carbon cycle and extreme changes in Earth's climate come from the Cretaceous and Paleogene Periods (e.g., oceanic anoxic events [OAEs] and the Paleocene/Eocene Thermal Maximum [PETM]). Little is known about the underlying causes and effects of these critical events in Earth's history, however. To a significant extent, these gaps in our understanding arise because of a lack of modern high-resolution paleoceanographic records from ocean drill sites, particularly from the tropics, that are so important in driving global ocean-atmospheric circulation. Drilling at Demerara Rise was targeted to access expanded sections of Cretaceous- and Paleogene-age deep-sea sediments, fulfilling priorities of the Ocean Drilling Program (ODP) Extreme Climates Program Planning Group and Long Range Plan. Demerara Rise represents an ideal drilling target for this purpose because the target sediments (1) are shallowly buried and, in places, crop out on the seafloor, (2) exist with good stratigraphic control in expanded sections, (3) contain spectacularly well preserved microfossils, and (4) were deposited within the core of the tropics in a proximal location to the equatorial Atlantic gateway.

During Leg 207, five sites were cored on the northern margin of Demerara Rise (Figs. F1, F2). The sites are located in a depth transect (present water depths are 1900–3192 m) along a grid of high-resolution multichannel seismic reflection lines supplemented by existing industry lines (Fig. F2). The transect of Cretaceous and Paleogene cores will be used to evaluate the following:

1. The history of Cretaceous anoxia in an equatorial setting and thereby test competing hypotheses for the causes and climatological effects of OAEs (particularly in relation to rapid emission and drawdown of greenhouse gases);
2. The detailed response of oceanic biotic communities across a range of paleowater depths to extreme perturbations in the geochemical carbon cycle and global climate;
3. Short- and long-term changes in greenhouse forcing and tropical sea-surface temperature (SST) response;
4. Key Cretaceous/Paleogene events of biotic turnover and/or inferred climate extremes, particularly across the Cretaceous/Paleogene (K/T) and the Paleocene/Eocene (P/E) boundaries; and
5. The role of equatorial Atlantic gateway opening in controlling paleoceanographic circulation patterns, OAEs, and cross-equatorial ocean heat transport into the North Atlantic.

Geologic History of Demerara Rise

Demerara Rise is a prominent submarine plateau located at ~5°N off the coasts of Surinam and French Guyana (Figs. F1, F2). The rise stretches ~380 km along the coast and is ~220 km wide from the shelf break to the northeastern escarpment, where water depths increase quickly from 1000 to >4500 m. Most of the plateau lies in shallow water (~700 m), but the northwest margin is a gentle ramp that reaches depths of 3000–4000 m. Much of the plateau is covered by 2–3 km of sediment. The sedimentary cover thins near the northeastern escarpment and exposes the lower parts of the sediment column and underlying

basement at depths of 3000 to >4500 m. In contrast, the gentle ramp on the northwest margin is covered by a nearly uniform drape of pelagic sediment down to water depths >4000 m.

Demerara Rise is built on rifted continental crust of Precambrian and early Mesozoic age. Tectonic reconstruction of the equatorial Atlantic places Demerara Rise south of Dakar, Senegal, prior to rifting of Africa from South America. The South American margin in the vicinity of Demerara Rise was one of the last areas in contact with West Africa during opening of the equatorial Atlantic. Rifting processes and related transform faulting separated the Guinea and Demerara Plateaus along an east-west-striking fault system during the earliest Cretaceous (Fig. F3). Barremian basaltic volcanics have been recovered in industry wells from the eastern Demerara Rise, suggesting that rifting began in the Early Cretaceous. Early Cretaceous en echelon faulting along the northwestern edge of Demerara Rise was caused by extensional movements and created a gently dipping ramp that reaches from present water depths between 1500 and 4000 m (Gouyet et al., 1994; Benkhelil et al., 1995).

Late Jurassic sandstones have been dredged in a water depth of 4400 m at the foot of the northern slope (Fox et al., 1972). The first known marine sediments on Demerara Rise are Neocomian in age (Fig. F4), and prior to Leg 207, the northern edge of the plateau is thought to have subsided rapidly and reached water depths of nearly 2 km by late Cenomanian time (Arthur and Natland, 1979). A striking angular unconformity is present across Demerara Rise, separating pre-Albian synrift sequences from Albian to present-age sediments. Upper Albian sediments are mostly green clayey carbonate siltstones. The Cenomanian–Santonian sequence consists almost exclusively of laminated black shale, with occasional stringers of limestone and chert. The black shale is a principal source rock for oil production in coastal French Guyana and Surinam and has total organic carbon (TOC) contents of up to 6–8 wt% in industry wells near the middle of the plateau. Laterally equivalent shales are important source rocks in basins west of Demerara Rise, and they are known as the Canje Formation (Guyana), Naparima Hill Formation (Trinidad), and La Luna Formation (Venezuela and Colombia). Campanian–Paleogene sediments are calcareous to siliceous oozes and chalks. A prominent submarine channel system and erosional surface developed in the late Oligocene–early Miocene. This surface can be traced across the entire northwestern plateau. The channels carried sediment east to west over the flank of the plateau and into feeder channels for a submarine fan that formed northwest of Demerara Rise. The channel system was short lived, and most of the Neogene sediments (hemipelagic and pelagic deposits) are thin or absent from the distal portions of the plateau.

DETAILED SCIENTIFIC OBJECTIVES

Oceanic Anoxic Events

OAEs represent major disruptions to the ocean system defined by massive deposition of organic carbon in marine environments (Schlanger and Jenkyns, 1976; Jenkyns, 1980; Herbert and Fischer, 1986; Arthur et al., 1990). Despite the fundamental role that OAEs are widely hypothesized to have played in the evolution of Earth's climatic and biotic history, very little is really known about the causes and effects of these events. Arguably, between two and six OAEs occurred during the mid–Late Cretaceous (OAEs 1a–1d, 2, and 3) (Jenkyns, 1980; Arthur et al., 1990; Erbacher and Thurow, 1997) (Fig. F5), and these are particularly important because they have left records, not merely in shallow seas but also in the deep oceans.

The $\delta^{13}C$ records from the Western Interior, English Chalk, and Italian Scaglia appear to confirm the initial designation of OAE 3 for the late Coniacian, but current resolution of Atlantic records is

insufficient to determine the existence of additional events in the late Turonian–Santonian (Jenkyns, 1980; Jenkyns et al., 1994). Similarly, until recently, comparatively little was known about the Albian OAEs (OAEs 1b–1d), but two new studies demonstrate the potential to improve constraints on the origin of different OAEs when diagenetically uncompromised microfossils become available from modern ocean drilling. Data from ODP Site 1049 suggest that pronounced water column stratification instigated OAE 1b (Erbacher et al., 2001), whereas records from nearby Site 1052 indicate that OAE 1d was triggered by the total collapse of upper ocean stratification, intense vertical mixing, and high oceanic productivity (Wilson and Norris, 2001). These antipodal hypotheses for the proximal causes of two OAEs within the same Cretaceous stage emphasize the utility of targeting sections that we know to contain records of multiple OAEs.

The two most prominent mid- to Late Cretaceous black shale events are the late early Aptian "Selli Event" (OAE 1a; ~120 Ma) and the Cenomanian/Turonian boundary ("Bonarelli Event") (OAE 2; ~93.5 Ma) (Fig. F5). Both OAEs 1a and 2 have sedimentary records in all ocean basins (Arthur et al., 1985, 1988, 1990; Bralower et al., 1994; Thurow et al., 1992), and the Aptian event is now known to have been truly cosmopolitan; its sedimentary expression extends even to the extremely shallow waters of mid-Pacific atolls (Jenkyns and Wilson, 1999). These findings and recent improvements to $\delta^{13}C$ records from land sections (both in outcrop and drill core) and the mid-Cretaceous seawater $^{87}Sr/^{86}Sr$ curve reveal three important factors concerning the possible origin of OAE 1a (Bralower et al., 1997; Menegatti et al., 1998; Erba et al., 1999; Jahrens et al., 2001; Jones and Jenkyns, 2001):

1. The response of the oceanic reservoir to increased sedimentary burial of organic carbon (as determined by the inferred increase in seawater $\delta^{13}C$) lacks black shale deposition during the Selli Event.
2. The onset of black shale deposition is associated with an extreme, short-lived negative $\delta^{13}C$ excursion in marine and terrestrial records and a carbonate dissolution "spike" that have been attributed to rapid greenhouse gas release (possibly methane as is hypothesized for the P/E boundary).
3. The foregoing events are associated with the onset of a pronounced decline in global seawater $^{87}Sr/^{86}Sr$ to its least radiogenic value in the past 125 m.y. (a second post-Jurassic minimum occurs around the time of OAE 2), suggesting a link between OAEs and oceanic plateau emplacement (Jones et al., 1994; Sinton and Duncan, 1997; Kerr, 1998) (Fig. F5).

The global presence of laminated sediments and a variety of geochemical records demonstrate that the response of the carbon cycle during OAE 2 was somehow related to dysoxic–euxinic conditions at the sediment/water interface (e.g., Sinninghe Damsté and Koster, 1998). However, the cause and dimensions of O_2 deficiency remain unclear and controversial. The substantial positive $\delta^{13}C$ excursion of seawater at the time of OAE 2 (Scholle and Arthur, 1980; Schlanger et al., 1987; Jenkyns et al., 1994) is widely attributed to increased global oceanic productivity and rates of C_{org} burial, but recent treatment of the problem using a simple model of the global carbon cycle indicates that this paradigm view requires more thorough investigation (Kump and Arthur, 1999). The process of sedimentary sequestration of C_{org} is hypothesized to act as a rapid negative feedback mechanism for global warming via drawdown of atmospheric carbon dioxide (Arthur et al., 1988; Kuypers et al., 1999).

The following scientific questions can be addressed using the sediments recovered from the Demerara Rise transect:

What is the history of OAEs in the tropical Atlantic as recorded on Demerara Rise?

What were the duration, cyclostratigraphy, and vertical extent of specific OAEs in the tropical Atlantic? Results from Demerara Rise will be used in conjunction with high-resolution records for OAE 2 from the shallow-water Tarfaya Basin (Kuhnt et al., 2001) to test (1) the predictions of the oxygen minimum zone model and (2) the role played by equatorial divergence in forcing the deposition of C_{org}-rich sediment (Handoh et al., 1999).

How does the type of C_{org} differ between (1) different OAE intervals and (2) these and non-OAE intervals? The sediments recovered from the Demerara Rise transect will provide an opportunity to examine the constraints that can be applied using modern geomicrobiological techniques.

What were the proximal and underlying causes of Cretaceous OAEs? In particular, it is important to determine whether carbon-cycle perturbations are the instigators or merely the consequence of OAEs. What role was played by sedimentation rate, clay content, and sea level change (Leckie et al., 2002)? The location of Demerara Rise will also allow the competing roles of gateway opening, plateau emplacement, and the hydrological cycle to be evaluated.

Are hypothesized increases in productivity during Cretaceous OAEs real? Current models of OAEs rely heavily on bulk carbonate $\delta^{13}C$ records from land sections, where preservation of microfossils is generally poor. Well-preserved microfossils from Demerara Rise will provide a way to test these records and their conventional interpretations by allowing the production of new types of data sets.

Are the lead, lag, and fractionation effects observed in existing records between the timing of C_{org} burial and the geochemical response (increase in inorganic and organic $\delta^{13}C$) reproducible in the core of the tropics at Demerara Rise? What mechanisms are responsible for these lead, lag, and fractionation effects?

What evidence (e.g., negative $\delta^{13}C$ excursions and depth-transect records of changes in the carbonate compensation depth [CCD]) exists to support the hypothesis that OAEs were driven by the sudden release of greenhouse gases (e.g., CH_4 as hypothesized for the P/E boundary)?

What was the impact of OAEs on chemical cycling in the oceans? High-resolution geochemical (e.g., trace element, strontium, and sulfur isotope) analysis of OAE 2 sediments can be used to test (1) the hypothesized link between large-scale hydrothermal activity and ocean anoxia (Brumsack, 1980) and (2) the impact of C_{org} and pyrite burial on the global sulfur, iron, and oxygen cycles (Brumsack and Lew, 1982; Ohkouchi et al., 1999).

Currently, a wide range of hypotheses invoke changes in ocean circulation and/or stratification to explain OAEs, but virtually no reliable geochemical data exist to constrain changes in the basic physical properties (temperature and salinity) of the water masses involved. These competing hypotheses can be tested using $\delta^{18}O$, trace element, and biomarker records using well-preserved microfossils and C_{org} from Demerara Rise.

Biotic Turnover

The tropics are widely viewed as an environment in which physicochemical factors and thus biotic compositions are inherently stable. Yet many low-latitude species have low environmental tolerances, thereby suggesting that relatively small climate changes may result in a substantial biological response (Stanley 1984). The so-called Cretaceous and Paleogene greenhouse was characterized by a series of significant marine and terrestrial biotic turnovers. Most of these events seem to be linked to major

changes in Earth's climate (Eocene–Oligocene transition and P/E boundary), paleoceanography, and/or the geochemical carbon cycle (Cretaceous OAEs and mid-Maastrichtian Event). Many of these events also produced synchronous turnovers in both terrestrial and marine biotas. The causes of most of these turnovers are poorly known because of the absence of expanded sections in the deep sea, where paleontological and isotopic studies can be carried out at high temporal resolution.

Widespread and presumably related isotopic, sedimentological, and paleontological changes are concentrated in the middle portions of the Maastrichtian (e.g., Barrera and Savin, 1999; Frank and Arthur, 1999; MacLeod and Huber, 2001). However, there are currently no established criteria for defining this interval. Some associated changes are graded over millions of years (e.g., high-latitude cooling), others are markedly diachronous (e.g., the last occurrence of bathyal inoceramids), others are not expressed in all areas (e.g., carbon isotopic excursion among benthic foraminifers), and still others are poorly dated (e.g., the collapse of rudist reefs). These uncertainties notwithstanding, in the subtropical North Atlantic and Tethys, the decline in abundance among inoceramids can first be resolved in the upper portion of Chron 31R, and their disappearance (except *Tenuipteria*) occurs in Chron 31N. This interval coincides with diversification among Tethyan planktonic foraminifers, with increased isotopic gradients among planktonic foraminifers on Blake Nose, an increase in the intensity of bioturbation at ODP Site 1052 and the Basque region, and proposed changes in the North Atlantic CCD. Thus, during Leg 207, mid-Maastrichtian changes are expected within the upper portion of Chron 31, in Zone CC25, and near the first occurrence datum of the planktonic foraminifer *Abathomphalus mayaroensis*.

The biotic turnovers of the mid-Cretaceous OAEs (OAEs 1b, 1d, and 2) are broadly comparable to one another even if the detailed causal factors are thought to have been different (Leckie, 1987; Erbacher and Thurow, 1997; Premoli Silva et al., 1999). A faunal crisis in nannoconids is well documented in the Aptian (Erba, 1994). Similarly, the early Albian OAE 1b strongly influenced the evolution of both planktonic foraminifers and radiolarians as did the other OAEs. Some events not only influenced planktonic groups but also benthic foraminifers, ammonites, bivalves, and even angiosperms. OAE 2 ranks as the eighth largest mass extinction in Phanerozoic Earth history (Sepkoski, 1986). Extension of the oxygen minimum zone (OMZ) and a rapid eutrophication of the oceans have been linked to extinction and a subsequent radiation of plankton and benthos alike (e.g., Hart, 1980; Caron and Homewood, 1983; Kaiho eand Hasegawa, 1994; Erbacher et al., 1996; Leckie, 1989). Documentation of fossilized photosynthetic green sulfur bacteria from Cenomanian/Turonian boundary black shales points to the existence of euxinic conditions in the proto–North Atlantic (Sinninghe Damsté and Koster, 1998; Kuypers et al., 2002). But interpretations differ as to whether the associated C_{org} burial was caused by OMZ expansion and C_{org} preservation or to enhanced productivity (Sinninghe Damsté and Koster, 1998).

The $\delta^{13}C$ excursions around three events (OAE 1b, 1d, and 2) have been interpreted in terms of increases in oceanic productivity, and this mechanism has been invoked to explain wide-scale carbonate platform drowning events in the Tethyan realm (Erbacher and Thurow, 1997; Weissert et al., 1998). On the other hand, results from the Pacific suggest that high tropical SSTs rather than eutrophication were responsible for platform drowning (Wilson et al., 1998; Jenkyns and Wilson, 1999). Cretaceous OAEs and extreme climates of the Paleogene (K/T and P/E boundaries and middle–late Eocene refrigeration) led to profound changes in plankton and benthos within the oceans (Thomas, 1998; Aubry, 1998).

The following questions concerning Cretaceous and Paleogene biotic turnover will be addressed using microfauna recovered from Demerara Rise:

Are leads and lags discernible, on the scale of ~10 k.y. or more, in the pattern of turnover between different groups of plankton and benthos that could elucidate the nature of gradual shifts in climate around a turnover pulse?

Are some species present only during transient climate shifts, and if so, how does their ecology (judged from faunal and isotopic data) compare with closely related species before and after the climatic anomaly? Answers could address (1) the rate of evolutionary response to climatic transients, (2) the magnitude or type of events needed to prompt evolutionary response, and (3) the extent to which species can accommodate environmental change by shifts in ecology rather than evolution (or extinction).

Are biotic changes permanent, or are major evolutionary changes offset from the transient climate shift? For example, the K/T extinction was abrupt, but the subsequent pattern of rediversification occurred over several million years. The long recovery appears to reflect structural changes in ecosystems wrought by the mass extinction (e.g., D'Hondt et al., 1998).

Are particular taxonomic groups more susceptible to extinction or radiation during turnovers?

Do different events (such as the various OAEs) generate predictable patterns of turnover within and between taxonomic groups? For example, thermocline dwelling species and those with complex life histories are believed to be particularly susceptible to extinction, and subsequent radiation, during OAEs (e.g., Hart, 1980; Caron and Homewood, 1983; Leckie, 1987), but these hypotheses have not been tested in detail with stable isotopic data.

Tropical Sea-Surface Temperatures and Greenhouse Forcing

A wide range of biotic observations suggest that substantially higher mid-latitude and polar temperatures relative to today prevailed during certain intervals of Earth history (e.g., mid-Cretaceous and early Paleogene), with tropical temperatures throughout the past ~150 m.y. probably at least as warm as today (Adams et al., 1990; Crowley and North, 1991). The $\delta^{18}O$ paleothermometry in deep-sea foraminiferal calcite supports the existence of these past "warm climates" (Fig. F6). These data show that deep and surface waters in the Cretaceous Antarctic during these intervals were significantly warmer than today (e.g., ~15°C for SSTs) (Huber et al., 1995). In contrast, broadly contemporaneous SSTs estimated in this way for the tropics are generally no warmer and sometimes much cooler (a minimum of ~12°–18°C) than today (Shackleton, 1984; Barrera, 1994; D'Hondt and Arthur, 1996). Such cool tropical SSTs contradict not only biotic observations but also basic theories of tropical ocean-atmosphere dynamics (Crowley, 1991). Attempts to simulate Cretaceous climates using numerical general circulation models have consistently demonstrated that (1) high levels of atmospheric CO_2 (four times present amounts) are needed to explain the warm polar SSTs derived from $\delta^{18}O$ paleothermometry and (2) this level of greenhouse forcing also yields increases in tropical SSTs beyond those indicated by $\delta^{18}O$ data sets (e.g., Manabe and Bryan, 1985; Barron, 1995; Bush and Philander, 1997; Poulsen et al., 1999; Otto-Bliesner et al., 2002). Explanations for the apparent paradox of the "cool tropical greenhouse" fall into two basic categories: (1) models of past warm climates fail to account adequately for polar ocean and/or atmospheric heat transport and (2) tropical $\delta^{18}O$ SST estimates are misleading.

Many artifacts plague existing records of tropical SST, including their extremely low resolution misidentification of true surface-dwelling species of foraminifers and the susceptibility of epipelagically secreted calcite to early diagenetic alteration in favor of artificially low SSTs (Douglas and Savin, 1975; Killingley, 1983; Schrag et al., 1995). Recent studies demonstrate that, under the correct geological circumstances, ancient carbonates (even highly metastable minerals) can be remarkably well preserved and yield $\delta^{18}O$ SSTs for the tropics that are significantly warmer than those provided by diagenetically suspect material (Wilson and Opdyke, 1996; Norris and Wilson, 1998; Wilson and Norris, 2001; Wilson et al., 2002; Norris et al., 2002; Pearson et al., 2001). These studies show that foraminifers recovered from

sections with clay-rich lithologies and/or shallow burial depths exhibit a distinctive "glassy" taphonomy similar to fauna recovered from modern-day sediment traps. This Cretaceous material includes epipelagic fauna that yield tropical $\delta^{18}O$ SSTs that match or, in some cases, exceed those measured today, thereby suggesting a thermal response to greenhouse forcing in the tropics.

The concept of a greenhouse mid- to Late Cretaceous Period is well supported by models of Earth's tectonic history. These models indicate that the mid- to Late Cretaceous was a time of exceptional rates of seafloor spreading and intraplate volcanism. This pulse in global oceanic crustal production is hypothesized to have caused increases in the levels of atmospheric carbon dioxide and global sea levels via increases in global oceanic ridge volumes, magmatic outgassing, and metamorphic decarbonation reactions (Schlanger et al., 1981; Larson, 1991; Berner, 1994; Larson and Erba, 1999). Fundamental problems, however, remain in terms of our understanding of these Cretaceous environments and their Paleogene equivalents.

One problem concerns our understanding of Cretaceous climate change at tectonic timescales. Maximum rates of Cretaceous–Cenozoic ocean crust cycling and, therefore, inferred atmospheric carbon dioxide levels are thought to have occurred during Aptian/Albian time (Larson, 1991; Larson and Erba, 1999), but this significantly predates Cretaceous climatic optima as perceived from mineralogical evidence and existing $\delta^{18}O$ paleothermometric records (Fig. F6.). One explanation for this discrepancy, consistent with the timing of peak Cretaceous–Cenozoic sea level (also Turonian), is that subducted crust and/or dating problems within the Cretaceous magnetic superchron (Superchron C34n) act to obscure a "hidden" Turonian pulse in ocean crust cycling (Wilson et al., 2002). Alternatively, the mismatch is real evidence of some other factor influencing CO_2 and/or SST (e.g., higher rates of $CaCO_3$ subduction) (Kump, 2002) during the Turonian relative to the Aptian–Albian (Wilson et al., 2002).

A second problem with our understanding of Cretaceous climate concerns the short-term stability of the so-called greenhouse state. High-resolution bulk carbonate $\delta^{18}O$ records from classic land sections in Italy reveal positive excursions that have been interpreted in terms of large-scale mid-Turonian and early Cenomanian glaciations superimposed on the middle of the Cretaceous greenhouse (Stoll and Schrag, 2000). Sedimentological and biotic records show no support for this hypothesis, but these records are of insufficient temporal resolution to provide a categorical test. Similarly, our highest resolution long-term $\delta^{18}O$ record from deep-sea sites for the Cretaceous comes from diagenetically altered bulk carbonate and has a temporal resolution of ~1 sample/200 k.y. (Clarke and Jenkyns, 1999). The best existing corresponding record from separates of planktonic foraminiferal calcite is also diagenetically suspect (it comes from chertified, deeply buried chalks in the Pacific) and is of very low resolution (<1 sample/m.y.; Aptian–Santonian) (Barrera, 1994). More recently, high-resolution sequence stratigraphic correlation of mid-Cenomanian sediments in northwest Europe and southeast India have been interpreted in terms of eustatic sea level change at an orbital timescale, possibly of glacial origin (Gale et al., 2002).

A third problem concerns the magnitude and origin of warmth of intermediate and deep waters in the Cretaceous oceans. A recent study of the dynamics of this problem demonstrates that the popular concept, instead of low-latitude "warm salty bottom water" formation, is essentially unsupported (Bice and Marotzke, 2001). A simpler way to explain the warm Cretaceous temperatures recorded by deep-sea benthic foraminifers is by water-mass formation at high latitudes that have warmer SSTs than today (presumably in response to pCO_2 forcing). However, the extraordinary magnitude of SST warmth indicated by a recent study for the Turonian high-latitude South Atlantic (Deep Sea Drilling Project [DSDP] Site 511; up to 32°C at ~60°S) (Bice et al., in press) raises severe questions concerning the levels of atmospheric pCO_2 forcing required.

The following scientific questions will be addressed using well-preserved microfossils and organic-rich sediments recovered from the Demerara Rise transect:

What is the history of changes in atmospheric CO_2 levels from the mid-Cretaceous to Paleogene time? Well-preserved microfossils and organic carbon-rich sediments from Demerara Rise will provide an ideal means to evaluate this question using multiple proxies for atmospheric pCO_2 (e.g., B isotope geochemistry in foraminiferal calcite and $\delta^{13}C$ geochemistry of bulk and biomarker organic carbon [e.g., 1989; Kuypers et al., 1999; Pearson and Palmer, 1999]).

What is the history of tropical SSTs in the tropical Atlantic? The presence of Demerara Rise within the core of the tropics throughout the entire Cretaceous and Paleogene provides a way to evaluate the relative strength of greenhouse forcing over long time periods. The combination of well-preserved calcareous microfossils and organic carbon–rich sediments recovered provides an excellent opportunity to address this problem using both well-established ($\delta^{18}O$) and newly developed (e.g., Mg/Ca; TEX_{86}) (Lear et al., 2000; Schouten et al., 2002) paleothermometry proxies. It is important to establish whether the persistent problem of "tropical overheating" in simulations of past warm climates is an artifact of poor SST records or the result of the existence of some tropical thermostatic regulator.

What evidence is there for rapid ocean warming associated with extreme perturbations in the geochemical carbon cycle (e.g., Cretaceous OAEs and P/E boundary)? High-resolution records from the Demerara Rise transect across these events will also provide a way to test the hypothesis that C_{org} burial during OAEs acted as a negative feedback for global warming.

Are hypothesized mid-Cretaceous glaciations real? Answers to this question have important consequences to (1) the long-standing problem of the mechanism responsible for perceived changes in global sea level prior to the icehouse and (2) our understanding of the stability of greenhouse climates.

Paleogene Events

The Paleogene record is rife with "critical boundaries" that offer significant opportunities for understanding the dynamics of greenhouse gas release, warm climate stability, biotic turnover associated with climate transitions, and extraterrestrial impacts. For example, the early Eocene warm period (~50–53 Ma) is the most extreme interval of global warming in the Cenozoic, but little is known about the number of hyperthermals within it, the range of temperatures, or their effects on biotic evolution (Thomas and Zachos, 1999). The Eocene warm period is succeeded by a long shift toward the lower temperatures and increased ice buildup of the late Eocene and Oligocene (Fig. F6), whose history and consequences for ocean circulation, carbon cycling, and biotic evolution are only vaguely understood. Similarly, extraterrestrial impacts in the early middle Eocene and the late Eocene offer the opportunity to study the climatological and biotic effects of impacts that were too small to precipitate global mass extinctions but were large enough to have engendered global changes in climate. Below, we discuss two events that are particularly well expressed by the sediments recovered from the Demerara Rise transect.

Thermal Maximum at the Paleocene/Eocene Boundary

The transient global warming at the end of the Paleocene is one of the best candidates for greenhouse warming in the geologic record. A growing body of evidence implicates a massive release of greenhouse gases into the atmosphere and ocean as a cause for ~5°–7°C warming in the Southern Ocean and

subtropics, a 35% –50% extinction of deep-sea benthic foraminifers, and widespread carbonate dissolution in the deep-ocean record (e.g., Zachos et al., 1993; Koch et al., 1995; Dickens et al., 1995). Recent studies utilizing high-resolution stable isotope analyses (Bains et al., 1999) and orbitally tuned chronologies (Norris and Röhl, 1999) suggest that carbon release occurred in a series of short steps, lasting a few thousand years, punctuated by catastrophic shifts in $\delta^{13}C$ and ocean temperature. Although these new data support the idea that the carbon may have been sourced from methane hydrate reservoirs, considerable uncertainty remains about how the carbon was released, what triggered the different phases of release, and what the biotic and climatological response was to the input of large amounts of greenhouse gas. We have little data to constrain fluctuations in the CCD during the P/E Event, a key parameter for understanding changes in CO_2 storage resulting from hypothesized methane outgassing. There also remain significant questions about the chronology of the P/E Event. Thus far, cycle-based chronologies are based mostly upon analysis of a single site (ODP Site 1051). Analysis of additional cyclostratigraphic records tied to magnetostratigraphy is needed to evaluate the accuracy of the existing chronology and allow us to calculate changes in accumulation rates, rates of evolutionary and ecological responses to climate change, and biogeochemical fluxes during the Paleocene–Eocene interval.

Cretaceous/Paleogene Boundary

Two decades of study have provided considerable information on the causes and evolutionary consequences of the Cretaceous/Paleogene (K/P) mass extinction. There is now widespread agreement that the extinction was precipitated by a large-body impact event that created the ~300-km-wide Chicxulub impact structure on the Yucatan Peninsula in eastern Mexico, nearly 5000 km from Demerara Rise. There is considerable evidence linking the Chicxulub impact event to the K/P extinction, ranging from the dating of impact glass to ~65.5 Ma (the currently accepted age for the K/P boundary) to the presence of impact-generated diamonds, high-pressure minerals, and chondritic ratios of platinum group elements in K/P boundary sections worldwide. Although some have continued to dispute the role of the impact event in the associated mass extinction, arguing that the impact predates the extinction or that there were multiple impacts, nearly all boundary layers that are generally agreed to be stratigraphically complete contain only one horizon rich in impact debris, and that layer is associated intimately with faunal and floral evidence for mass extinction.

Recently, it has become apparent that the impact event led to significant disruption of the stratigraphic record both above and below the boundary. Seismicity produced by the impact (an event with a Richter scale magnitude of ~10–13) and the effects of tsunamis produced by the impact eroded or caused mass wasting of Maastrichtian sediments throughout the Gulf of Mexico, the Caribbean, the North Atlantic, and Baja, California. Accordingly, it is not surprising that nearly all cores recovered from these areas display sedimentary disruptions or hiatuses associated with the boundary. The mass extinction, in turn, greatly diminished the supply of biogenic sediment to the seafloor, resulting in a significant drop in the sedimentation rate and, therefore, stratigraphic acuity in the earliest Paleogene. Hence, nearly all known K/P boundary sequences do not have rates of sedimentation sufficient to resolve many of the most pressing issues for analysis of extinction processes such as the climatic conditions that prevailed in the few hundred or even thousand years following the impact.

There are a series of outstanding issues that could be addressed by drilling on Demerara Rise:

Where does the K/P boundary fall within Magnetochron C29r? Although the position and age of the boundary has been evaluated using cyclostratigraphic work in the South Atlantic, the cycle counts

were not entirely unambiguous (within more than two precession cycles; ~42 k.y.) and require testing through further cyclostratigraphy and magnetostratigraphy work.

How does the distribution of ejecta and impact-generated mass wasting on South America differ from that observed around the western and eastern North Atlantic? Experience with eastern North Atlantic sites suggests that if an ejecta layer exists on Demerara Rise it is only a few millimeters thick and may rest on a slumped sequence of Maastrichtian sediments.

What is the pattern of climate evolution in the first several thousand years of the Danian, and what does this signify about the mechanisms of extinction and the environmental conditions associated with the subsequent radiation of surviving species?

Does the vertical $\delta^{13}C$ gradient really disappear as proposed in models of extinction-related shutdown of biological production in the oceans? Thus far, there have been no studies of the K/P boundary along depth transects where changes in vertical gradients in carbonate ion concentration, nutrient proxies, and deepwater circulation could be studied in a single area.

Equatorial Atlantic Gateway Opening, Oceanic Circulation, and Heat Transport

The opening of the equatorial Atlantic gateway was driven by the separation of Africa and South America and is widely hypothesized to have had a significant effect on both oceanic circulation patterns and heat transport over wide areas of the Cretaceous Atlantic. Yet, the timing of the opening of this gateway remains poorly constrained. Based on the biogeographic distribution of foraminifers and cephalopods, a shallow-water passage is thought to have been initiated between the North and South Atlantic Oceans at some time during the Albian (Moullade and Guerin, 1982; Förster, 1978; Wiedmann and Neugebauer, 1978; Moullade et al., 1993). Results from ODP Leg 159 on the eastern side of the equatorial Atlantic gateway suggest that a strong relationship existed between stepwise deepening and widening of the gateway and black shale deposition on the west African margin from the Albian to the Turonian (Wagner and Pletsch, 1999). Cessation of black shale deposition in the Late Cretaceous is interpreted to result from increasingly vigorous circulation between the North and South Atlantic. Hence, marking the transition from a Mesozoic longitudinal circulation system through the Tethyian and the central Atlantic Oceans to a more Cenozoic-like oxidizing latitudinal circulation pattern through the Atlantic gateway.

Analysis of the subsidence history of Demerara Rise will contribute to interpretations of the history of the opening of the equatorial Atlantic gateway. High-resolution sampling of distinct time slices across a range of paleowater depths will help to constrain the following questions:

What were the timings of the establishment of oceanographically significant throughflow in the equatorial Atlantic gateway (i.e., the onset of throughflow of upper intermediate and deeper water masses)? Results will help to determine the paleoceanographic consequences of connecting the previously restricted South Atlantic to the North Atlantic–Tethyian realm.

What was the specific role played by the equatorial Atlantic gateway in controlling the development of Cretaceous black shale deposition? By comparing the high-resolution OAE records from Demerara Rise with earlier DSDP mapping, it will be possible to evaluate whether this gateway merely controlled OAE sedimentation in the more restricted South Atlantic or whether its influence extended to the tropical North Atlantic–Tethys.

What is the long-term history of cross-equatorial heat transport into the North Atlantic? Demerara Rise is positioned in an ideal location to sample meriodonal circulation and delivery of heat northward from Cretaceous to Oligocene time (Fig. F1).

RESULTS

Site 1257

Site 1257 is located in 2951 m of water on a terrace above the steep northern slope >10° northwest of Demerara Rise, ~400 km north of Suriname. As the second deepest location, Site 1257 serves as an intermediate member of the paleoceanographic depth transect across Demerara Rise. It was promoted to recore DSDP Site 144, which was spot cored during Leg 144 in 1970. The major objectives were the following:

1. Core and log an Albian–Oligocene section to evaluate paleoceanographic and paleoclimatic changes during the Paleogene and Cretaceous, with emphasis on major and abrupt events during this interval such as the Eocene/Oligocene (E/O) boundary, the P/E boundary, and the Cretaceous OAE.
2. Reconstruct the history of the opening of the equatorial Atlantic gateway by obtaining benthic proxy data. These data will help understand changes in bottom water circulation over Demerara Rise during the gradual opening of the seaway.
3. Define the depth of key seismic reflectors for a detailed planning of the remaining sites along the Demerara Rise depth transect.

The steep northwestern slope of Demerara Rise, where Site 1257 is located, is part of the southern transform fault that separated South America and West Africa during the rift phase of the southern central Atlantic in the Late Jurassic–Early Cretaceous. Although spot cored, results from Site 144 demonstrated the potential for presence of all the target sediments.

Seismic Stratigraphy

Within 2.5 km northwest and 1.5 km north and northeast of the drill site, the seafloor begins to fall off at a 10° angle, from the site elevation of 2951 meters below sea level (mbsl) to the abyssal plain of 4400 mbsl. The site itself is on a slight mound that appears to be an erosional remnant. Reflector "A" representing the top of this erosional unconformity crops out at the seafloor at the site (within the resolution of the survey data). Between Reflector A (the seafloor in this case) and Reflector "B" is seismic Unit 2 (seismic Unit 1 is missing at this site). It is 173 ms thick (in two-way traveltime) at this location, calculated to be 144 meters below seafloor (mbsf) by the check shot and downhole logging velocity information. Seismic Unit 2 shows an incoherent reflection character here, describing a disturbed sediment package or being affected by side echoes from local complex topography. A high-amplitude reflection event of short lateral duration occurs at 110 ms (90 mbsf) at the site.

Reflector "B′" at 173-ms subbottom (144 mbsf) marks the top of seismic Unit 3. It is a flat-lying sequence at this site that dips gently to the northeast at an angle of 1.7°. Reflection event B is hummocky on a local scale, probably cut by channels, and is underlain by several high-amplitude reflections and then a short transparent zone to the top of Reflector B at 217-ms subbottom (181 mbsf). Subunit 3b underlies

3a and is the sequence between Reflectors B′ and Reflector "C," which occurs at 272-ms subbottom (232 mbsf).

Most acoustic energy is lost below Reflector C in the survey data, and the section is difficult to describe. A few hyperbolic reflections in this interval are visible. Industry line C2206 crosses in a northeast-southwest direction just 1 km northeast of the drill site. In this profile, the sequence of reflectors below Horizon C appears folded into a possible small anticline below the drill site and contacts Reflector C as an angular unconformity.

At Site 1257, one advanced piston corer/extended core barrel (APC/XCB) hole and two rotary core barrel (RCB) holes were cored. Hole 1257A was APC cored to 40.6 mbsf, but lithification in this part of the sediment column stopped APC coring earlier than desired. The hole was completed with XCB coring to a total depth of 284.7 mbsf, with 75.9% recovery (Table T1). XCB coring proved slow and resulted in poor quality cores (biscuiting), so RCB coring was used for Holes 1257B and 1257C. The upper 40 m of the succession was washed at Hole 1257B, and the section between 40 and 227.3 mbsf was RCB cored with 62.1% recovery. At Hole 1257C, the upper 82 m was washed and RCB cored between 82 and 235.9 mbsf, with 62.8% recovery. Porcellanite, limestone, and chert beds at ~90 mbsf and between 170 and 225 mbsf reduced recovery of both XCB and RCB coring.

Wireline logging was conducted with the triple combination (triple combo) tool string and the Formation MicroScanner (FMS)-sonic tool string through Hole 1257A. The Well Seismic Tool (WST) was used to undertake a check shot survey. Results provided accurate traveltime data for calibrating velocity logs and providing formation velocity information for time-to-depth conversion of seismic data.

Sediments at Site 1257 range in age from Miocene to Albian. A 1.5-m-thick veneer of Neogene nannofossil ooze directly overlies lower Oligocene sediment. Chalk spanning the E/O boundary was recovered in Hole 1257B. Paleogene sedimentation is cut by two hiatuses in the upper Eocene and uppermost Paleocene. In Hole 1257C, sediments spanning the P/E boundary were recovered. Good core recovery of an expanded upper Paleocene section allowed construction of a complete composite section of this interval. Foraminiferal packstone boulders intercalated in a 2- to 3-m-thick slumped sequence represent the early Paleocene. The Cretaceous sequence of Site 1257 is cut by three hiatuses in the upper Maastrichtian and lower Campanian. The Santonian–latest Cenomanian is represented by a 44-m-thick sequence of laminated black shales that include OAEs 3 and 2. Hard limestone and chert layers in this interval prevented good core recovery. Recovery improved in the lower part of the succession and three copies of the black shale intervals in Holes 1257A, 1257B, and 1257C will possibly allow a complete postcruise reconstruction of this interval. An unconformity underlying the black shales separates the latest Cenomanian from upper to middle Albian sediments.

Recovery of Critical Intervals

The main objective of Leg 207 was the recovery of sediments with microfossils of major and abrupt events of the Paleogene and Cretaceous Periods, such as the E/O boundary, P/E boundary, and the OAEs. In Hole 1257A, sediment with a continuous lower Oligocene–upper Eocene transition was recovered, presumably including the prominent stable isotope shift associated with the dramatic growth of ice sheets on Antarctica.

Sediments spanning the P/E boundary were recovered in Hole 1257C. This transient global warming period at the end of the Paleocene is one of the best candidates for study of abrupt change resulting from greenhouse warming in the geologic record. A growing body of evidence implicates a massive release of greenhouse gases into the atmosphere and ocean as a cause for dramatic warming in the Southern Ocean

and subtropics. The P/E boundary record in Hole 1257C comprises a 3.5-cm-thick dark greenish clay that represents carbonate dissolution associated with the P/E boundary in deep oceans. Shore-based investigations will show if the succession above the event is complete.

A 44-m-thick succession of laminated black shales, including OAEs 3 and 2, was recovered in all three holes at Site 1257. OAEs represent major disruptions in the ocean system, defined by massive deposition of organic carbon in marine environments. They are hypothesized to have played a major role in the evolution of Earth's climatic and biotic history. OAE 3 is an interval of organic-rich and laminated sediment, roughly defined as covering the Santonian and Coniacian epochs. They have been described from various locations around the central Atlantic and the Western Interior Basin in the USA. OAE 2 is a well-defined latest Cenomanian to earliest Turonian event that has a global distribution. It is paralleled by a set of distinctive positive stable carbon isotope excursions pointing to a severe disturbance of the global carbon cycle associated with the burial of organic-rich sediments. Although the recovery in the black shale interval at Site 1257 was not as good as desired, a comparison of all three holes will probably allow for fairly complete coverage of the OAEs. A shore-based refinement of the stratigraphy including stable carbon isotope measurements will help to better define the OAE intervals. The preservation of foraminifers in this section varies between moderate and very good and has good promise for shore-based paleotemperature studies.

Stratigraphy of Site 1257

Lithologic description of the cores and biostratigraphic age assignments exposed a number of hiatuses and highly condensed intervals within the sedimentary succession at Site 1257. A veneer of upper Miocene nannofossil ooze was defined as lithologic Unit I. The unit is characterized by a gradual color change downcore from pale brown to pale olive. The sediment is strongly mottled, and iron sulfide is present in discrete burrows and as mottling throughout the unit. Unit I unconformably overlies lower Oligocene–uppermost Eocene light greenish gray to greenish gray chalk and ooze. Less lithified intervals may be related to variations in clay content. Microfossil assemblages of this interval are rich in well-preserved diatoms and radiolarians. Below this section, a 20-m-thick interval of middle Eocene biosiliceous chalk disconformably overlies lower Eocene chalks with biogenic silica. The latter intervals have been grouped as lithologic Unit II, which was divided into Subunits IIA and IIB in the transition from ooze to chalk at 22 mbsf. The transition coincides with an significant increase of siliceous microfossil abundance. Sedimentation rates in the Oligocene–Eocene varied from 5 to 9 m/m.y., with increasing values in the lower Eocene.

The Paleocene comprises foraminiferal nannofossil chalks that were described as lithologic Subunit IIIA. Siliceous microfossils of the upper Paleocene were replaced by zeolite, which is abundant throughout the subunit. The presence of occasional porcellanite stringers also indicates diagenetic alteration of biogenic silica. Good recovery of an expanded upper Paleocene sequence (sedimentation rates = ~10 m/m.y.) allowed the construction of a spliced section that shows a pronounced cyclicity, possibly representing a 20- to 50-k.y. periodicity.

An early to late Paleocene gravity flow deposit marks the lower boundary of Subunit IIIA. No upper Maastrichtian sediments were recovered. The subjacent lower Maastrichtian–lower Campanian zeolitic chalk (Subunit IIIB) is similar to that of the Paleocene. Well-preserved radiolarians are present in the upper Campanian but absent below. A condensed glauconite-rich horizon marks the base of Campanian sediments, where a sharp irregular contact with underlying black shales of lithologic Unit IV is present (Core 207-1257A-20X).

The black shales of Unit IV primarily consist of dark olive-gray to black finely laminated calcareous claystone with carbonaceous material. Carbonate contents range from ~40 to 60 wt% in dominant lithologies and as high as 78 wt% in individual carbonate-rich layers. TOC reaches values up to 16 wt%, and hydrogen index and oxygen index values indicate that the black shales contain Type II kerogen, indicating a marine source of the organic matter. The unit shows very well developed submillimeter-scale laminations and has a strong petroliferous odor, although the organic matter is thermally immature. Rhythmic color variations (dark olive-gray to black) are present on a decimeter scale throughout. Lighter intervals are relatively rich in prismatic inoceramid shell material. Olive laminated calcareous porcellanite and limestone as thick as 30 cm, gray and black chert nodules, and concretions of nannofossil chalk with foraminifers are present in minor amounts. Preservation of calcareous microfossils varies between moderate to very good. Pristine glassy foraminiferal tests also are observed in this unit. Microfossil ages yield Santonian, Coniacian, and Turonian ages and date the base of the black shale as Cenomanian. Sedimentation rates of the Upper Cretaceous sediments vary between 4 and 6 m/m.y.

A sharp contact between the laminated black shales and the underlying pyrite-rich clayey carbonate siltstone (Unit V) was recovered in Core 207-1257C-15R. Foraminifers within a sandstone date the top of the unit in Section 207-1257A-25-CC as Cenomanian. The bottom of Hole 1257A has an upper to middle Albian age.

Geochemistry

Pore waters are characterized by the presence of a brine with maximum chlorinity of 823 mM, a ~50% increase over average seawater chlorinity. The maximum chlorinity is centered ~200 mbsf in the black shales (Unit IV), decreasing above and below the unit. The combination of the chlorinity and salinity profiles, a low-temperature anomaly recorded by the downhole logging Temperature/Acceleration/Pressure (TAP) tool, and high-porosity intervals in shales suggest that the brines are sourced externally through the black shales. Sulfate decreases downhole and is depleted by ~160 mbsf. Below 220 mbsf, sulfate increases to ~5 mM at the base of the cored interval. Methane first appears at ~108 mbsf, increasing rapidly to reach a broad maximum between 180 and 218 mbsf within black shales, largely coincident with the interval of sulfate depletion, before decreasing downhole. High methane-to-ethane ratios and the absence of measurable higher molecular weight hydrocarbons indicate that the methane was generated microbially.

Physical Properties and Logging

Core physical property data (multisensor track [MST] and discrete measurements) and downhole logging physical property data show excellent agreement. Density and velocity values are uncharacteristically high for such shallow sediments but reflect their age and degree of cementation. Nonetheless, these physical property profiles demonstrate, in general, a relatively normal depth-consolidation profile that cementation appears not to have altered. On a higher frequency scale, there are significant characteristics to these data that reflect lithostratigraphic changes and trends, and patterns of cyclicity are obvious in some intervals. The most pronounced change correlates with lithologic Unit IV, the black shales. In this case, the unit is characterized by lower density and velocity values but with a high degree of scatter. Very high peak values correlate with calcified beds. Other significant deviations from the normal consolidation trend correlate with events and hiatuses identified in the lithostratigraphy, such as the lower Eocene hiatus, the upper Paleocene hiatus, the P/E boundary, and the top and bottom of the

black shale sequence. These strong physical property contrasts yield strong reflection characteristics and allow for good correlation with the seismic stratigraphy.

Depositional History

Shallow marine Albian synrift sediments are the oldest sequence recovered at Site 1257. They are unconformably overlain by Cenomanian–Santonian laminated black shales. These organic-rich shales reflect high productivity in surface waters and low oxygen levels in the bottom water. Regional oceanic upwelling conditions are believed to be the reason for this long-lasting (~17 m.y.) phase of black shale deposition at Demerara Rise. Similar facies have been described from the Tarfaya Basin on the northwest African margin of the Atlantic and from Venezuela, Colombia, and Costa Rica.

Oxic conditions were established by the early Campanian when pelagic and open marine marls were deposited on Demerara Rise. However, the abundance of trace fossils indicating dysoxic environments points toward oxygen deficiency at the seafloor. The upper Campanian–Neogene pelagic record at Site 1257 is interrupted by several hiatuses and slump deposits reflecting the position of the site on the topographic slope of Demerara Rise. Paleobathymetric assignments of these sediments are difficult to provide, but water depths similar to the present probably were reached by the late Maastrichtian to Paleocene. Sedimentation and subsidence have probably kept pace since that time.

Site 1258

Site 1258 is located at a depth of 3192.2 mbsl on the gently dipping western slope ~2° of Demerara Rise, ~380 km north of Suriname. The site is located on a ridge of Paleogene sediments outcropping on the seafloor. Site 1258 is the distal and deepest end-member of the paleoceanographic depth transect across Demerara Rise. The major objectives are similar to those of Site 1257:

1. Core and log a Paleogene–Albian section to evaluate paleoceanographic and paleoclimatic changes, with emphasis on major and abrupt events during this interval such as the E/O boundary, the P/E boundary, and the Cretaceous OAE.
2. Reconstruct the history of the opening of the equatorial Atlantic gateway by obtaining benthic proxy data. These data will help understand changes in bottom water circulation over Demerara Rise during the gradual opening of the seaway.
3. Recover continuous and expanded sediment records of the Paleogene and Cretaceous to reconstruct short- and long-term changes in greenhouse forcing.

The seismic stratigraphy established for Demerara Rise, including Horizons A, B, B′, and C, have been correlated to Site 1258 strata. Reflector A, representing the top of a presumably early Miocene erosional unconformity, crops out at the seafloor at the site (within the resolution of the survey data). Between Reflectors A and B, seismic Unit 2 is 300 ms thick (265 mbsf), using downhole logging velocity information. Seismic Unit 3, between Reflector B at 300-ms subbottom and Reflector C at 480-ms subbottom, is a 94-m-thick flat-lying sequence that dips 1.5° to the north-northwest.

Seismic Unit 2 shows an echo character of reasonably coherent but slightly contorted reflections with offsets, which probably describes a sediment sequence that has undergone mass failure and rotational displacement. Seismic Unit 3 is divided into two subunits: the basal subunit (Subunit 3b) lies between Horizons B′ and C (450- to 515-ms subbottom; 417–480 mbsf). It is defined on the basis of a series of

strong, parallel, coherent reflections that are laterally contiguous and have been shown to correlate to the black shale interval.

At Site 1258, three RCB holes were cored. Hole 1258A was cored to 447.5 mbsf, with 83.9% recovery, and Hole 1258B to 460.9 mbsf, with 76.3% recovery (Table T1). Hole 1258C was washed from 0 to 120.0 mbsf. To obtain a splice for a lower–lower middle Eocene succession, missing because of faulting in Hole 1258A, Hole 1258C was spot cored between 120.1 and 206.1 mbsf. Spot coring the interval between 245.3 and 274.2 mbsf obtained a third copy of the K/T boundary interval. Subsequent washing until 384.8 mbsf was followed by coring of the hole until a total depth of 485.0 mbsf. The average recovery in Hole 1258C was 74.9%. Hard beds between 320 and 380 mbsf and between 415 and 420 mbsf reduced core recovery in these intervals.

Stratigraphy of Site 1258

Lithologic description of the cores and biostratigraphic age assignments revealed a rather continuous sedimentary succession with only a few hiatuses. Sediments at Site 1258 range in age from Miocene to middle Albian. An ~8-m-thick package of Miocene nannofossil ooze unconformably overlies a drape of calcareous ooze with radiolarians and diatoms of early Oligocene age. This sequence, in turn, unconformably overlies an expanded 143-m-thick succession of lower middle Eocene (planktonic foraminiferal Zone P10; calcareous nannoplankton Zone NP15) to lower Eocene nannofossil chalk. With a sedimentation rate of ~20 m/m.y., the middle–lower Eocene succession is a remarkably expanded and complete (to zonal level) section. Excellent RCB recovery provided continuous core overlap from the middle Eocene to ~10 m below the P/E boundary. The periodic variability present in the Eocene magnetic susceptibility data at Site 1258 will provide a good basis for postcruise cyclostratigraphic studies. Age control is excellent, with well-defined paleomagnetic datums present in the section (e.g., the top of Subchron C21n and the base of Subchron C22r). Preliminary investigation suggests that the dominant frequencies of the magnetic susceptibility data are likely Milankovitch Periods, with significant power at ~20, 40, and 100 k.y.

At all three holes, we recovered an apparently expanded section across the P/E boundary. As at Site 1257, the upper Paleocene clayey nannofossil chalk sequence is relatively thick. Zeolite or locally abundant opal-CT lepispheres replace siliceous microfossils in this interval. In all three holes, we recovered the K/T boundary, and the KT-ejecta layer is present in Core 207-1258B-27R. The subjacent upper Maastrichtian greenish gray nannofossil chalk with foraminifers and clay and lower Maastrichtian–lower Campanian zeolitic nannofossil claystone display cyclic color banding between light greenish gray and greenish gray on a decimeter scale. The succession is considerably expanded with planktonic foraminifers missing in most of the samples investigated. Radiolarians in the Campanian are well preserved. The lithology becomes increasingly clay rich downhole, and carbonate contents decrease to 35%. Foraminifers and nannofossils are rare in this interval, and a significant increase in abundance of diagenetic calcite and carbonate debris is observed. *Planolites, Chondrites,* and *Zoophycos* burrows are abundant as are barite and pyrite crystals. Average sedimentation rates in the Maastrichtian–Campanian interval were 12 m/m.y.

A condensed glauconite-rich horizon in Core 207-1258B-44R separates the Campanian clayey chalk from the ~60-m-thick black shale sequence below. This interval contains the lower part of OAE 3, a complete OAE 2, and an expanded succession of laminated shales of Cenomanian–middle Albian age. The preservation and abundance of calcareous microfossils is poor to good, with glassy foraminifers present in the Cenomanian part of the black shales. A middle Albian disconformity separates the laminated black

shales and limestones from the underlying TOC-rich claystones with phosphatic concretions. Although rich in predominantly marine organic matter (up to 5%), the sediments lack obvious laminations. Clay-rich beds in the latter yield some extremely well preserved microfossils. In addition, ammonites as small as a centimeter in diameter are abundant in some laminae. Rare and thin bioclastic limestone intervals are intercalated; they may represent occasional small-scale storm deposits. The base of Site 1258 is dated as late early Albian age (*Tenuipteria primula* planktonic foraminiferal zone and Subzone NC8a–b).

Recovery of Critical Intervals

The main objective of Leg 207 was to recover sediments containing microfossils through major and abrupt paleoclimate events of the Paleogene and Cretaceous Periods, such as the E/O boundary, P/E boundary, and the OAEs.

In the three holes cored at Site 1258, sediments spanning the P/E boundary were recovered. The boundary interval comprises the last occurrence of benthic foraminifer *Gavelinella beccariiformis,* followed by a sharp contact between light green chalk and dark green clay. The sharp contact reflects the sudden decrease of carbonate content from values of ~60 wt% $CaCO_3$ in the upper Paleocene to ~13 wt% in the lowermost Eocene associated with the P/E boundary. Green clay-rich sediments prevail from the P/E boundary to ~1.90 m above the boundary. Light green carbonate-rich sediments are the dominant lithology of the lower Eocene. Site 1258 appears to provide the first highly expanded P/E boundary succession known from tropical oceans.

The K/T boundary was recovered in all the three holes cored at Site 1258, and the K/T-ejecta layer is present in Core 207-1258B-27R. The base of the K/T boundary is marked by a 1-mm-thick layer of clayey spherules overlying upper Maastrichtian chalks and is covered by a thin (2–3 mm) drape of whitish nannofossil chalk of potentially reworked upper Maastrichtian sediments. Alternatively, this lower lamina of spherules may represent particles that settled through a soupy portion of fine carbonate (nannofossils) that had been either fluidized or suspended by dewatering of the upper Maastrichtian sediment column induced by the K/T impact. The 2-mm-thick white layer is overlain by a 2-cm-thick graded bed of medium to fine sand-sized green spherules, which are, in turn, overlain by gray clay. The *Parvulorugoglobigerina eugubina* planktonic foraminiferal zone (Pα) is remarkably expanded (~3 m thick) and is overlain by planktonic foraminifers belonging to Danian foraminiferal Subzones P1a–P1c, suggesting that the recovered succession is expanded and complete (at the zone level). The recovery of the ejecta layer is, to our knowledge, the first such in South America. Demerara Rise lies ~5000 km southeast of the impact crater in Yucatan. The distribution of documented ejecta deposits west, north, and northeast of Yucatan is one of the supporting lines of evidence to suggest the K/T bolide approached from a southeasterly direction.

A ~60-m-thick Coniacian–Albian succession of laminated black shales and laminated limestones, including OAE 2, was recovered in all three holes at Site 1258. Average recovery of this interval was 77%, and correlation between the holes and the high quality FMS logs will allow for a continuous reconstruction of the interval. The transition between Campanian chalks and the underlying black shales is represented by a hiatus covering the entire Santonian. Coniacian organic-rich sediments are slumped or missing. OAE 2 is represented by an interval of distinctly laminated black shales with TOC values up to 28 wt%. The main lithology consists of dark olive-gray to black finely laminated calcareous claystone with organic matter (black shale) and clayey chalk and limestone with organic matter. The unit shows well-developed submillimeter-scale laminations and has a strong petroliferous odor. Rhythmic color variations between dark olive gray to black are visible on a decimeter scale. Carbonate contents vary between 5 and

95 wt%, and the constituents include nannofossils (concentrated in fecal pellets), foraminifers, and shell fragments. TOC values range from ~5 to 28 wt% in the black shales. Rock-Eval analyses indicate Type II kerogen, which is consistent with a marine origin of the organic matter. Fish scales, bone fragments, and amorphous to cryptocrystalline phosphatic nodules are common. The black shales facies continue until the upper middle Albian, including the middle Cenomanian Event, and the lowermost black shales are dated as late middle Albian (*Biticinella breggiensis* planktonic foraminiferal zone). Storm deposits with oyster and other pelecypod fragments are present, especially toward the base of the black shale interval. Occasional layers of diagenetic calcite with a distinct bluish tint are noted. Microscope analysis reveals that the morphology of the calcite growth resembles that of authigenic methane carbonate cements and may derive from the high methane content in the black shales. To date, no upper Albian biostratigraphic markers have been identified that would enable a stratigraphic definition of the uppermost Albian OAE 1d.

Geochemistry

Active microbial organic matter diagenesis is focused within the organic-rich black shales of Unit IV, similar to Site 1257. Pore water sulfate decreases linearly throughout the overlying units to the top of the black shales at ~390 mbsf. Correspondingly, ammonium, which is produced by organic matter degradation, increases linearly through the same interval. In contrast, alkalinity, a byproduct of sulfate reduction, does not increase linearly with depth but varies with multiple maxima and minima. The correspondence between alkalinity and calcium profiles and intervals of increased lithification suggests alkalinity and calcium variability is controlled by carbonate diagenesis. As expected, where pore water sulfate approaches zero (approximately the top of the black shales), methane contents increase sharply to high values (~3000–60,000 ppmv). Interstitial gas volumes and methane/ethane ratios are higher at Site 1258 than at Site 1257, probably reflecting the higher TOC contents of Units IV and V at Site 1258. Unlike Site 1257, however, Site 1258 pore waters are not characterized by the presence of brine. Salinity and chlorinity decrease with depth beginning at ~300 mbsf, then sharply decrease within the clayey chalks of Unit V. The minimum chloride value at the base of the hole is 465 mM, a 17% decrease from seawater chlorinity. At present, the origin of the low-salinity fluids is undetermined.

Physical Properties and Logging

Core physical property data (MST and discrete measurements) and downhole logging physical property data show excellent agreement. The downhole profiles show marked variability linked to lithologic change. In general, they exhibit a normal consolidation profile down to ~267 mbsf, with a strong negative excursion in velocity and density encompassing the P/E boundary. Below 267 mbsf, the profiles remain constant or decrease slightly, correlating with lithologic Subunit IIC to Unit V. The data variability in this interval also shows patterns of cyclicity. The most pronounced change correlates with lithologic Unit IV, the black shales. In this case, lower density and highly variable velocity values, which reach in excess of 2600 m/s, characterize the unit. Other significant deviations from the normal consolidation trend correlate with events and hiatuses identified in the lithostratigraphy, such as the P/E boundary, the K/T boundary, and the top and bottom of the black shale sequence. These pronounced physical property contrasts yield strong reflection characteristics and allow for good correlation with the seismic stratigraphy.

Depositional History

Lower–middle Albian clayey and TOC-rich sediments represent the oldest sequence recovered at Site 1258 and reflect open marine conditions in a marginal or epicontinental setting. They are unconformably overlain by middle Albian–Coniacian black shales. At present, it remains unclear whether the contact between these two lithologies represents Reflector C, which separates synrift from drift sediments on Demerara Rise. If so, the change between synrift and drift sedimentation at Site 1258 occurred within one planktonic foraminiferal zone, which would give the reflector a late middle Albian age (*B. breggiensis* planktonic foraminiferal zone). Although no major facies change is observed between middle Albian and upper Cenomanian, the lack of late Albian index fossils point to a hiatus in this interval. The abundance of storm deposits in the lower part of the succession might indicate a paleowater depth above storm-wave base and continuous deepening characterizes the remaining Lower Cretaceous succession. During the OAE 2, highest TOC values and very distinct laminations indicate severe bottom water anoxia. Slumping and reworking of organic-rich sediments and black shales occurred during the Coniacian. The top of the black shales is represented by a hiatus covering the Santonian and lower Campanian. At present, it is unclear whether the observed mass flows in the Coniacian are part of the tectonic movements related to the opening of the equatorial Atlantic gateway. The contact between upper Coniacian slumped black shales and condensed lower Campanian glauconite-rich chalk is erosional.

Oxic conditions were established by the early Campanian, when sedimentation on Demerara Rise changed from hemipelagic to pelagic. The abundance of radiolarians in the Campanian, however, indicates increased surface water productivity. The cyclic distribution of trace fossils, indicative of oxygen deficiency, suggests recurring decreases of bottom water oxygenation. The rather continuous Maastrichtian–Eocene pelagic record at Site 1258 records the results of the K/T impact with a graded bed of spherules. The spherules are up to 2.5 mm in diameter, an exceptional size considering the distance to the proposed impact crater.

Interpretation of the seismic records, in conjunction with the observation of mass-wasting deposits and "missing" intervals between holes, indicates that a significant portion of the cored stratigraphic column has failed in a slope instability event or events. The likely scenario is a rotational slump whereby material has been displaced but not transported far and the stratigraphy is left largely intact.

Site 1259

Site 1259 is located at a water depth of 2354 mbsl on the gently dipping (~1°) north-facing slope of Demerara Rise, ~380 km north of Suriname. The site is located on a ridge of Paleogene sediments subcropping near the seafloor and is the second shallowest of all sites forming the intended paleoceanographic depth transect across Demerara Rise. The major objectives were the following:

1. Core and log a Paleogene–Albian section to evaluate paleoceanographic and paleoclimatic changes, with emphasis on major and abrupt events during this interval that include the E/O boundary, the P/E boundary, and the Cretaceous OAE.
2. Reconstruct the history of the opening of the equatorial Atlantic gateway by obtaining benthic proxy data. These data will help to understand changes in bottom water circulation over Demerara Rise during the gradual opening of the seaway.
3. Recover continuous and expanded sediment records of the Paleogene and Cretaceous to reconstruct short- and long-term changes in greenhouse forcing.

The seismic stratigraphy established for Demerara Rise, including Horizons A, B, B′, and C, has been correlated proximally to Site 1259 with line GeoB219; the closest of the three holes drilled at this site is 170 m from this line. The slope angle near the drill site is gentle (~1°) but increases downslope from the site. Reflector A, representing the top of a presumably lower Miocene erosional unconformity, outcrops at the seafloor on the nearest seismic line. The Miocene section recovered in the core is probably not present at the extrapolated site position on the seismic line.

Between Reflectors A and B, seismic Unit 2 is 465 ms thick (~405 mbsf using laboratory-measured velocity information). The topmost sequence (180 ms; ~130 m) within this seismic unit consists of incoherent reflections. Below this interval, Unit 2 is represented by a sequence of high-amplitude, parallel, coherent reflections that are relatively flat lying. This package is about 120 m thick, terminating at 300-ms subbottom (240 mbsf). Below this section to its base at Reflector B, the horizons are still parallel and coherent but lower in amplitude. The entire unit dips to the north slightly less than the seafloor, at ~0.6°. Reflector B, at 463-ms subbottom (442 m), is a high-amplitude, laterally coherent reflector that correlates with the approximate position of the K/T boundary. Seismic Unit 3, between Reflectors B and C at 571 ms, is a ~100-m-thick flat-lying sequence that dips 1° to the north. The upper part of this unit, between Reflectors B and B′, is acoustically incoherent and relatively transparent. The basal part lies between Horizons B′ and C (503- to 571-ms subbottom; ~495–545 mbsf) and is defined on the basis of a series of strong, parallel, coherent reflections that are laterally contiguous for several kilometers, below which is another thin (20 m) transparent zone.

Reflector C is an angular unconformity at Site 1259, with underlying reflections cropping against it at relatively shallow angles (~2°), as they appear on the strike line GeoB2219. On the industry seismic line C2206a that intersects the site in a dip profile (northwest), these low-angle reflections are not resolved and the underlying sequence appears locally conformable (a disconformity).

At Site 1259, three RCB holes were cored. Hole 1260A was cored to 558.8 mbsf, with 66.6% recovery. Hole 1259B was washed to 305 mbsf and cored to 381.9 mbsf. It was then washed to 420.5 mbsf and cored to 556.2 mbsf. Recovery was 69.2% within the cored intervals (Table T1). Hole 1259C was washed to 308.0 mbsf and cored to 373.3 mbsf. It was washed to 436 mbsf, and one core was taken between 436.0 and 445.6 mbsf to obtain a third copy of the K/T boundary interval. The following succession was washed again until 490 mbsf, where continuous coring proceeded until 553.7 mbsf. Recovery in Hole 1259C was 80% within the cored intervals.

Sandy intervals between 120 and 300 mbsf and hard layers between 380 and 400 and 490 and 520 mbsf hampered core recovery in these intervals.

Stratigraphy of Site 1259

Lithologic descriptions of the cores and biostratigraphic age assignments revealed a rather continuous sedimentary succession with only a few hiatuses. Sediments at Site 1259 range in age from Miocene to Cenomanian. The deepest unit recovered in Site 1259 did not yield any age diagnostic microfossils. A thin veneer of Holocene foraminiferal ooze at the top of the section unconformably overlies an ~30-m-thick slide of reworked lower Oligocene calcareous ooze with nannofossils and planktonic foraminifers. A disconformity separates this slide from a concordant succession of lower Miocene calcareous ooze and chalk. Another disconformity separates the Miocene from lower Oligocene to upper Eocene foraminiferal chalk. The latter is represented by a condensed interval of calcareous chalks and overlies an expanded, 235-m-thick succession of middle Eocene (planktonic foraminiferal Zone P14; calcareous nannoplankton Zone NP17) to lower Eocene nannofossil chalk with abundant and well-preserved radiolarians in the

middle Eocene part of this succession. Excellent RCB recovery provided continuous core overlap between holes for the lower Eocene. The periodic variability present in the lower Eocene at Site 1259 will provide a good basis for postcruise cyclostratigraphic studies. Age control is excellent, with well-defined paleomagnetic datums present in the section (e.g., Chrons C30n and C32n). Preliminary investigation suggests the dominant periodicities of the magnetic susceptibility data are Milankovitch in nature.

In all three holes, we recovered an apparently expanded section across the P/E boundary. As at Sites 1258 and 1260, the upper Paleocene clayey nannofossil chalk sequence is relatively thick. Zeolites or locally abundant opal-CT lepispheres replace siliceous microfossils in this interval. Each hole recovered the K/T boundary with ejecta layers. The subjacent upper Maastrichtian greenish gray nannofossil chalk with foraminifers and clay and the lower Maastrichtian–upper Campanian zeolitic nannofossil claystone displays cyclic color banding between light greenish gray and greenish gray on a decimeter scale. Radiolarians in the Campanian are well preserved. The lithology becomes increasingly clay rich downhole, and carbonate contents decrease to 30%. Foraminifers and nannofossils are rare in this interval, and a significant increase in abundance of diagenetic calcite and carbonate debris is observed. *Planolites, Chondrites,* and *Zoophycos* burrows are abundant, as are barite and pyrite crystals. Average sedimentation rates in the Maastrichtian–Campanian interval were 4.5 m/m.y. The periodic variability present in the Campanian–Maastrichtian intervals at Site 1259 will provide a good basis for postcruise cyclostratigraphic studies. Age control is excellent, with well-defined paleomagnetic datums present in both sections (Chrons C30n and C32n; see "Paleomagnetism"). Preliminary investigation suggests the dominant periodicities of the magnetic susceptibility data are Milankovitch in nature.

The abundance of very dark intervals (cyclic in appearance) and glauconitic layers increase in the lower part of the clayey chalk. A condensed interval of glauconite-rich horizons and firmgrounds separates the Campanian clayey chalk from the ~50-m-thick laminated black shale sequence. The top of the black shale unit contains a 1.2-m-thin sliver of Santonian age sediments that unconformably overlies 15 m of lower Coniacian black shales with some debris flows and slumped horizons. The Turonian and OAE 2 are virtually complete and expanded, but only 15 m of Cenomanian-age black shales represents the thinnest occurrence of Cenomanian sediments of Leg 207. The preservation and abundance of calcareous microfossils is poor to good, with glassy foraminifers present in the Santonian–Cenomanian part of the black shales. The maximum TOC content in these sediments is 29 wt%. A disconformity separates the lower Cenomanian laminated black shales and limestones from the underlying silty claystone calcareous siltstone and quartz sandstone that did not yield any age diagnostic microfossils and represents the oldest sediments cored at Site 1259. Sedimentary structures and the presence of shallow-water fossils (brachiopods, oysters, and echinoderms) suggest a very shallow marine to tidal origin of these sediments.

Recovery of Critical Intervals

The main objective of Leg 207 was to recover sediments containing microfossils through major and abrupt paleoclimate events of the Paleogene and Cretaceous Periods, such as the E/O boundary, P/E boundary, and the Cretaceous OAEs.

Sediments spanning the P/E boundary were recovered in all three holes at Site 1259. The boundary interval comprises the last occurrence of benthic foraminifer *Aragonia velascoensis,* a species that became extinct at the P/E boundary, followed by a sharp contact between light green chalk over dark green clay. The sharp contact reflects the sudden decrease of carbonate content between the upper Paleocene and the lowermost Eocene associated with the P/E boundary. Planktonic foraminifers are absent from the base of the distinctive green clay horizon until at least 20 cm above the P/E boundary, although this interval

contained a small number of benthic foraminifers and abundant, but poorly preserved, spumularian radiolarians. A sample 50 cm above the P/E boundary contains a moderately well preserved foraminiferal assemblage with abundant *Morozovella allisonensis* and *Acarinina soldadoensis* and rare *Acarinina africana, Acarinina sibaiyaensis, Subbotina patagonica,* and *Parasubbotina varianta*. Three of these species, *M. allisonensis, A. africana,* and *A. sibaiyaensis,* are associated with P/E boundary sections in other tropical and subtropical sites (Central Pacific, Egypt, Spain, New Jersey, and the Blake Plateau) and are known as the "excursion fauna" because of their abundance and near restriction to the PETM. An unusual element of these assemblages is *Parasubbotina paleocenica*—a clavate species that has previously been reported only from ODP Site 1220 in the equatorial Pacific and its type area in coastal Senegal. The West African and equatorial Pacific settings of these previous discoveries suggest that *P. paleocenica* is associated with upwelling conditions. Hence, we infer that the excursion fauna may also represent an expansion of relatively productive waters during the PETM.

The K/T boundary was recovered in all three holes cored at Site 1259, and the ejecta layer is present in each of them. A 1.9-cm-thick layer of clayey spherules overlying upper Maastrichtian chalks marks the base of the K/T boundary. Above the boundary, the lower Danian planktonic foraminiferal Zones P2 to Pα were distinguished. The lower Danian planktonic foraminiferal Subzone P1c to Zone Pα have a thickness of 8 m. The thickness of the spherule layer is similar to that at Site 1258 and 1260, suggesting that the spherule bed at both sites is a result of fallout rather than redeposition.

A ~50-m-thick Santonian–Cenomanian succession of laminated black shales and laminated foraminiferal limestones, including OAEs 3 and 2, was recovered in both holes at Site 1259. The quasiperiodic variability of the claystone and chalks/limestone comprising the black shales resulted in strong signal-to-noise ratios in both the gamma ray attenuation (GRA) bulk density and natural gamma ray data sets. These data sets, combined with good RCB recovery over a significant portion of the black shale interval, allowed for the construction of a continuous composite section from ~520 to 555 meters composite depth (mcd), the Turonian–Cenomanian interval of the black shales including OAE 2. Poor recovery from 495 to 520 mcd precluded the construction of a composite section in this upper interval of the Cretaceous black shales (OAE 3).

The transition between Campanian chalks and the underlying black shale sequence is represented by a condensed section covering the early Campanian and entire Santonian epochs. The thickness of Coniacian organic-rich sediments is comparable to other sites. OAE 2 is represented by an interval of distinctly laminated black shales. The main lithology consists of dark olive-gray to black finely laminated calcareous claystone with organic matter (black shale) and clayey chalk and limestone with organic matter. Occasional coarse-grained glauconite-rich horizons are present. The unit shows well-developed submillimeter-scale laminations and has a strong petroliferous odor. Rhythmic color variations, between dark olive gray and black, are visible on a decimeter scale. TOC values range from ~5 to 29 wt% in the black shales, with the highest values deriving from the basal upper Cenomanian part of the succession. Rock-Eval analyses indicate Type II kerogen, which is consistent with a marine origin of the organic matter. Fish scales, bone fragments, and amorphous to cryptocrystalline phosphatic nodules are common.

Geochemistry

Similar to the pore waters of Site 1257, Site 1259 is characterized by the presence of a brine, with maximum chlorinity of 832 mM, a ~50% increase over average seawater chlorinity. The combination of the chlorinity and salinity profiles and high-porosity intervals in the black shales suggest that the brine is sourced laterally through these organic-rich claystones of Unit IV. Interstitial water (IW) chemical profiles

associated with the degradation of organic matter are dominated by the presence of black shales and associated organic matter-rich sediments. Sulfate decreases downhole and is depleted by ~490 mbsf, the top of Unit IV, whereas ammonium increases to more than 1 mM. Below the sulfate reduction zone, methane increases sharply to reach a maximum of 76,000 parts per million by volume (ppmv) near the base of black shales before dropping to 2000 ppmv in Unit V. As at previous Leg 207 sites, the calcium and alkalinity profiles show the effects of carbonate diagenesis. In particular, decreases in calcium and alkalinity indicate an interval of carbonate precipitation between 300 and 490 mbsf.

Physical Properties

Index properties, compressional (*P*)-wave velocities, and GRA densities were measured on core samples from Site 1259. No downhole logs were run at this site because of concerns about hole conditions in the topmost part of the formation. In general, the physical property data reflect normal consolidation down to about 365 mbsf, with relatively linear profiles. Small excursions in properties appear at about 95 mbsf and between 200 and 280 mbsf, the latter correlating with a middle Eocene radiolarian-rich interval of calcareous nannofossil chalk. Porosity data show strong periodic signals superimposed on the normal consolidation trend through the lower Eocene, suggesting that cyclical variations may be readily determined.

Lithologies become richer in clay below 365 mbsf. Velocity and density profiles tend to flatten with much higher scatter in magnitudes than above. A strong increase in velocity and density corresponds with the K/T boundary, and probable cyclicity is again apparent in data through the Maastrichtian sedimentary sequence. The black shale facies is highlighted particularly well by the physical property data, with a distinct drop in average values but a high degree of scatter. Velocity and density maximums correspond with limestone or sandstone beds and low values in density and velocity correspond with organic-rich intervals. The largest peaks in velocity and density appear in the quartz sandstone and siltstone below the black shales (values up to 3500 m/s and 2.4 g/cm^3).

Depositional History

Probable tidal flat deposits of unknown age (Albian?), which were deposited in a marginal marine setting, represent the oldest sequence recovered at Site 1259. They are unconformably overlain by a black shale sequence that dates from late Cenomanian to Santonian, but most of it is Turonian, with thinner Cenomanian, Coniacian, and Santonian intervals. Occasional clayey bentonite layers indicate the proximity of volcanoes. Calcareous nannofossils of the genus *Ephrolitus* form very dark TOC-rich shales at the base of the succession point to marginal marine environments. The laminated, coarse-grained foraminiferal limestones in the succession may be related to winnowing, grain flows, or reflect changes in carbonate productivity. Continuous deepening characterizes the remaining Upper Cretaceous succession. During OAE 2, high TOC values and very distinct laminations indicate bottom water anoxia. The top of the black shale interval is represented by a condensed interval covering the Santonian and lower Campanian. At present, it is unclear whether the observed mass flow deposits in the upper Turonian and Coniacian are part of the tectonic movements related to the opening of the equatorial Atlantic gateway.

Oxic conditions were established by the late Campanian, when sedimentation on Demerara Rise changed from hemipelagic to pelagic. The abundance of radiolarians in the Campanian, however, indicates increased surface water productivity. The cyclic pattern of trace fossil abundance suggests reduction in bottom water oxygenation recurs.

Maastrichtian- to Oligocene-age sediments at Site 1259 consist of pelagic deep marine nannofossil chalks and oozes. Sedimentation rates varied from 4.5 m/m.y. in the Maastrichtian–late Paleocene, 12 m/m.y. in the late Paleocene–late Eocene, and ~13 m/m.y. in the early Miocene. The succession is interrupted by a few hiatuses—a lower Paleocene hiatus covering ~1 m.y., an ~3-m.y. hiatus at the middle/upper Eocene boundary, and a upper Oligocene interval of hiatuses and condensed intervals representing ~3 m.y. These hiatuses may reflect periods of slow deposition and/or erosion.

Site 1260

Site 1260 is located at a water depth of 2549 mbsl on the gently dipping (~1°) northwest-facing slope of Demerara Rise, ~380 km north of Suriname. The site is located on a ridge of Paleogene sediments subcropping near the seafloor. Site 1260 is at an intermediate depth of the intended paleoceanographic depth transect across Demerara Rise. The major objectives were the following:

1. Core and log a Paleogene–Albian section to evaluate paleoceanographic and paleoclimatic changes, with emphasis on major and abrupt events during this interval that include the E/O boundary, the P/E boundary and the Cretaceous OAE.
2. Reconstruct the history of the opening of the equatorial Atlantic gateway by obtaining benthic proxy data. These data will help to understand changes in bottom water circulation over Demerara Rise during the gradual opening of the seaway.
3. Recover continuous and expanded sediment records of the Paleogene and Cretaceous to reconstruct short- and long-term changes in greenhouse forcing.

The seismic stratigraphy established for Demerara Rise, including Horizons A, B, B′, and C, have been correlated to Site 1257 and 1258 strata. The seafloor in the proximity of the drill site appears hummocky in the downslope direction but reasonably flat in the contour parallel direction. Reflector A, representing the top of a presumably lower Miocene erosional unconformity, subcrops near the seafloor at the site. Between Reflectors A and B, seismic Unit 2 is 365 ms thick (~315 mbsf using laboratory-measured downhole logging and check shot velocity information). The topmost sequence within this seismic unit consists of contorted reflectors that pinch out against the seafloor within 1.5 km downslope. This sequence may represent a slumped interval. Below this slumped interval, Unit 2 is represented by a sequence of crenulated but coherent reflection horizons, separated by transparent or incoherent intervals. In the downslope direction, these reflectors are reasonably flat lying, dipping slightly less than the angle of the seafloor.

Seismic Unit 3, between Reflector B at 365-ms subbottom and Reflector C at 522 ms, is a ~170-m-thick, flat-lying sequence that dips 1.5° to the north-northwest. The basal part of this unit lies between Horizons B′ and C (464- to 522-ms subbottom; ~392–485 mbsf) and is defined on the basis of a series of strong, parallel, coherent reflections that are laterally contiguous. This seismic interval has been shown to correlate to the black shale interval.

At Site 1260, two RCB holes were cored. Hole 1260A was cored to 491.9 mbsf, with 79.6% recovery (Table T1). Hole 1260B was washed to 40 mbsf and cored from 40 to 136.5 mbsf. It was then washed to 235 mbsf and cored to 509 mbsf. Recovery was 88.2% within the cored intervals. Hard beds between 130 and 154, 180 and 211, and 480 and 509 mbsf hampered core recovery in these intervals.

Stratigraphy of Site 1260

Lithologic descriptions of the cores and biostratigraphic age assignments revealed a rather continuous sedimentary succession with only a few hiatuses. Sediments at Site 1260 range in age from Oligocene to early Albian. A thin veneer of Pleistocene carbonate-poor clayey ooze with quartz and glauconite at the top of the section unconformably overlies ~30 m of heavily slumped and reworked lower Oligocene calcareous chalk with nannofossils and planktonic foraminifers. The late Eocene is represented by a condensed interval of calcareous chalks and overlies an expanded 235-m-thick succession of middle Eocene (planktonic foraminiferal Zone P13; calcareous nannoplankton Zone NP17) to lower Eocene nannofossil chalk, with abundant and well preserved radiolarians in the middle Eocene part of this succession. With the exception of a hiatus spanning the lower/middle Eocene boundary, the lower–middle Eocene succession is remarkably expanded (average sedimentation rate = ~20 m/m.y.) and complete. Excellent RCB recovery provided continuous core overlap between holes for the middle Eocene. The periodic variability present in the middle Eocene color reflectance and GRA bulk density data at Site 1260 will provide a good basis for postcruise cyclostratigraphic studies. Age control is excellent, with well-defined paleomagnetic datums present in the section (e.g., Subchrons C19n and C20n). Preliminary investigation suggests the dominant periodicities of the magnetic susceptibility data are Milankovitch in nature, with significant power at 40 k.y.

In both holes, we recovered an apparently expanded and laminated section across the P/E boundary. As at Site 1258, the upper Paleocene clayey nannofossil chalk sequence is relatively thick and sedimentation rates in the lower Eocene to Paleocene interval drop to values averaging ~12 m/m.y. Zeolite or locally abundant opal-CT lepispheres replace siliceous microfossils in this interval. In both holes, we recovered the K/T boundary with ejecta layers. The subjacent upper Maastrichtian greenish gray nannofossil chalk with foraminifers and clay and the lower Maastrichtian to upper Campanian zeolitic nannofossil claystone display cyclic color banding between light greenish gray and greenish gray on a decimeter scale. The succession is considerably expanded. Almost complete coring in both holes allowed for the construction of a splice with only one gap in the lower Maastrichtian. Radiolarians in the Campanian are well preserved. The lithology becomes increasingly clay rich downhole, and carbonate contents decrease to 30 wt%. Foraminifers and nannofossils are rare in this interval, and a significant increase in abundance of diagenetic calcite and carbonate debris is observed. *Planolites, Chondrites,* and *Zoophycos* burrows are abundant, as are barite and pyrite crystals. Average sedimentation rates in the Maastrichtian–Campanian interval were 12 m/m.y.

A condensed glauconite-rich horizon in Core 207-1260A-42R separates the Campanian clayey chalk from the ~90-m-thick black shale sequence, with TOC content up to 14 wt%. This interval contains a thin Coniacian interva, and thus the lower part of OAE 3, and a virtually complete Turonian. OAE 2 overlies an expanded succession of laminated shales of Cenomanian age. The preservation and abundance of calcareous microfossils is poor to good, with glassy foraminifers present in the Turonian and Cenomanian part of the black shales. A disconformity separates the lower Cenomanian laminated black shales and limestones from the underlying silty claystone and silty limestone, which dated as late early Albian age (*T. primula* planktonic foraminiferal zone; Subzones NC8a–b) and represents the oldest sediments cored at Site 1260.

Recovery of Critical Intervals

The main objective of Leg 207 was to recover sediments containing microfossils through major and abrupt paleoclimate events of the Paleogene and Cretaceous Periods, such as the E/O boundary, P/E boundary, and the Cretaceous OAEs.

Sediments spanning the P/E boundary were recovered in both holes at Site 1260. The boundary interval comprises the last occurrence of benthic foraminifer *Aragonia velascoensis,* a species that became extinct at the P/E boundary, followed by a sharp contact between light green chalk over dark green clay. The sharp contact reflects the sudden decrease of carbonate content between the upper Paleocene and the lowermost Eocene associated with the P/E boundary. The uppermost Paleocene chalk contains distinct laminations until 12 cm above the boundary, where the first bioturbation occurs. Pervasive bioturbation returns within about 30 cm above the boundary. Bioturbated, light green, carbonate-rich sediments are the dominant lithology of the lower Eocene.

The K/T boundary was recovered in both holes cored at Site 1260, and the ejecta layer is present in Cores 207-1260A-36R and 207-1260B-23R. An 1.8-cm-thick layer of clayey spherules overlying upper Maastrichtian chalks marks the base of the K/T boundary. In the core from Hole 1260A, the spherule layer is covered by a thin (5 mm) drape of whitish nannofossil chalk of potentially reworked upper Maastrichtian sediments. The section is similar in Hole 1260B, but the spherule layer is only 1 mm thick, probably because of drilling disturbance. Above the boundary, the lower Danian planktonic foraminiferal Zones P2 to Pα were distinguished. The thickness of the spherule layer is similar to that at Site 1258, suggesting that the spherule bed at both sites is a result of fallout rather than redeposition.

A ~90m-thick Coniacian–Albian succession of laminated black shales and laminated foraminiferal limestones, including OAE 2, was recovered in both holes at Site 1260. Average recovery of this interval was 80%, and correlation between the holes and the high quality FMS logs will allow for a continuous reconstruction of the interval.

The transition between Campanian chalks and the underlying black shale sequence is represented by a hiatus or condensed section covering the entire Santonian. Coniacian organic-rich sediments are very thin. OAE 2 is represented by an interval of distinctly laminated black shales. The main lithology consists of dark olive-gray to black finely laminated calcareous claystone with organic matter (black shale) and clayey chalk and limestone with organic matter. Occasional coarse grained glauconite-rich horizons are present. The unit shows well-developed submillimeter-scale laminations and has a slight petroliferous odor. Rhythmic color variations, between dark olive gray and black, are visible on a decimeter scale. TOC values range from ~5 to 14 wt% in the black shales. Rock-Eval analyses indicate Type II kerogen, which is consistent with a marine origin of the organic matter. Fish scales, bone fragments, and amorphous to cryptocrystalline phosphatic nodules are common. The lower part of the black shales consists of distinctly laminated shales that are composed almost exclusively of fecal pellets. The black shale facies continues until the lower Cenomanian and thus comprises the mid-Cenomanian Event.

Geochemistry

IW profiles at Site 1260 document reactions similar to those at earlier Leg 207 sites, with remarkably comparable profiles to Site 1258 in particular. Microbially mediated organic matter remineralization is largely centered within Unit IV, the black shales. Sulfate decreases linearly downcore to zero near the top of Unit IV at ~390 mbsf, with a corresponding increase in ammonium to values in excess of 2 mM. Below the depth of sulfate depletion, methane contents increase sharply to maximum values (~68,000 ppmv) within the black shales, then decrease below. As at Site 1258, alkalinity and calcium profiles document

intervals of active carbonate diagenesis. Within the upper 400 mbsf, chloride profiles at Site 1260 are strikingly similar to the upper 400 mbsf at Site 1258, including two coincident 3% decreases at ~310 and 370 mbsf. Below 400 mbsf, the Site 1260 chloride profile only increases slightly (577–582 mM) and shows neither the presence of the brine documented at Site 1257 nor the pronounced pore water freshening that was observed at Site 1258.

Physical Properties and Logging

Index properties, *P*-wave velocities, and GRA densities were measured on core samples from Site 1260. Logging runs consisted of two passes with the triple combo tool string and two passes with the FMS-Sonic tool. In addition, a check shot velocity run was conducted, comprising 14 downhole stations. Hole conditions were excellent for the logging tools, and data are of extremely high quality. In general, the physical property data reflect normal consolidation down to ~328 mbsf. Anomalously high velocities and porosities in the top 40 m reflect a slump deposit within this interval. Porosity, resistivity, and FMS data show strong periodic signals superimposed on the normal consolidation trend through the Eocene interval, suggesting cyclical variations may be readily determined.

Lithologies become richer in clay below 328 mbsf. Velocity and density profiles tend to flatten with much higher scatter in magnitudes than above. All logs correlate very closely with lithologic changes identified from core descriptions. Natural gamma logs delineate the black shale facies particularly well, but all logs show distinctive changes in profile shape and a high degree of data variability in this interval. Critical intervals that are visually distinct, like the P/E and K/T boundaries, are readily distinguished with logging and physical property data as well. As a consequence, lithologic changes and these event deposits can be correlated to the seismic reflection data with a high degree of confidence.

Depositional History

Clayey quartz siltstone of lower Albian age, which was deposited in a marine marginal or epicontinental shelf setting, represents the oldest sequence recovered at Site 1260. It is unconformably overlain by a black shale sequence that dates from Cenomanian to Coniacian, but most of it is Cenomanian, with thinner Turonian and Coniacian intervals. Debris flows, wood fragments, and quartz are found at the base of the organic-rich black shale section, which indicate shallow water depths. The laminated, coarse-grained foraminiferal limestones in the succession may be related to winnowing or grain flows or may reflect changes in carbonate productivity. Continuous deepening characterizes the remaining Upper Cretaceous succession. During OAE 2, highest TOC values and very distinct laminations indicate bottom water anoxia. The top of the black shale interval is represented by a hiatus covering the Santonian and lower Campanian. At present, it is unclear whether the observed mass flow deposits in the upper Turonian and Coniacian are part of the tectonic movements related to the opening of the equatorial Atlantic gateway. The contact between upper Coniacian slumped black shales and condensed Campanian glauconite-rich chalk is erosional.

Oxic conditions were established by the Campanian, when sedimentation on Demerara Rise changed from hemipelagic to pelagic. The abundance of radiolarians in the Campanian, however, indicates increased surface water productivity. The cyclic pattern of trace fossil abundance suggests that reductions in bottom water oxygenation recur.

Maastrichtian- to Oligocene-age sediments at Site 1260 consist of pelagic deep marine nannofossil chalks and oozes. Sedimentation rates vary from 4.3 m/m.y. in the Maastrichtian–upper Paleocene, 12.1 m/m.y. in the upper Paleocene–lower Eocene, ~20.5 m/m.y. in the middle Eocene, and ~6.7 m/m.y. in the

upper Eocene. The succession is interrupted by several hiatuses—a upper Paleocene hiatus representing ~1 m.y., an ~1.5-m.y. hiatus at the lower/middle Eocene boundary, an upper–middle Eocene hiatus of ~5 m.y., and an lower Oligocene hiatus of ~2 m.y. These hiatuses may reflect periods of slow deposition and/or erosion.

Site 1261

Site 1261 is located at a water depth of 1899 mbsl on the gently dipping (~1°), northwest-facing slope of Demerara Rise, ~350 km north of Suriname. Sites 1260 and 1258 are to the northwest. and Sites 1257 and 1259 are to the north. Site 1261 is the shallowest site, forming the paleoceanographic depth transect across Demerara Rise. The major objectives were the following:

1. Core and log a Paleogene–Albian section to evaluate paleoceanographic and paleoclimatic changes, with emphasis on major and abrupt events during this interval that include the E/O boundary, the P/E boundary, and the Cretaceous OAE.
2. Reconstruct the history of the opening of the equatorial Atlantic gateway by obtaining benthic proxy data. These data will help to understand changes in bottom water circulation over Demerara Rise during the gradual opening of the seaway.
3. Recover continuous and expanded sediment records of the Paleogene and Cretaceous to reconstruct short- and long-term changes in greenhouse forcing.

The seismic stratigraphy established for Demerara Rise, including the Horizons A, B, B′, and C, was correlated to Site 1261 with line GeoB213. Lines GeoB204 and GeoB208 are orthogonal to GeoB213 and pass within 5 km of the site to the northwest and southeast, respectively. Industry line C2206a passes orthogonal to GeoB213 as well, 8 km to the northwest of the drill site.

The seismic stratigraphy for Demerara Rise shows increasing sediment thickness to the south (in board). At Site 1261, the uppermost sediment section has not been defined previously. It consists of a thin (30 ms; 24 m) package of parallel, coherent reflections that offlap from the upslope direction (south) and truncate against the seafloor ~10 km downslope from the site. This sequence is likely Quaternary in age, and the base of it is termed Reflector "O."

What has previously been defined as seismic Unit 1 (Miocene–Pliocene) underlies Reflector O. It is largely missing at the other sites. In the immediate vicinity of Site 1261, Unit 1 comprises a well-defined set of coherent seismic reflections of varying amplitudes. The topmost reflections truncate against the Reflector O, sometimes in an angular fashion. The base of the unit is Reflector A, just above which is a 50-ms-thick (~40 m) zone of incoherent reflections capped by a bright reflector. This interval appears to be a debris flow. Unit 1 is 415 ms thick (~367 m) at the drill site.

Unit 2 is below Reflector A, which is the presumed lower Miocene erosional unconformity. The base of seismic Unit 2 is correlated to Reflector B at 586-ms subbottom (550 mbsf). It is represented by a sequence of high-amplitude, parallel, coherent reflections that are relatively flat lying, dipping 0.5° to the north. Seismic Unit 3, between Reflectors B and C, is estimated to be 150 ms thick (175 m). Much of the acoustic energy in the high-resolution site survey profile (line GeoB213) is lost within the highly reflective Unit 2. Little detail is resolved in Unit 3 as a result. It appears as an acoustically transparent package with occasional semicoherent reflectors at the top and at the very base, just above Horizon C. It is difficult to correlate the Horizon B′ and thus to distinguish Subunits 3a and 3b resulting from this low reflectivity. Horizon B′ has been correlated to the base of the slightly coherent section near the top of Unit 3, but the tie is uncertain.

Reflector C, at the base of the section of interest, is an unconformity. No coherent subsurface data are recognizable in the survey data, but the nearby industry line C2206a shows the underlying section. At Site 1261, the unconformity appears as a disconformity, and it is difficult to actually pick up Reflector C as a single event. Further below, reflections form a broad anticline, fault bounded to the southwest and folded into a syncline to the northeast.

A listric normal fault is shown on line GeoB213 5 km southeast of the drill site. This fault has offset the entire sediment column. Apparent displacement across the fault is ~30–60 ms in the deeper portion of the section (at Reflector C), whereas in the upper portion, it is on the order of 200 ms. This discrepancy in offset can be accounted only by invoking either significant rotation or slumping in the upper sediment column. The fault splays at 300-ms subbottom to the seafloor, showing significant tilting of reflections in the interval between offsets and providing further evidence of slumping.

At Site 1261, two RCB holes were cored. Hole 1261A was spot cored to a depth of 236.9 mbsf, with cores taken between 0 and 22.5, 69.7 and 79.3, 131.4 and 141.1, and 189.1 and 198.7 mbsf. Continuous coring proceeded from 236.9–659.8 mbsf. The recovery in Hole 1261A was 73.4% for the cored intervals (Table T1). Hole 1261B was washed to 525.3 mbsf and cored to 674.1 mbsf. Recovery was 62.2% within the cored intervals.

Stratigraphy of Site 1261

Lithologic descriptions of the cores and biostratigraphic age assignments reveal a sedimentary succession with several hiatuses. Sediments at Site 1261 range in age from Pleistocene to Cenomanian. Approximately 13 m of nannofossil ooze of Pleistocene age at the top of the section unconformably overlie an apparently continuous ~300-m-thick succession of lower middle Pliocene–upper Miocene nannofossil clay. Sedimentation rates in the Neogene are extraordinarily high with values of 65 m/m.y. A ~60-m-thick upper Miocene matrix-supported conglomerate is the base of the Neogene at Site 1261. A disconformity separates this debris flow from a concordant succession of middle (planktonic foraminiferal Zone P14; calcareous nannoplankton Zone NP17) to lower Eocene calcareous chalk, porcellanite, and limestone. A 4-m.y. hiatus covering the lower Eocene (planktonic foraminiferal Zone P6) lies above the P/E boundary, which was recovered in Hole 1261A.

As at the other Leg 207 sites, the upper Paleocene clayey nannofossil chalk contains zeolites or locally abundant opal-CT lepispheres that replaced siliceous microfossils in this interval. Foraminifers in the middle part of this succession are very well preserved. The K/T boundary layer is absent from this site because of a hiatus covering most of the lower Danian (planktonic foraminiferal Zone P1). The subjacent upper Maastrichtian greenish gray to upper Campanian claystone with nannofossils is fairly condensed and displays cyclic color banding between light greenish gray and greenish gray on a decimeter scale. Foraminifers and nannofossils are rare in this interval, and a significant increase in abundance of diagenetic calcite and carbonate debris is observed. *Planolites, Chondrites,* and *Zoophycos* burrows are abundant, as are barite and pyrite crystals. Average sedimentation rates in the Maastrichtian–Campanian interval were 3.3 m/m.y. Magnetostratigraphic age control in this interval is excellent, with well-defined paleomagnetic datums C29r to C32r present in both holes.

There are numerous very dark-colored intervals, cyclic in appearance, in the lower part of the Campanian. A condensed glauconite-rich interval separates the claystone from a ~8-m-thick laminated black shale sequence. The contact between upper Campanian and the mid-Cretaceous black shales is very sharp and may represent a hardground. Site 1261 represents the most expanded black shale sequence of the Leg 207 paleoceanographic depth transect. Approximately 10 m of Santonian sediments overlies ~10

m of lower Coniacian black shales. The Turonian epoch is virtually completely represented and underlain by 40 m of upper Cenomanian black shales. Preservation and abundance of calcareous microfossils is rated poor to moderate. The maximum TOC content in these sediments is 16 wt%. Rock-Eval analyses indicate Type II kerogen, which is consistent with a marine origin of the organic matter. Fish scales, bone fragments, and amorphous to cryptocrystalline phosphatic nodules are common.

A disconformity separates the Cenomanian-age laminated black shales and limestones from the underlying quartz sandstone and silty claystone that is upper Albian–Cenomanian in age, according to a single nannofossil datum. The oldest sediment cored at Site 1261 is a limestone with abundant oysters of the genus *Aucillina*.

Recovery of Critical Intervals

The main objective of Leg 207 was to recover sediments containing microfossils through major and abrupt paleoclimate events of the Paleogene and Cretaceous Periods, such as the E/O boundary, P/E boundary, and the Cretaceous OAEs.

Sediments spanning the P/E boundary were recovered in Hole 1261A. The boundary interval comprises a sharp contact between light green chalk over dark green clay followed by a reddish clay-rich interval similar to Sites 1258 and 1259. The sharp contact reflects the sudden decrease of carbonate content between the upper Paleocene and the lowermost Eocene associated with the P/E boundary. The K/T boundary was not represented at this site.

A ~87-m-thick Santonian to upper Cenomanian succession of laminated black shales and laminated foraminiferal limestones, including OAEs 3 and 2, was recovered in both holes at Site 1261. This interval is the most expanded record of the Santonian to Coniacian OAE 3 of Leg 207 (20 m). The variability of the claystone and chalks/limestone comprising the black shales resulted in strong signal-to-noise ratios in both the GRA bulk density and natural gamma ray data sets. These data sets, combined with good RCB recovery over a significant portion of the black shale interval, allowed for the construction of a continuous composite section with only three small gaps. If these alternations prove to be periodic, then there is a good opportunity for high-resolution age control with orbital tuning.

Geochemistry

Site 1261 is the third of the five sites dominated by the presence of an IW brine. Chloride increases in a linear fashion to the base of the black shales, where the highest chlorinity encountered on Demerara Rise is observed (907 mM; 62% greater than standard seawater). Unfortunately, it was not possible to extract pore water from the very thin interval of quartz sandstone that was recovered immediately below the shales. It could not be verified, therefore, whether the brine was sourced laterally through the black shale sequence, as was suggested by the Site 1257 chloride profile.

Unlike previous Leg 207 sites, organic matter degradation reactions occur outside the organic-rich black shales. Sulfate decreases to zero in the upper 200 mbsf within the rapidly deposited (65 m/m.y.) Pliocene nannofossil clay. Correspondingly, ammonium, a common respiration product of organic matter diagenesis, increases sharply to ~1.5 mM within the upper 140 mbsf, and then slowly increases with depth to a maximum of 1.8 mM in the black shales. Methane increases modestly to ~2,000 ppmv in the upper 500 mbsf, then increases sharply near the top of the black shales to a maximum of ~110,000 ppmv. In contrast, alkalinity does not increase with depth as expected within the sulfate reduction zone, but decreases from the seafloor to a minimum at ~480 mbsf. The decreasing alkalinity corresponds with a

decrease in calcium between ~250 and 375 mbsf and the interval of well-cemented Eocene chalks and limestones, indicating carbonate precipitation.

Physical Properties and Logging

Index properties, *P*-wave velocities, and GRA densities were measured on core samples from Site 1261. Downhole logging runs included the triple combo and the FMS-sonic tool strings, acquiring borehole caliper, acoustic velocity, formation density, porosity, electrical resistivity, and natural gamma ray emission data. The WST was run for check shot velocities, but the tool could not be lowered past a bridge at 210 mbsf. Five WST stations were acquired in this upper interval. Logging data show the seafloor to be at 1887.8 mbsl, 12.1 m shallower than the drillers depth.

Logging data in the upper ~380 mbsf are highly suspect as a result of a highly variable hole diameter through this interval. Consequently, correlation between laboratory-measured densities and logging densities are poor. Log velocity data are not affected as severely by the hole diameter and correlate well with discrete core measurements in the laboratory and the check shot velocities measured with the WST tool. Physical property data show this interval is normally consolidated, with linear increases in density and velocity and a decrease in porosity. A significant perturbation in the porosity and velocity curves correlates with a major debris flow interval between ~320 and 380 mbsf.

Logging density data become stable below ~380 mbsf. They show a significant increase between 380 and 500 mbsf, concomitant with higher velocities. This interval corresponds with the Eocene sequence that has high clay and siliceous fractions relative to overlying sediments. A gradual decline in velocity and density corresponds with the P/E boundary. A subsequent sudden increase in these properties correlates with the K/T boundary and the underlying Maastrichtian chalk sequence. Absolute values show an overall drop with a high degree of scatter through the Cenomanian and Turonian black shale sequence. Velocity and density maximums in this interval correspond with limestone or coarse-grained beds, and low values in density and velocity correspond with organic-rich intervals.

Depositional History

Shallow marine quartz sandstones with ammonite casts and limestones with oysters represent the oldest sequence recovered at Site 1261. They are overlain by a black shale sequence that dates from upper Cenomanian to Santonian, but most of it is Cenomanian to Turonian with thinner Coniacian and Santonian intervals. Occasional clayey bentonite layers indicate the proximity of volcanoes. The laminated, coarse-grained foraminiferal limestones in the succession may be related to winnowing, grain flows, or reflect changes in carbonate productivity. Continuous deepening characterizes the remaining Upper Cretaceous succession. During the OAE 2, high TOC values and very distinct laminations indicate bottom water anoxia. The top of the black shale interval is a sharp contact between the Santonian and overlying glauconite-rich upper Campanian claystones. At present, it is unclear whether the observed glauconite-rich intervals in the black sediment deposits of the Turonian and Coniacian reflect periods of oxygenation, condensation, or both.

Oxic conditions were established by the late Campanian, when sedimentation on Demerara Rise changed from hemipelagic to pelagic. The cyclic pattern of trace fossil abundance, however, suggests that a reduction in bottom water oxygenation recurs.

Maastrichtian- to Pleistocene-age sediments at Site 1261 consist of pelagic deep marine clayey chalk, claystone, limestone, and clays. Sedimentation rates varied from 3.3 m/m.y. in the Maastrichtian, 7 m/m.y. in the Paleocene and early Eocene, to 8.9 m/m.y. in the middle Eocene. These are the lowest values

observed during Leg 207 for these intervals. Average sedimentation rates for the upper Miocene–lower Pliocene reach the extremely high values of 65 m/m.y. The pelagic succession is interrupted by a few hiatuses—an lower Paleocene hiatus covering ~4 m.y., a ~2.5-m.y. hiatus in the lower Eocene, and a hiatus representing ~31 m.y. covering the upper Eocene, Oligocene, and lower Miocene. These hiatuses may reflect periods of slow deposition and/or erosion.

DISCUSSION AND CONCLUSIONS

Lithostratigraphy

The five sites cored during Leg 207 recovered sedimentary sequences that record the sedimentary and paleoceanographic history of the tropical Atlantic. The sedimentary pile can be divided into three broad styles of deposition—synrift clastics, restricted marine "black shales," and open marine chalk and calcareous claystones (Fig. F8). Synrift deposits show a variety of lithologies, and important questions remain regarding depositional water depth, terrigenous sources, transport paths, and possible differences in age within and among the sites. Pelagic deposition included long intervals of relatively constant sedimentation recovered at multiple sites suitable for detailed chronostratigraphic and paleoceanographic studies. In addition, the changing proportions of terrigenous and biogenic components, the distribution of regional hiatuses, and benthic isotopic studies should help constrain the evolution of circulation within the tropical Atlantic. The most dramatic lithologic features recovered during Leg 207, however, were the sedimentological expression of the P/E and K/T boundary events and black shale deposition encompassing several OAEs.

Paleocene/Eocene Boundary

The P/E boundary is placed at the level of a greenish clay bed ~30-cm thick that is unique at each site (Fig. F9A). It is provisionally interpreted as the record of the shoaling of the CCD following the P/E boundary event and is expected to coincide with both the benthic foraminiferal extinction event and the carbon isotopic excursion. The 1–5 cm of the Paleocene below the clay shows a progressive increase in clay content toward the boundary. Above the boundary, the clay is relatively thick and distinctly laminated at Site 1260, but this fabric is not seen at the other sites. Either the record at Site 1260 is exceptionally complete or there were paleobathymetric differences in expression of the event on Demerara Rise. A 12- to 20-cm-thick red interval begins 2–20 cm above the P/E boundary at Sites 1258, 1259, and 1261 but not at Sites 1257 or 1260, documenting additional site-to-site variability.

Magnetic susceptibility measurements suggest that the clay-rich part of the boundary sequence ranges from ~1 m in thickness at Site 1261 to ~2 m in thickness at Site 1258. The differential thickness of the magnetic susceptibility peak may reflect depth-related changes in carbonate preservation or variations in sedimentation rate. All the sites display pronounced cyclicity in physical property measurements and sediment color. Cyclicity is particularly pronounced at Site 1259, where a short period cycle with an ~25- to 30-cm wavelength is modulated by an ~1- to 1.5-m cycle that resembles the modulation of the orbital precession cycle with a period of ~21 k.y. by the 100-k.y. eccentricity cycle. The pervasive cyclicity in physical property records from the lower Eocene offers the possibility not only of refining the chronology of the P/E boundary event, but also cross-checking the results between sites.

Cretaceous/Tertiary Boundary

Compared to the P/E boundary, the lithologic character of the K/T boundary is remarkably consistent at the three sites in which it was recovered (Fig. F9B). At each site, sediments ~0.5 m above and below the boundary have a yellowish brown tinge, but the causal relationship of these colors to the boundary is unclear. The boundary itself occurs within an interval of pelagic sediment with no visible change in depositional style until 0.3 cm below an apparent ejecta layer marking the boundary. This layer is 1.5–2 cm thick and is composed of normally graded, green spherules. Spherules decrease in diameter from ~1 mm at the base to ~0.25 mm at the top; the uniformity of this layer among sites suggests settling of ejecta material without subsequent reworking (i.e., an air fall deposit). The spherule bed sits on a ~3-mm-thick gray fine-grained homogeneous layer, probably composed of Maastrichtian nannofossils. Possible interpretations of this layer include (1) fine material suspended or elutriated by impact shaking, (2) a thin layer of reworking between the time of the impact and the arrival of the first spherules, and (3) a diagenetic artifact related to rapid burial and alteration of the spherules. The spherule bed is overlain by a clay-rich interval containing characteristic earliest Tertiary as well as bloom foraminifers and nannofossils. Carbonate content gradually increases over ~0.5 m, and the basal Danian seems to be expanded, suggesting that details of the paleoceanographic conditions in the earliest Tertiary may be preserved on Demerara Rise.

Black Shales

In contrast to these two event layers, tens of meters of organic-rich laminated sediments (black shale) were recovered at all sites during Leg 207 (Fig. F8). These rocks represent the local equivalent of widespread organic-rich sedimentation in the southern part of the mid-Cretaceous North Atlantic (Kuhnt et al., 1990). They include the globally recorded OAE 2 around the Cenomanian/Turonian boundary.

On Demerara Rise, black shale sedimentation began abruptly in the early Cenomanian and extended into the Campanian. The black shales unconformably overlie Albian shallow-water siliciclastic sediments, including a unit interpreted as a tidal flat deposit. Some of the Albian claystones have a high organic carbon content, but organic matter composition and a lack of lamination distinguishes them clearly from the younger black shales. During the Coniacian, and especially in the Santonian, oceanographic conditions in the region were apparently less stable, as indicated by intercalated glauconitic and bioturbated intervals. Bioturbation affected large intervals of the organic-rich claystones and destroyed the lamination. Furthermore, probable tectonic instability on Demerara Rise lead to widespread mass wasting, resulting in numerous debris flows affecting the Coniacian–Santonian part of the black shale sequence. Sediment clasts of Campanian age in one debris flow indicate mass wasting lasted at least into the Campanian. The lithologic transition from the black shales into the overlying Campanian pelagic deposits at some sites occurs over several meters of glauconite-rich bioturbated claystone. At other sites, it is a sharp contact at the top of a debris flow deposit. The basal Campanian chalks typically contain some glauconite, quartz, and a strong accumulation of zeolite-replaced radiolarians.

The black shales are characterized by the following three facies:

1. Laminated organic-rich claystones with variable carbonate content (5–50 wt%) and up to 30 wt% TOC of marine origin; this facies is particularly well developed in the upper Cenomanian–Turonian part of the black shale interval.

2. Lighter laminated to finely bedded foraminifer wackestone to packstone forms either light–dark cycles with the organic-rich claystones or show a sharp base and a gradual transition (storm deposits?) into overlying sediments.
3. Glauconitic bioturbated intervals that might represent periods of oxygenation. Burrows in the latter extend deeply into the underlying sediment (~1 m). These glauconite-rich intervals can be correlated between holes and eventually also between the shallower sites. No equivalent has been found at the deeper sites.

Throughout the sediment and in particular the organic-rich claystone is characterized by a distinct and sometimes very high content of well-preserved fish debris and phosphatic nodules (~2 cm). These occurrences form either discrete layers/intervals or are scattered in the background sediment. Diagenetic calcite formation is common at the shallower sites. Calcite replaces organic-rich sediment in the form of "beef" or cone-in-cone structures up to several centimeters thick.

Black shale sediments seem to have been deposited in a shallow to moderately deepwater environment. Existing seismic lines do not support a silled basin model but rather an intensified oxygen-minimum layer impinging on Demerara Rise. This interpretation is further supported by occasional glauconite-rich bioturbated intervals at the shallower sites marking the weakening or even retreat of the oxygen minimum zone.

Biostratigraphy

A principal objective of Leg 207 was to recover relatively expanded, shallowly buried Paleogene and Cretaceous sediments that could be used for paleoceanographic study of the tropical Atlantic. Of the five sites drilled, all recovered multiple sequences of Cenomanian and Turonian black shales, Campanian–Maastrichtian chalk, as well as Paleocene, lower Eocene, and middle Eocene chalk. In aggregate, the recovered sections form a continuous record of tropical sedimentation from the late middle Eocene (~38 Ma) to the late Campanian (~76 Ma) and from the Santonian (~83.5 Ma) to the late early Cenomanian (~98 Ma). The oldest sedimentary rocks recovered during Leg 207 are lower and middle Albian claystones (Site 1258), and the youngest are Pliocene–Pleistocene clay-rich nannofossil oozes (Site 1261). At all but one site (1261), the Paleogene was exposed at the seafloor or by <90 m of burial beneath Neogene sedimentary cover.

Neogene or Oligocene calcareous ooze is present at the seafloor at all the Leg 207 sites and consists mostly of winnowed foraminifer sands. The thickest Neogene sequence is present at Site 1261, where 370 m of Pleistocene, Pliocene, and upper Miocene strata is present above chalk of late middle Eocene age. The Neogene section at Site 1261 was spot cored through most of its thickness but appears to comprise an expanded sequence of lower Pliocene and upper Miocene deposits that form a drape over the shallower parts of Demerara Rise shoreward of the Leg 207 drill sites. Elsewhere, drilling encountered lower Miocene and lower Oligocene calcareous ooze below a thin veneer of Pleistocene foraminifer nannofossil ooze. At Site 1259, nearly 125 m of Oligocene and lower Miocene strata is present, but at least the upper 28 m represents a remobilized sequence that was slumped or eroded and redeposited in inverse stratigraphic order. Redeposited lower Oligocene calcareous ooze also is present at Site 1260. The E/O boundary is unconformable or highly condensed at all sites.

There are widespread Paleogene unconformities in the upper Eocene, the lower middle Eocene, and upper Danian (Figs. F10, F11). However, with the exception of the upper Eocene, the other hiatuses are mostly represented by sediment in at least one of the sites. Most notably, the widespread lower Eocene–

middle Eocene hiatus, which is found virtually everywhere in the North Atlantic, is represented by apparently continuous sedimentation at Site 1258. Indeed, recovery at Site 1258 appears to include the most complete lower Eocene section cored by DSDP and ODP in the tropical oceans (Figs. F10, F11). In the Cretaceous, there is a condensed surface or unconformity across the Santonian–lower Campanian and another one between the upper Albian and lower Cenomanian (Figs. F12, F13). Further biostratigraphic work may well recover zonal markers for parts of the lower Campanian in the sequence of glauconitic sands that is present at the contact between the Turonian–Santonian black shales and the upper Campanian chalk. The age of the Albian–Cenomanian unconformity may be diachronous with the oldest Cenomanian section present at Sites 1258 and 1260, whereas Cenomanian sedimentation began slightly later in the late Cenomanian at the other sites.

Preservation of microfossils is highly variable at all Leg 207 sites. Calcareous microfossils are best preserved in parts of the Albian at Site 1258, the black shale sequence, and the Paleocene—all sequences rich in clay. In some cases, particularly in the black shales, foraminifers are preserved with translucent skeletons and primary microstructure. Much of the lower and middle Eocene suffers from extensive reprecipitation and recrystallization of calcite. Siliceous microfossils (mainly radiolarians) are present in parts of the middle Eocene, the lower Eocene, and Campanian and in spots within the black shales and underlying Albian claystone. Middle Eocene siliceous nannofossil chalks at Site 1260 are particularly notable for their expanded sequence of middle Eocene radiolarian zones with excellent preservation.

Paleocene/Eocene Boundary

During Leg 207, we recovered the P/E boundary at all five sites, with a remarkable 10 cores spanning the boundary interval. At all sites, the P/E boundary is represented by dark green clay-rich beds that form a sharp contact with underlying chalk. The chalk below the boundary is frequently well lithified and shows a transition to slightly darker sediment that is often laminated ~1–2 cm below the first dark green clay. The green beds themselves are either massive (e.g., Sites 1257–1259) or display fine laminations (e.g., Sites 1260 and 1261) in the lower parts. Its preservation throughout the depth transect implies nearly equivalent paleowater depths at the time of deposition. Bioturbation gradually returns between 5 (Site 1261) and ~30 cm (Site 1259) above the base of the green bed.

Samples taken from the massive green beds at Sites 1258 and 1259 contain few calcareous foraminifers but common, poorly preserved radiolarians. Calcareous microfossils begin to appear at about the same level that the massive or laminated sequence begins to become bioturbated. The foraminiferal assemblages are characteristic of dissolved faunas, consisting mostly of small benthic foraminifers. However, as preservation improves, a distinct fauna of planktonic foraminifers appears. These species include *M. allisonensis, A. sibaiyensis,* and *A. africana,* all of which have been named the excursion fauna because they have been previously recognized only in the interval of the $\delta^{13}C$ anomaly. Leg 207 sites appear to contain a few additional, as yet unnamed, species of the excursion fauna (e.g., Kelly et al., 1996). In addition, the foraminiferal assemblage from Site 1259 includes a clavate species, *P. paleocenica,* which has thus far been described only from coastal Senegal and the equatorial Pacific (Site 1220). About 2 m above the base of the green beds at Site 1259, the excursion fauna appears to be rare or absent, but several other foraminifer species are present that may be undescribed. These include a nearly biconvex variant of *Morozovella aequa*.

Cretaceous/Tertiary Boundary

Although Demerara Rise is located some 3500 km southeast of and therefore upwind from the Chicxulub impact site, ejecta layers ~1.0–2.0 cm thick were cored at the K/T boundary in six holes at three sites (Fig. F14). This is the first such evidence of the event reported from the South American continent proper.

The ejecta usually rests on a 1- to 2-mm-thick white calcareous layer (Fig. F14) composed of Cretaceous microfossils that were possibly suspended into the water column by the seismic shock of the impact. The ejecta itself is typically laminated, sometimes consisting of sublayers of darker and lighter color with different concentrations of spherules, black or dark to light green in color. These are often graded upward, and individual spherules may range in size from 1 to 3 mm in diameter.

Above the ejecta layer, the dark green boundary clay is relatively soft, low in carbonate, and sometimes drilling disturbed. In the most complete sections (at Sites 1258 and 1259) (Fig. F14), the greenish chalk beneath contains the latest Maastrichtian-age calcareous nannofossils *Micula prinzii* and *Micula murus* along with the corresponding planktonic foraminifers *Abathomphalus mayaroensis* and the rare *Plummerita hantkenoids,* which suggests that the Leg 207 sites preserve an unusually complete record of latest Cretaceous paleoclimate and biotic evolution.

Immediately above the boundary clay, the "disaster forms" *Braarudosphaera* and *Thoracosphaera* are present, but other nannofossils are difficult to extract from the more lithified Danian chalk farther uphole. Instead, planktonic foraminifers provide better age control for the biotic "recovery," beginning with rather small specimens of *P. eugubina* and associated forms that distinguish the basal Tertiary Zone Pα and hence progressing upsection through Subzone P1b or Zone P2 before a disconformity intervenes.

Black Shales

Each of the five sites (Sites 1257–1261) drilled in the course of Leg 207 recovered a sequence of claystones rich in organic matter, referred here to as black shales (Fig. F13). The black shale sequence has been attributed a Cenomanian–earliest Campanian age based on biostratigraphic observations (Fig. F12). Throughout the depth transect covered by the five sites, the thickness of the black shales is relatively consistent (Site 1261: shallow; 89 m; Site 1259: shallow; 56 m; Site 1260: intermediate; 93 m; Site 1257: deep; 57 m; Site 1258: deep; 56 m).

The black shales rest on shallow marine to nonmarine sediments of Albian–earliest Cenomanian age:

Upper Albian–lower Cenomanian: silt–sandstones (Site 1261),
Lower Cenomanian: silt–sandstones (Site 1259),
Lower–middle Albian: claystones (Site 1260),
Upper Albian: siltstones (Site 1257), and
Upper –middle Albian: black shales and claystones (Site 1258).

The black shales rest on shallow marine to non-marine sediments of Albian to earliest Cenomanian age: upper Albian–lower Cenomanian silt–sandstones (Site 1261), lower Cenomanian silt–sandstones (Site 1259), lower – middle Albian claystones (Site 1260), upper Albian siltstones (Site 1257) and upper –middle Albian black shales and claystones (Site 1258). The onset of the black shale sedimentation occurred, except at Site 1258, in the Cenomanian over a period of ~3 m.y. (Fig. F13). Because of the low resolution, poor preservation, and absence of both calcareous nannofossils and planktonic foraminifers in the lower part of the black shale succession at most sites, an accurate age assignment of the basal part is impossible. The

current biostratigraphic data cannot solve the question of whether the onset of the black shales at the various sites is synchronous or diachronous over a period of ~3 m.y. within the Cenomanian. A very dark black shale interval, intercalated in the lower part of the black shale succession of the shallow sites (1259 and 1261) is of late Cenomanian–early Turonian age and may equate the OAE 2.

The top of the black shale succession is diachronous, with ages ranging from latest Turonian (Site 1258) to mid-Coniacian (Site 1260) to late Santonian (Site 1261) to early Campanian (Sites 1257 and 1259). The different ages of the cessation of black shale deposition are partly caused by postdepositional erosion and/or condensation.

Paleomagnetism

Shipboard paleomagnetic measurements of chalks generally indicate a polarity pattern consistent with chrons expected from the biostratigraphy. Chrons C30n through C32r were resolved in Maastrichtian–Campanian clayey chalks at most sites; the upper Paleocene succession at Site 1257 displayed Chrons C24r–C26n, and Chrons C18–C19r were observed in mid-Eocene (upper Lutetian to lower Bartonian) siliceous chalk.

Shipboard assignment of polarity zones within some white to green-gray chalk intervals, especially the lower–middle Eocene (lower Lutetian), was difficult. In this facies, the magnetic intensities after low alternating-field (AF) demagnetization steps approached the background noise level of the pass-through cryogenic magnetometer. In addition, when the color of the lithified clayey chalk was brownish to reddish, such as within the upper–lower Eocene (upper Ypresian) and uppermost Maastrichtian, it was not possible to remove secondary overprints by AF demagnetization. Magnetostratigraphy within similar facies at ODP sites requires progressive thermal demagnetization of minicores in a magnetically shielded room and analysis with a cryogenic magnetometer, having an additional order-of-magnitude sensitivity. Therefore, we collected a large set of oriented minicores for shore-based analyses, which should enable resolution of the full Eocene–Campanian polarity pattern.

An exciting discovery of Leg 207 was ubiquitous cyclic sediments in expanded sections of lower to middle Eocene (55035 Ma) siliceous chalks and in Maastrichtian–upper Campanian (80–65 Ma) clayey chalks at all five sites on Demerara Rise. Both of these time slices lack direct cyclostratigraphic calibration of the magnetic polarity pattern and associated geological time scale. Similar cycle-magnetic tuning of the Paleocene timescale (Chrons C29–C24; ~66–53 Ma) has been accomplished with Leg 171 and other DSDP/ODP sites. Therefore, the array of Leg 207 sites will complete a high-resolution astronomically tuned magnetic polarity timescale spanning the 50 m.y. of the Campanian–Eocene.

Sedimentation and Accumulation Rates

Linear sedimentation rates (LSRs) were derived from age-depth models at each of the Leg 207 sites. At all sites and with current stratigraphic resolution, the sediment sequences can be characterized by continuous but variable rates of sedimentation separated by distinctive hiatuses, condensed intervals, and/or mass flows. Each of the hiatuses comprises, based on biostratigraphic dating, at least 1 m.y.

Linear Sedimentation Rates of Cretaceous Black Shales

The absence of biostratigraphic zonal markers, as well as the extensive normal polarity Superchron C34n, restricted the age assignment in most of the Lower–Upper Cretaceous sequences recovered during Leg 207 (Albian–Santonian). Therefore, LSRs calculated for these intervals should be considered as

imprecise estimates. These intervals include the black shale sequences (Cenomanian–Santonian) that were characterized by LSRs of 3–5 m/m.y. at Sites 1257, 1258, and 1259 and slightly higher values of ~8.5 m/m.y. at Sites 1260 and 1261 (corresponding to 0.3–0.9 cm/k.y. in Fig. F15). In addition, mass accumulation rate (MAR) calculations were limited by the lack of reliable dry bulk density (DBD) data at Sites 1258 and 1259.

Significant Increase in Linear Sedimentation Rates and Mass Accumulation Rates across the Cretaceous/Tertiary Boundary

Average LSRs increased markedly across the K/T boundary interval at all sites (Fig. F15). They were at least 1.5 and up to 2.8 times higher during the Paleogene (Paleocene–Eocene) than rates recorded during the latest Cretaceous (Campanian–Maastrichtian). Highest LSRs are consistently recorded for the Paleocene and Eocene, with no discernible change in LSRs across the P/E boundary interval at all Leg 207 sites (Fig. F15). Late Paleocene and early Eocene LSRs ranged from 7 to 15 m/m.y. (Fig. F15), characteristic for pelagic nannofossil chalk, which is the dominant lithology in this interval. The middle Eocene interval is characterized by a distinct decrease in LSRs from 11 m/m.y. (during the early Eocene) to 3 m/m.y. at Site 1257, whereas a relative increase in LSRs is recorded for the same time interval at Sites 1260 (from 12 to 20.5 m/m.y.) and 1261 (from 7 to 9 m/m.y.) (Fig. F15).

MAR calculations, using the LSRs and average DBD data, allow for a better assessment of sedimentation processes because the influence of compaction has been taken into account. This effect is clearly illustrated at Site 1261, where overburden by Neogene sediments on the Paleogene chalks is greatest and, hence, is reflected in lowest LSRs calculated for the Paleogene sequences on Demerara Rise. However, MARs are comparable to those found at the deeper Site 1257 (Fig. F15).

In contrast at Site 1258, where the change in LSR across the K/T boundary was least pronounced, MARs only increased by 10% during the Paleocene and Eocene, compared to 50% using LSR only (Fig. F15). Nevertheless, the conclusion that sedimentation rates, hiatuses notwithstanding, were higher overall during the Paleogene than during the Late Cretaceous still holds when MARs are considered.

Glimpses of Neogene Sedimentation Rates: Site 1261

Neogene oozes recovered during Leg 207 are too thin relative to sampling density at four of the five sites for a meaningful sedimentation rate to be calculated. In addition, slumping and hiatuses are present in these sequences. At Site 1261, however, the upper 368 m is unique among the five sites cored during Leg 207. The youngest interval is Pleistocene in age, which is separated by a gap of ~3 m.y. from an interval of Pliocene–upper Miocene nannofossil clay and nannofossil ooze. Sedimentation rates in this section are the highest calculated for Demerara Rise (65 m/m.y.) (Fig. F15). This interval of high sedimentation rate sits above a thick (60 m) series of mass flow deposits that occupy a stratigraphic position corresponding to a >30-m.y. gap in pelagic sedimentation.

Cyclostratigraphy

Intervals of complete stratigraphy were recovered by multiple coring, particularly through the middle–upper Eocene and Cenomanian–Campanian (Fig. F16). Rotary coring and moderate recovery prevented sampling complete stratigraphy everywhere, however. Where overlap existed in the Paleocene–lower Eocene (Fig. F17) and Campanian and Maastrichtian (Fig. F18) sequences, magnetic susceptibility was generally the best correlation tool, reflecting varying percentages of carbonate and clay. Within the

Cenomanian–Santonian black shales, GRA bulk density allowed good correlation between holes where organic-rich laminated claystones alternate with more calcareous well-indurated sediments (Fig. F19).

In the lower and middle Eocene, splices were created for Sites 1258, 1259, and 1260 (Fig. F16). At these sites, the splice sections span the P/E boundary. Splices also were constructed that span the K/T boundary at Sites 1259 and 1260, where the boundary is conformable and contains the ejecta layer (Figs. F17, F18). A splice also was generated for Site 1257, where the base of the Paleocene is an unconformity. It was possible to create a splice section that covered the entire Campanian–Maastrichtian succession at Sites 1259 and 1260. For Sites 1259, 1260, and 1261, sampling splices were created that cover all or nearly all of the Cretaceous black shales.

Organic Geochemistry

Cenomanian–Santonian sequences, extraordinarily rich in organic carbon, were recovered at all five sites cored during Leg 207. The finely laminated, dark-colored organic-rich claystones typically contain between 2 and 15 wt% organic carbon, and they range in thickness from 30 m at Site 1258 to 95 m at Sites 1260 and 1261. These thick and extensive black shales are part of the global burial of huge amounts of organic carbon on the seafloor during OAEs 2 and 3.

Organic geochemical properties of the black shales that were measured during Leg 207 reveal aspects of the exceptional conditions of organic matter production and preservation involved in their formation. The results of Rock-Eval pyrolysis show that the bulk of the organic matter originates from algal and microbial primary production (Fig. F20). Extractable biomarker hydrocarbon compositions suggest that relative proportions of algal and microbial contributions of organic matter vary in different parts of the black shale sequences. Hydrocarbon distributions from some parts are dominated by the acyclic tetraterpenoid lycopane, which is indicative of microbial productivity (Brassell et al., 1981). In other parts, the algal C_{15}–C_{19} *n*-alkanes dominate. The presence of both algal and microbial biomarkers suggests that organic matter production was enhanced by a consortium of primary producers. Brassell et al. (1981) postulate expansion of an intensified oxygen minimum zone into the photic zone led to black shale deposition at DSDP Site 144, which was recored as Site 1257 during Leg 207. This paleoenvironment probably permitted the coexistence of algae and the photosynthetic microbes that function best under dysaerobic and anaerobic conditions.

Organic matter is thermally immature, as shown by both the high Rock-Eval hydrogen index and low T_{max} values (Fig. F20) and also by the dominance of nonrearranged steranes. In addition, improved organic matter preservation is implied by $C_{organic}/N_{total}$ ratios that increase to ~40 as organic carbon concentrations increase (Fig. F21). Values above ~20 are usually considered typical of land-plant organic matter, but such elevated ratios are also common to Cretaceous black shales (Meyers, 1997). Consequently, most of the elevated C/N values that mimic those of land-derived organic matter are likely to be the result of retarded, selective alteration of algal and microbial organic matter. A likely scenario is that nitrogen-rich components were more readily degraded than other organic matter components during sinking of organic matter through a strongly developed oxygen minimum zone, thereby elevating the C/N ratio of the surviving organic matter (Twichell et al., 2002).

Contributions of land-derived organic matter are also evident in the black shales. Some of the *n*-alkane distributions of the 10 samples that comprise the biomarker survey are dominated by the C_{29} and C_{31} components diagnostic of land-plant waxes. These hydrocarbon compositions do not indicate a dominance of land-plant organic matter in the black shales, inasmuch as land plants contain larger proportions of hydrocarbons than do algae and microbes (e.g., Meyers, 1997), but they do confirm the

presence of continental plant debris. However, the proportion of land-plant material appears to become important in some of the lower Cenomanian black shales from Site 1260 in which C/N ratios are between 40 and 60 (Fig. F21).

Concentrations of interstitial methane in the sediment sequences at all five Leg 207 sites increase abruptly in the black shales, where they reach their peak values. The possible relation between sediment organic matter contents and gas concentrations was tested by measuring the organic carbon concentrations of the headspace sediment samples at three of the sites. A rough correspondence exists between higher TOC and greater gas concentrations. Marked excursions from a simple linear relation suggest that the type of organic matter, and not simply the amount, affects gas generation from the black shales. Because of the low thermal maturity of organic matter at all five sites (Fig. F20) and the predominance of methane in the interstitial gases, the origin of all the gases is almost certainly from in situ microbial activity. Dramatic decreases in methane concentration at the tops of the black shale boundaries suggest that methane oxidation, which consumes interstitial sulfate, proceeds in overlying units (see "Interstitial Water Geochemistry"). Moreover, active generation of gas must exist to replace the gas that migrates out of this lithologic unit and to maintain the elevated gas concentrations within the black shales.

Interstitial Water Geochemistry

IWs from 152 samples were collected at all five sites cored on Demerara Rise, covering a depth range from the sediment/seawater interface to 648 mbsf. This comparably dense IW sampling program was conducted to understand the impact of relatively deep-seated organic matter–rich black shale sequences on diagenetic processes along the paleoceanographic transect. At all sites (except Site 1261), sulfate and ammonium gradients are essentially linear from the sediment/seawater interface to the top of the black shale sequence (Fig. F22A, F22B). These results indicate the following:

1. Nearly 100 m.y. after deposition, the black shale sequence continues to act as a bioreactor that dominates IW chemistry.
2. Sulfate reduction is of minor importance at shallower depth intervals.
3. The resulting downhole profiles are controlled by the existence of one major stratigraphic sulfate sink and ammonium source (Cretaceous black shales) and simple compensatory diffusion from and/or to the sediment/seawater interface. We interpret the linearity of these profiles to reflect minimal accumulation of sediments younger than middle Eocene age at Sites 1257–1260. Methane diffusing upward from the black shales may furnish metabolic activity above the black shale unit, possibly anaerobic methane oxidation.

Despite the reducing character of the sedimentary column at all Leg 207 sites, only very low IW concentrations of manganese and iron are attained within the black shales (Fig. F22D, 22E). Our favored working hypothesis for this observation is that these redox-sensitive metals were completely remobilized during or shortly after the host organic matter–rich units were deposited, implying conditions of severe synsedimentary oxygen depletion. In contrast, high dissolved barium levels (>300 µM) are attained in the black shales (Fig. F22C), indicating ongoing mobilization of barium where sulfate concentrations are lowest. Uphole diffusion of Ba and downhole diffusion of sulfate from the sediment/water interface give rise to authigenic barite formation in the overlying Campanian to Paleogene sediments (see "Lithostratigraphy").

The other prominent features seen in the Leg 207 IW data set are chloride anomalies (Fig. F22F). At Sites 1257, 1259, and 1261, we see increases in chloride concentration downhole to >60% relative to standard seawater. Based on the depth profiles obtained at Site 1257 (where data are available from significantly below the black shales), we infer that the shales acts as an aquifer for brines at these sites. At Sites 1258 and 1260, we observe relatively low salinity and chloride concentration anomalies between about 300 and 500 mbsf (up to 17% freshening relative to seawater). Low-chlorinity anomalies such as those seen at Site 1258 are not easy to interpret with confidence on the basis of shipboard data alone. The presence of significant concentrations of methane in headspace gas analyses (>50,000 ppmv) (see "Organic Geochemistry") are consistent with the anomalies having been caused by dissociation of gas hydrates. Alternative explanations for the chloride anomalies are clay dehydration reactions and dilution by meteoric water. The former possibility seems unlikely given the lithologies encountered, but the latter possibility cannot be excluded even though the nearest landmass is located ~350–400 km away.

Physical Properties and Downhole Measurements

The main objectives of Leg 207 were the recovery of continuous black shale sequences and critical boundaries such as the K/T, P/E, and E/O and the acquisition of a high-resolution stratigraphy vital to investigating these events. Four of the five sites were logged during Leg 207 (Holes 1257A, 1258C, 1260B, and 1261B). Downhole logging runs included the triple combo tool string with the Multi-Sensor Spectral Gamma Ray Tool (MGT) and the FMS-sonic and WST tool strings, acquiring borehole diameter and wall imagery, formation acoustic velocity, density, porosity, electrical resistivity, natural gamma radiation, and direct acoustic traveltimes. Logging data from Leg 207 show a high degree of correlation with the physical property data, which includes index properties, *P*-wave velocities, GRA densities, and NGR emissions measured on all recovered core samples.

Index property trends, corroborated by the porosity, density, and velocity logs, generally indicate normal consolidation from the surface to the depth of the K/T boundary. Significant perturbations in these profiles are found coincident with the P/E and K/T boundaries as well as various hiatuses. At Sites 1257–1260, acoustic velocity increases linearly with depth until the P/E boundary (Fig. F23). In the interval between the P/E and K/T boundaries, velocity remains about a fixed baseline, varying with cyclical changes in sediment composition and degree of lithification. These variations are well represented in the high-resolution FMS images, MGT gamma ray and porosity logs, and MST GRA densities, all providing an excellent opportunity for cyclostratigraphic analysis. At Site 1261, a 310-m-thick Neogene sequence of normally consolidated clay-rich material overlies a 60-m-thick debris flow and a highly indurated middle Eocene sequence that is unique in character to this particular site (Fig. F23).

Across the K/T and through most of the Cretaceous, all sites show a high degree of similarity in the physical property and downhole logs. Highly lithified Maastrichtian chalks gradationally change to low-velocity, high-porosity calcareous claystones with glauconite-rich horizons at their base. This change is readily tracked in both the downhole MGT natural gamma ray logs and the NGR records from the MST.

Through the black shale intervals, the wireline data have provided a continuous record of the stratigraphy that is readily interpreted in terms of organic-rich, clay-rich intervals interbedded with carbonate-cemented layers. High-resolution MST data through the shales shows excellent agreement with the downhole logs. Coupled with high recovery through these sequences, the generation of a core-log composite stratigraphy at all logged sites should be possible. Figure F24 shows the black shale sequence in Hole 1260B, with the carbonate-cemented layers readily picked out as low gamma ray and porosity and high resistivity (white bands in the FMS images), density, velocity, and photoelectric effect values.

Gamma ray levels through the shales are characteristically high and correlate exceptionally well between the log and MST profiles. All the sites show a distinct two level division within the sequence. Spectral information from the Hostile-Environment Natural Gamma Ray Sonde (HNGS) and MGT suggest that this is mainly a function of uranium content, which may indicate leaching or postdepositional concentration (Fig. F24).

An overall increase in the porosity of the organic-rich claystones tends to be more significant at Sites 1261, 1259, and 1257, where a slight increase in the porosity profile may reflect the existence of excess pore pressures or subtle lithologic variations (Fig. F23).

Seismic Stratigraphy

The seismic stratigraphy for the Demerara Rise study area is characterized by key reflectors (Reflectors O, A, B, B′, and C) were introduced that defined four main seismostratigraphic units (Units 1–4) and one minor unit (Unit Q). A seismic track map with seafloor bathymetry is presented in Figure F2. Within each site chapter, physical property data (in particular, velocity and density) derived from laboratory measurements on core and from downhole logging were used to generate synthetic seismograms. These seismograms were matched to seismic reflection profiles across each site to provide quantitative ties from core and logging results, which are in the depth domain to seismic data that are in the time domain. The results of these ties are summarized in Figure F25. Although these data are presented in each site chapter, there was no attempt to correlate seismic reflection profile data to lithology. Using the information derived from the synthetic seismograms, seismic profiles across each drill site have been depth migrated and matched against the summary lithologic column (Figs. F26, F27, F28, F29, F30). These results permit the seismic profiles to be interpreted with certainty and allow lithologic units to be correlated site to site and regionally across Demerara Rise with confidence.

Reflector C is clearly defined as the base of the black shales, and the underlying sediments of Unit 4 are Albian-age claystone, clayey siltstone, and sandstone. Site 1260 sampled the deepest below Horizon C (40 m). It is uncertain as to whether any of these sediments were truly synrift or whether they represent undeformed shallow water clastic sediments following rifting. Horizon C is presently ~2650 mbsl at Site 1261 (the shallowest site) and dips 0.7° to the north (Fig. F31). At Site 1258 (the deepest site), Horizon C is 3700 mbsl.

The complete sediment sequence from the seafloor to Horizon C is in excess of 1000 m to the south of Site 1261. It gradually thins to the north and rapidly thins near the flanks of the rise. It is ~200 m thick on the upper slope of the flank and then rapidly drops to zero, as the sediment is not sustained on the very steep slopes.

Seismic Unit 3 lies between Reflectors C and B. Horizon B is within seismic Unit 3, and it correlates with the top of the black shale sequence (lithologic Unit IV) at each site, except Site 1259. At this location, it correlates slightly above Unit IV, probably due to an expanded gradational sequence of organic-rich glauconitic claystone above the black shales. The top of seismic Unit 3 is Reflector B, a regional high-amplitude reflector that correlates with the K/T boundary at every site. This surface dips rather uniformly at ~1° to the northwest. The thickness of Unit 3 is locally variable but, in general, increases from ~120 m in the south (Site 1261) to >300 m thick in the northwest between Sites 1258 and 1260.

Seismic Unit 2 lies between Reflectors B and A. Horizon A correlates everywhere to the top of lithologic Unit II, a variable nannofossil chalk sequence that is mostly Eocene in age but possibly as young as early Miocene. Reflector A is believed to result from an episode of extensive erosion during the early Miocene. The surface of Reflector A dips toward the northwest and is ~2100 mbsl at Site 1261 and 3200 mbsl at Site

1258. This surface appears to be channelized, but seismic line density is insufficient to discern details. Unit 2 is highly variable in thickness as a result of differential amounts of erosion but, in general, thins toward the northwest. At Site 1260, for example, the seismic unit is 180 m thick, whereas at Site 1259 it is 400 m thick.

Reflector A forms the base of seismic Unit 1. Its top is typically the seafloor because Reflector O and seismic Unit Q are rarely present. Unit 1 correlates with unlithified or semilithified sediment, such as the 300-m-thick succession of Miocene–Pliocene nannofossil clay at Site 1261. The unit is absent at other sites. Seismic lines show that its thickness is highly variable because its lower bounding surface is Reflector A. Its maximum thickness is >350 m, and it thins toward the west and northwest.

Seismic Unit Q rarely is resolved on seismic reflection profiles, but at Site 1261, it is nearly 30 m thick (Fig. F30). At this location, Reflector O correlates with the base of lithologic Subunit IA, a Pleistocene nannofossil ooze. Reflector O represents an unconformity, separating Pleistocene and younger sediment from the middle Miocene. Reflections within Unit 1 sometimes truncate against Reflector O.

In summary, strong physical property contrasts in lithologic units, as described from Leg 207 drilling results on Demerara Rise, translate to excellent correlation with seismic units and even with some single-reflection events. Depth-migrated seismic reflection profiles consistently match summary lithologic columns as a result. Seismic reflection data can be used to confidently correlate from site to site and across the Demerara Rise study area.

Cretaceous–Neogene Depositional History of Demerara Rise

The stratigraphy of sites cored along the depth transect during Leg 207 were integrated to interpret the mid-Cretaceous (Albian) to Neogene history of Demerara Rise. This history reflects multiple depositional episodes during the late rifting and drifting stage of a continental margin that saw different sedimentological regimes separated by several hiatuses of varying duration. Transform movements related to the opening of the equatorial Atlantic gateway are believed to have influenced the sedimentary history during the Cenomanian–Campanian stages.

The oldest sediments recovered during Leg 207 are early Albian in age. At the deepest site of the depth transect (Site 1258), they are represented by organic carbon–rich claystones with phosphatic pebbles. Ammonites and microfossils recovered from this interval indicate open marine conditions in a probable epicontinental basin. Upslope (at Site 1260), an increase of siliciclastic detritus indicates a sedimentary environment closer to the sediment source. Probable tidal flat deposits of unknown age (Albian?), which were deposited in a marginal marine setting, represent the oldest sequence recovered at the shallow end of the transect (Site 1259). These deposits suggest that Demerara Rise was a submarine high separated from South America by a shallow marine epicontinental basin as early Cretaceous shallow-water carbonates and Aptian–Albian open marine marls have been recovered in industry wells farther south.

Shallow-water environments are also indicated by marine quartz sandstone with occasional ammonite casts and shell debris recovered at the shallow sites (Sites 1261 and 1259) and at Site 1257, where they unconformably overly middle to upper Albian open marine clays. These sandstones are late Albian to upper Cenomanian in age.

Black shale deposition at Demerara Rise started in the middle Albian at the deep end of the transect. At this location, they are overlain by a lower–middle Cenomanian sequence of storm-induced layers intercalated within black shales, which might be laterally equivalent to the quartz sandstone upslope. No upper Albian sediments have been identified. Elsewhere, middle–late Cenomanian black shales overlie a

prominent unconformity that separates them from the underlying Albian–lower Cenomanian clays and sandstones, which represent the synrift deposits on Demerara Rise.

Cyclic successions of middle–upper Cenomanian organic matter–rich black shale with abundant phosphatic pebbles and fish remains and laminated foraminiferal packstone are believed to represent the first shallow hemipelagic sediments on Demerara Rise. They reflect high surface water productivity and dysoxic bottom water conditions. The thickness of the Cenomanian sequence on Demerara Rise changes greatly (8–80 m). This may be the result of either varying subsidence histories of different small slope basins or the middle–early Turonian sea level rise and the consequent transgressive onlap. However, the onset of black shale deposition at the shallow sites dates late Cenomanian. There, very dark TOC-rich shales yield very reduced planktonic faunas and calcareous nannoplankton of the genus *Ephrolitus,* which indicate a very shallow marine to lagoonal setting.

High-productivity conditions, probably related to local upwelling, continued until the Coniacian with most extreme conditions during the OAE 2. Clayey bentonite layers indicate the proximity of volcanoes. Occasional glauconite-rich horizons are interpreted as either an oxygenation event or resulting from reduced sedimentation rates or both. Debris flow deposits, slumped intervals, and condensed horizons in the upper Turonian–lower Campanian indicate the position of the Leg 207 sites at a steeper slope and with turbulent sedimentary conditions. Black shale deposition on Demerara Rise ends in the Santonian–early Campanian.

No middle–late early Campanian-age sediments have been recovered, and the upper Campanian yields glauconite-rich horizons indicating reduced sedimentation rates. It is believed that the cessation of black shale sedimentation, very reduced deposition, rates, and hiatuses are related to oceanographic modifications and transform motions following the opening of the equatorial Atlantic gateway. Oxic conditions were established by the late Campanian, when sedimentation on Demerara Rise changed from hemipelagic to pelagic. The abundance of radiolarians in the Campanian, however, indicates increased surface water productivity. The cyclic pattern of trace fossil abundance suggests recurrence of a reduction in bottom water oxygenation.

Maastrichtian–Oligocene-age sediments at Demerara Rise consist of pelagic deep marine nannofossil and foraminiferal chalks and oozes deposited in an upper bathyal setting. The succession records the lithologic consequences of the K/T boundary impact and the abrupt global warming associated with the P/E boundary. The high abundance of radiolarians in middle Eocene sediments is related to upwelling conditions. Because of a major erosional event in the early Miocene, Oligocene sediments on Demerara Rise are often reworked or reduced in thickness.

The presence of Neogene sediments on the slopes of Demerara Rise is rather patchy. As a probable result of Amazon plumes, upper Miocene- to Pliocene-age sediments are clay rich and sedimentation rates can be very high (Site 1261). However, no upper Pliocene and only very thin veneers of Pleistocene and Holocene clay-rich sediments are present.

REFERENCES

Adams, C.G., Lee, D.E., and Rosen, B.R., 1990. Conflicting isotopic and biotic evidence for tropical sea-surface temperatures during the Tertiary. *Palaeogeogr., Palaeoclimatol., Palaeoecol.,* 77:289–313.

Arthur, M.A., Brumsack, H.-J., Jenkyns, H.C., and Schlanger, S.O., 1990. Stratigraphy, geochemistry, and paleoceanography of organic carbon-rich Cretaceous sequences. *In* Ginsburg, R.N., and Beaudoin, B. (Eds.), *Cretaceous Resources, Events and Rhythms:* Dordrecht (Kluwer), 75–119.

Arthur, M.A., Dean, W.E., and Pratt, L.M., 1988. Geochemical and climatic effects of increased marine organic carbon burial at the Cenomanian/Turonian boundary. *Nature,* 335:714–717.

Arthur, M.A., Dean, W.E., Schlanger, S.O., 1985. Variations in the global carbon cycle during the Cretaceous related to climate, volcanism, and changes in atmospheric CO_2. *In* Sundquist, E.T., and Broecker, W.S. (Eds.), *The Carbon Cycle and Atmospheric CO_2: Natural Variations Archean to Present.* Geophys. Monogr., Am. Geophys. Union, 32:504–529.

Arthur, M.A., and Natland, J.H., 1979. Carbonaceous sediments in the North and South Atlantic: the role of salinity in stable stratification of Early Cretaceous basins. *In* Talwani, M., Hay, W., and Ryan, W.B.F. (Eds.), *Deep Drilling Results in the Atlantic Ocean: Continental Margins and Paleoenvironment.* Geophys. Monogr., Maurice Ewing Ser., Am. Geophys. Union, 3:375–401.

Aubry, M.-P., 1998. Early Palaeogene calcareous nannoplankton evolution: a tale of climatic amelioration. *In* Aubry, M.P., Lucas, S., and Berggren, W.A. (Eds.), *Late Paleocene–Early Eocene Climatic and Biotic Events in the Marine and Terrestrial Records:* New York (Columbia Univ. Press), 158–203.

Bains, S., Corfield, R.M., and Norris, R.D., 1999. Mechanisms of climate warming at the end of the Paleocene. *Science,* 285:724–727.

Barrera, E., 1994. Global environmental changes preceding the Cretaceous-Tertiary boundary: early-late Maastrichtian transition. *Geology,* 22:877–880.

Barrera, E., and Savin, S.M., 1999. Evolution of Campanian–Maastrichtian marine climates and oceans. *In* Barrera, E., and Johnson, C.C. (Eds.), *Evolution of the Cretaceous Ocean-Climate System,* Geol. Soc. Amer. Special Paper, 332:245–282.

Barron, E.J., 1995. Tropical climate stability and implications for the distribution of life. *In* Stanley, S.M. (Ed.), *Effects of Past Global Change on Life:* Washington, D.C. (National Academy Press), 108–117.

Benkhelil, J., Mascle, J., and Tricart, P., 1995. The Guinea continental margin: an example of a structurally complex transform margin. *Tectonophysics,* 248:117–137.

Berner, R.A., 1994. GEOCARB II: a revised model of atms. CO_2 over Phanerozoic time. *Am. J. Sci.,* 294:56–91.

Bice, K.L., and Marotzke, J., 2001. Numerical evidence against reversed thermohaline circulation in the warm Paleocene/Eocene ocean. *J. Geophys. Res.,* 106:11529–11542.

Bice, K. L., B. T. Huber, and R. D. Norris, in press. Extreme polar warmth during the Cretaceous greenhouse? The paradox of the Late Turonian Record at DSDP Site 511. *Paleoceanography.*

Bralower, T.J., Arthur, M.A., Leckie, R.M., Sliter, W.V., Allard, D.J., and Schlanger, S.O., 1994. Timing and paleoceanography of oceanic dysoxia/anoxia in the Late Barremian to Early Aptian. *Palaios,* 9:335–369.

Bralower, T.J., Fullagar, P.D., Paull, C.K., Dwyer, G.S., and Leckie, R.M., 1997. Mid-Cretaceous strontium-isotope stratigraphy of deep-sea sections. *Geol. Soc. Am. Bull.,* 109:1421–1442.

Brassell, S.C., Wardroper, A.M.K., Thomson, I.D., Maxwell, J.R., and Eglinton, G., 1981. Specific acyclic isoprenoids as biological markers of methanogenic bacteria in marine sediments. *Nature,* 290:693–696.

Brumsack, H.-J., 1980. Geochemistry of Cretaceous black shales from the Atlantic Ocean (DSDP Legs 11, 14, 36 and 41). *Chem. Geol.,* 31:1–25.

Brumsack, H.-J., and Lew, M, 1982. Inorganic geochemistry of Atlantic Ocean sediments with special reference to Cretaceous black shales. *In* von Rad, U., Hinz, K., Sarnthein, M., Seibold, E. (Eds.), *Geology of the Northwest African Continental Margin:* Berlin (Springer-Verlag), 661–685.

Bush, A.B.G., and Philander, S.G.H., 1997. The Late Cretaceous: simulation with a coupled atmosphere-ocean general circulation model. *Paleoceanography,* 12:495–516.

Caron, M., and Homewood, P., 1983. Evolution of early planktic foraminifers. *Mar. Micropaleontol.,* 7:453–462.

Clarke, L.J., and Jenkyns, H.C., 1999. New oxygen isotope evidence for long-term Cretaceous climatic change in the Southern Hemisphere. *Geology,* 27:699–702.

Crowley, T., 1991. Past CO_2 changes and tropical sea surface temperatures. *Paleoceanography,* 6:387–394.

Crowley, T.J., and North, G.R., 1991. *Paleoclimatology: Oxford Monographs on Geology and Geophysics:* New York (Oxford Univ. Press).

D'Hondt, S., and Arthur, M.A., 1996. Late Cretaceous oceans and the cool tropic paradox. *Science,* 271:1838–1841.

D'Hondt, S., Donaghay, P., Zachos, J.C., Luttenberg, D., and Lindinger, M., 1998. Organic carbon fluxes and ecological recovery from the Cretaceous-Tertiary mass extinction. *Science,* 282:276–279.

Dickens, G.R., O'Neil, J.R., Rea, D.K., and Owen, R.M., 1995. Dissociation of oceanic methane hydrate as a cause of the carbon isotope excursion at the end of the Paleocene. *Paleoceanography,* 10:965–971.

Douglas, R.G., and Savin, S.M., 1975. Oxygen and carbon isotope analyses of Tertiary and Cretaceous microfossils from Shatsky Rise and other sites in the North Pacific Ocean. *In* Larson, R.L., Moberly, R., et al., *Init. Repts. DSDP,* 32: Washington (U.S. Govt. Printing Office), 509–520.

Erba, E., 1994. Nannofossils and superplumes: the early Aptian "nannoconids crisis." *Paleoceanography,* 9:483–501.

Erba, E., Bartolini, A.C., Channel, J.E.T., Larson, R.L., Opdyke, B.N., Premoli Silva, I., Salvini, G., and Torricelli, S., 1999. An integrated stratigraphy of the Cismon

APTICORE (Southern Alps, Italy): a reference section for the Hauterivian–Aptian interval at low latitudes. *European Union of Geosciences 10: 28th March–1st April 1999, Strasbourg, France:* Cambridge (Cambridge Publications), 221. (Abstract).

Erbacher, J., Huber, B.T., Norris, R.D., and Markey, M., 2001. Intensified thermohaline stratification as a possible cause for an ocean anoxic event in the Cretaceous period. *Nature,* 409:325–327.

Erbacher, J., and Thurow, J., 1997. Influence of oceanic anoxic events on the evolution of mid-Cretaceous radiolaria in the North Atlantic and western Tethys. *Mar. Micropalaeontol.,* 30:139–158.

Erbacher, J., Thurow, J., and Littke, R., 1996. Evolution patterns of radiolaria and organic matter variations: a new approach to identify sea-level changes in mid-Cretaceous pelagic environments. *Geology,* 24:499–502.

Förster, R., 1978. Evidence for an open seaway between northern and southern proto-Atlantic in Albian times. *Nature,* 272:158–159.

Fox, P.J., Schreiber, E., and Peterson, J., 1972. Compressional wave velocities in basalt. *In* Hayes, D.E., Pimm, A.C., et al., *Init. Repts. DSDP,* 14: Washington (U.S. Govt. Printing Office), 773–776.

Frank, T.D., and Arthur, M.A., 1999. Tectonic forcings of Maastrichtian ocean-climate evolution. *Paleoceanography,* 14:103–117.

Gale, A.S., Hardenbol, J., Hathaway, B., Kennedy, W.J., Young, J.R., and Phansalkar, V., 2002. Global correlation of Cenomanian (Upper Cretaceous) sequences: evidence for Milankovitch control on sea level. *Geology,* 30:291–294.

Gouyet, S., Unternehr, P., and Mascle, A., 1994. The French Guyana margin and the Demerara Plateau: geologic history and petroleum plays. *In* Mascle, A. (Ed.), *Hydrocarbon and Petroleum Geology of France*. Spec. Publ.—Eur. Assoc. Pet. Geosci., 4:411–422.

Handoh, I.C., Bigg, G.R., Jones, E.J.W., Inoue, M., 1999. An ocean modeling study of the Cenomanian Atlantic: equatorial paleo-upwelling, organic-rich sediments and the consequences for a connection between the proto-North and South Atlantic. *Geophys. Res. Lett.,* 26:223–226.

Hart, M.B., 1980. A water depth model for the evolution of the planktonic Foraminiferida. *Nature,* 286:252–254.

Herbert, T.D., and Fischer, A.G., 1986. Milankovitch climatic origin of mid-Cretaceous black shale rhythms in central Italy. *Nature,* 321:739–743.

Huber, B.T., Hodell, D.A., and Hamilton, C.P., 1995. Mid- to Late Cretaceous climate of the southern high latitudes: stable isotopic evidence for minimal equator-to-pole thermal gradients. *Geol. Soc. Am. Bull.,* 107:1164–1191.

Jahren, A.H., Arens, N.C., Sarmiento, G., Guerrero, J., and Amundson, R., 2001. Terrestrial record of methane hydrate dissociation in the Early Cretaceous. *Geology,* 29:159–162.

Jenkyns, H.C., 1980. Cretaceous anoxic events: from continents to oceans. *J. Geol. Soc. London,* 137:171–188.

Jenkyns, H.C., Gale, A.S., and Corfield, R.M., 1994. Carbon- and oxygen-isotope stratigraphy of the English Chalk and Italian Scaglia and its palaeoclimatic significance. *Geol. Mag.,* 131:1–34.

Jenkyns, H.C., and Wilson, P.A., 1999. Stratigraphy, palaeoceanography and evolution of Cretaceous Pacific guyots: relics from a greenhouse Earth. *Am. J. Sci.,* 299:341–392.

Jones, C.E., and Jenkyns, H.C., 2001. Seawater strontium isotopes, oceanic anoxic events, and seafloor hydrothermal activity in the Jurassic and Cretaceous, *Amer. J. Sci.,* 301:112–149.

Jones, C.E., Jenkyns, H.C., Coe, A.L., and Hesselbo, S.P., 1994. Strontium isotopic variations in Jurassic and Cretaceous seawater. *Geochim. Cosmochim. Acta.,* 58:3063–3074.

Kaiho, K., and Hasegawa, T., 1994. End-Cenomanian benthic foraminiferal extinctions and oceanic dysoxic events in the northwestern Pacific Ocean. *Palaeogeogr., Palaeoclimatol., Palaeoecol.,* 111:29–43.

Kelly, D.C., Bralower, T.J., Zachos, J.C., Premoli Silva, I., and Thomas, E., 1996. Rapid diversification of planktonic foraminifera in the tropical Pacific (ODP Site 865) during the late Paleocene thermal maximum. *Geology,* 24:423–426.

Kerr, A.C., 1998. Oceanic plateau formation: a cause of mass extinction and black shale deposition around the Cenomanian-Turonian boundary? *J. Geol. Soc. London,* 155:619–626.

Killingley, J.S., 1983. Effects of diagenetic recrystallization on $^{18}O/^{16}O$ values of deep-sea sediments. *Nature,* 301:594–597.

Koch, P.L., Zachos, J.C., Dettman, D.L., 1995. Stable isotope stratigraphy and palaeoclimatology of the Palaeogene Bighorn Basin. *Palaeogeogr., Palaeoclimatol., Palaeoecol.,* 115:61–89.

Kuhnt, W., Chellai, E.H., Holbourn, A., Luderer, F., Thurow, J., Wagner, T., El Albani, A., Beckmann, B., Herbin, J.-P., Kawamura, H., Kolonic, S., Nederbraght, S., Street, C., and Ravilious, K., 2001. Morocco Basin's sedimentary record may provide correlations for Cretaceous paleoceanographic events worldwide. *Eos, Trans., Am. Geophys. Union,* 82:361–364.

Kuhnt, W., Herbin, J.P., Thurow, J., and Wiedmann, J., 1990. Distribution of Cenomanian-Turonian organic facies in the western Mediterranean and along the adjacent Atlantic margin. *In* Huc, A.Y. (Ed.), *Deposition of Organic Facies*. AAPG Stud. Geol., 30:133–160.

Kump, L.R., 2002. Reducing uncertainty about carbon dioxide as a climate driver. *Nature,* 419:188–190.

Kump, L.R., and Arthur, M.A., 1999. Interpreting carbon-isotope excursions: carbonates and organic matter. *Chem. Geo.,* 161:181–198.

Kuypers, M.M.M., Blokker, P., Erbacher, J., Kinkel, H., Pancost, R.D., Schouten, S., Sinninghe Damsté, J.S., 2001. Massive expansion of marine archaea during a mid-Cretaceous oceanic anoxic event. *Science,* 293:92–94.

Kuypers, M.M.M., Pancost, R.D., and Damste, J.S.S., 1999. A large and abrupt fall in atmospheric CO_2 concentration during Cretaceous times. *Nature,* 399:342–345.

Kuypers, M.M.M., Pancost, R.D., Nijenhuis, I.A., and Sinninghe Damsté, J.S., 2002. Enhanced productivity led to increased organic carbon burial in the euxinic North Atlantic basin during the late Cenomanian oceanic anoxic event. *Paleoceanography,* 17:10.1029/222PA000569.

Larson, R.L., 1991. The latest pulse of Earth: evidence for a mid-Cretaceous superplume. *Geology,* 19:547–550.

Larson, R.L., and Erba, E., 1999. Onset of the Mid-Cretaceous greenhouse in the Barremian–Aptian: igneous events and the biological, sedimentary and geochemical responses. *Paleoceanography,* 14:663–678.

Lear, C.H., Wilson, P.A., and Elderfield, H., 2000. Palaeotemperature and ocean chemistry records for the early Palaeogene from Mg/Ca and Sr/Ca in benthic foraminiferal calcite. *GFF,* 122:93.

Leckie, R.M., 1987. Paleoecology of mid-Cretaceous planktonic foraminifera: a comparison of open ocean and epicontinental sea assemblages. *Micropaleontology,* 33:164–176.

————, 1989. A paleoceanographic model for the early evolutionary history of planktonic foraminifera. *Palaeogeogr., Palaeoclimatol., Palaeoecol.,* 73:107–138.

Leckie, R.M., Bralower, T.J., and Cashman, R., 2002. Oceanic anoxic events and plankton evolution: biotic response to tectonic forcing during the Mid-Cretaceous. *Paleoceanography,* 17:10.1029/2001PA000623.

Macleod, K.G., and Huber, B.T., 2001. The Maastrichtian record at Blake Nose (western North Atlantic) and implications for global palaeoceanographic and biotic changes. *In* Kroon, D., Norris, R.D., and Klaus, A. (Eds.), *Western North Atlantic Paleogene and Cretaceous Paleoceanography.* Spec. Publ.—Geol. Soc. London, 183:111–130.

Manabe, S., and Bryan, K., 1985. CO_2-induced change in a coupled ocean-atmosphere model and its paleoclimatic implications. *J. Geophys. Res.,* 90:11689–11708.

Menegatti, A.P., Weissert, H., Brown, R.S., Tyson, R.V., Farrimond, P., Strasser, A., and Caron, M., 1998. High resolution $\delta^{13}C$ stratigraphy through the early Aptian "Livello Selli" of the Alpine Tethys. *Paleoceanography,* 13:530–545.

Meyers, P.A., 1997. Organic geochemical proxies of paleoceanographic, paleolimnologic, and paleoclimatic processes. *Org. Geochem.,* 27:213–250.

Moullade, M., and Guérin, S., 1982. Le problème des relations de l'Atlantique Sud et de l'Atlantique Central au Crétacé moyen: nouvelles données microfauniques d'après les forages D.S.D.P. *Bull. Soc. Geol. Fr.,* 24:511–517.

Moullade, M., Mascle, J., Benkhelil, J., Cousin, M., and Tricart, P., 1993. Occurrence of marine mid-Cretaceous sediments along the Guinean slope (*Equamarge II* cruise): their significance for the evolution of the central Atlantic African margin. *Mar. Geol.,* 110:63–72.

Norris, R.D., Bice, K.L., Magno, E.A., and Wilson, P.A., 2002. Jiggling the tropical thermostat in the Cretaceous hothouse. *Geology,* 30:299–302.

Norris, R.D., and Röhl, U., 1999. Carbon cycling and chronology of climate warming during the Palaeocene/Eocene transition. *Nature,* 401:775–778.

Norris, R.D., and Wilson, P.A., 1998. Low-latitude sea-surface temperatures for the mid-Cretaceous and the evolution of planktic foraminifera. *Geology,* 26:823–826.

Ohkouchi, N., Kawamura, K., Kajiwara, Y., Wada, E., Okada, M., Kanamatsu, T., Taira, A., 1999. Sulfur isotopes records around Livello Bonarelli (Northern Apennines, Italy) black shale at Cenomanian-Turnonian boundary. *Geology,* 27, 535-538.

Otto-Bliesner, B.L., Brady, E.C. and Shields, C, 2002. Late Cretaceous ocean: coupled simulations with the national center for atmospheric research climate system model art. *J. Geophys. Res.,* 107:4019.

Pearson, P.N., Ditchfield, P.W., Singano, J., Harcourt-Brown, K.G., Nicholas, C.J., Olsson, R.K., Shackleton, N.J., and Hall, M.A., 2001. Warm tropical sea surface temperatures in the Late Cretaceous and Eocene epochs. *Nature,* 413:481–487.

Pearson, P.N., and Shackleton, N.J., 1995. Neogene multispecies planktonic foraminifer stable isotope record, Site 871, Limalok Guyot. *In* Haggerty, J.A., Premoli Silva, I., Rack, F., and McNutt, M.K. (Eds.), *Proc. ODP, Sci. Results,* 144: College Station, TX (Ocean Drilling Program), 401–410.

Poulsen, C.J., Barron, E.J., and Wilson, P.A., 1999. A re-interpretation of mid-Cretaceous shallow-marine temperatures through model-data comparison. *Paleoceanography,* 14:679–697.

Premoli Silva, I., Erba, E., and Salvini, G., 1999. Biotic changes in Cretaceous oceanic anoxic events. *European Union of Geosciences 10: 28th March–1st April 1999, Strasbourg, France:* Cambridge (Cambridge Publications), 220. (Abstract).

Schlanger, S.O., Arthur, M.A., Jenkyns, H.C., and Scholle, P.A., 1987. The Cenomanian-Turonian oceanic anoxic event, I. Stratigraphy and distribution of organic carbon-rich beds and the marine $\delta^{13}C$ excursion. *In* Brooks, J., and Fleet, A.J. (Eds.), *Marine Petroleum Source Rocks*. Spec. Publ.—Geol. Soc. London, 26:371–399.

Schlanger, S.O., and Jenkyns, H.C., 1976. Cretaceous oceanic anoxic events: causes and consequences. *Geol. Mijnbouw,* 55:179–184.

Schlanger, S.O., Jenkyns, H.C., and Premoli-Silva, I., 1981. Volcanism and vertical tectonics in the Pacific Basin related to global Cretaceous transgressions. *Earth Planet. Sci. Lett.,* 52:435–449.

Scholle, P.A., and Arthur, M.A., 1980. Carbon isotope fluctuations in Cretaceous pelagic limestones: potential stratigraphic and petroleum exploration tool. *AAPG Bull.,* 64:67–87.

Schrag, D.P., DePaolo, D.J., and Richter, F.M., 1995. Reconstructing past sea surface temperatures: correcting for diagenesis of bulk marine carbonate. Geochim. Cosmochim. Acta, 59:2265–2278.

Sepkoski, J.J., 1986. Phanerozoic overview of mass extinction. *In* Raup, D., and Jablonski, D. (Eds.), *Patterns and Processes in the History of Life:* Berlin (Springer-Verlag), 277–295.

Shackleton, N.J., 1984. Oxygen isotope evidence for Cenozoic climatic cooling. *In* Brenchley, P.J. (Ed.), *Fossils and Climate:* Chichester (Wiley), 27–34.

Shouten, S., Hopmans, E.C., Schefuss, E., Sinninghe Damsté, J.S., 2002. Distributional variations in marine crenarchaeotal membrane lipids: a new tool for reconstructing ancient sea water temperatures? *Earth Planet Sci. Lett.,* 204:265–274.

Sinninghe Damsté, J.S., and Koester, J., 1998. A euxinic southern North Atlantic Ocean during the Cenomanian/Turonian oceanic anoxic event. *Earth Planet. Sci. Lett.,* 158:165–173.

Sinton, C.W., and Duncan, R.A., 1997. Potential links between ocean plateau volcanism and global ocean anoxia at the Cen/Tur boundary. *Econ. Geol.,* 92:836–842.

Stanley, S.M., 1984. Temperature and biotic crises in the marine realm. *Geology,* 12:205–208.

Stoll, H., and Schrag, D.P., 2000. High resolution stable isotope records from the upper Cretaceous of Italy and Spain: glacial episodes in a greenhouse planer? *Geol. Soc. Am. Bull.,* 112:308–319.

Thomas, E., 1998. Biogeography of the late Paleocene benthic foraminiferal extinction. *In* Aubry, M.-P., Lucas, S.G., and Berggren, W.A. (Eds.), *Late Paleocene-Early Eocene: Climatic and Biotic Events in the Marine and Terrestrial Records:* New York (Columbia Univ. Press), 214–235.

Thomas, E., and Zachos, J.C., 1999. Was the LPTM a unique event? *In* Schmitz, B., Sundquist, B., and Andreasson, F.P. (Eds.), *Early Paleogene Warm Climates and Biosphere Dynamics*. Geol. Soc. Sweden, 122:169–170.

Thurow, J., Brumsack, H.-J., Rullkötter, J., Littke, R., and Meyers, P., 1992. The Cenomanian/Turonian boundary event in the Indian Ocean—a key to understand the global picture. *In* Duncan, R.A., Rea, D.K., Kidd, R.B., von Rad, U., and Weissel, J.K. (Eds.), *Synthesis of Results from Scientific Drilling in the Indian Ocean.* Geophys. Monogr., Am. Geophys. Union, 70:253–273.

Twichell, S.C., Meyers, P.A., and Diester-Haass, L., 2002. Significance of high C/N ratios in organic-carbon-rich Neogene sediments under the Benguela Current upwelling system. *Org. Geochem.,* 33:715–722.

Wagner, T., and Pletsch, T., 1999. Tectono-sedimentary controls on Cretaceous black shale deposition along the opening Equatorial Atlantic Gateway (ODP Leg 159). *In* Cameron, N., Bate, R., and Clure, V. (Eds.), *The Oil and Gas Habitat of the South Atlantic*. Geol. Soc. Lon. Spec. Publ., 153:241–265.

Weissert, H., Lini, A., Föllmi, K.B., and Kuhn, O., 1998. Correlation of early Cretaceous carbon isotope stratigraphy and platform drowning events: a possible link? *Palaeogeogr., Palaeoclimatol., Palaeoecol.,* 137:189–203.

Wiedmann, J., and Neugebauer, J., 1978. Lower Cretaceous ammonites from the South Atlantic Leg 40 (DSDP), their stratigraphic value and sedimentologic properties. *In* Bolli, H.M., Ryan, W.B.F., et al., *Init. Repts. DSDP,* 40: Washington (U.S. Govt. Printing Office), 709–734.

Wilson, P.A., Jenkyns, H.C., Elderfield, H., and Larson, R.L., 1998. The paradox of drowned carbonate platforms and the origin of Cretaceous guyots. *Nature,* 392:889–894.

Wilson, P.A., and Norris, R.D., 2001. Warm tropical ocean surface and global anoxia during the mid-Cretaceous period. *Nature,* 412:425–429.

Wilson, P.A., Norris, R.D., and Cooper, M.J., 2002. Testing the Cretaceous greenhouse hypothesis using glassy foraminiferal calcite from the core of Turonian tropics on Demerara Rise. *Geology,* 30:607–610.

Wilson, P.A., and Opdyke, B.N., 1996. Equatorial sea-surface temperatures for the Maastrichtian revealed through remarkable preservation of metastable carbonate. *Geology,* 24:555–558.

Zachos, J.C., Lohmann, K.C., Walker, J.C.G., and Wise, S.W., Jr., 1993. Abrupt climate changes and transient climates during the Paleogene: a marine perspective. *J. Geol.,* 101:191–213.

Zachos, J.C., Pagani, M., Sloan, L., Thomas, E. and Billups, K., 2001. Trends, rhythms, and aberrations in global climate 65 Ma to present. *Science,* 292:686–693.

TABLE CAPTION

Table T1. Leg 207 operations summary.

FIGURE CAPTIONS

Figure F1. Regional location map. The boxed area represents the approximate Leg 207 operational area on Demerara Rise, which is shown in detail on Figure F2.

Figure F2. Seismic survey track lines over bathymetry. The bathymetry was compiled from the seafloor pick of the seismic data.

Figure F3. Global paleogeographic reconstruction of the Late Cretaceous, showing the position of Demerara Rise in the early South Atlantic.

Figure F4. Stratigraphy of industry well A2-1 in relation to multichannel seismic (MSC) line SU7657A. TD = total depth.

Figure F5. Summary of major geochemical, tectonic, sea level, and plankton evolutionary events associated with mid-Cretaceous oceanic anoxic events (OAEs) (from Leckie et al., 2002). Planktic = planktonic, Foram = foraminifer, Biostrat = biostratigraphy.

Figure F6. Comparison of Cretaceous $\delta^{18}O$-temperature records indicate a 20- to 40-m.y. mismatch between peak Cretaceous–Cenozoic warmth and peak Cretaceous–Cenozoic tectonic CO_2 production inferred from ocean crust cycling (after Wilson et al., 2002). Open symbols = "glassy" foraminifers from the low-latitude western Atlantic, Gulf Coast, and Tanzania. Solid symbols = bulk carbonate from the high-latitude southern Indian Ocean. All temperatures are conservative values calculated assuming δw = mean Cretaceous seawater and would be 3°–6°C higher if modern latitudinal trends in δw were applied. VPDB = Vienna Peedee belemnite.

Figure F7. Cenozoic events in climate, tectonics, and biota vs. $\delta^{18}O$ and $\delta^{13}O$ in benthic foraminiferal calcite (after Zachos et al., 2001). VPDB = Vienna Peedee belemnite.

Figure F8. Schematic illustration of the distribution of lithologic units and major breaks in sedimentation recognized during Leg 207. Unit V is dominated by clastics, Unit IV by organic-rich deposits, and Units I–III by pelagic microfossils with variable clay contents.

Figure F9. Close-up photographs of the P/E and K/T boundary intervals recovered during Leg 207. Each section is in meters above and below the boundary intervals. **A.** The P/E boundary interval is hung on the clay layer interpreted as the lithologic expression of shoaling of the CCD associated with the benthic extinction event and carbon isotope excursion. **B.** The K/T boundary interval is hung on the base of the spherule layer interpreted as a primary air fall deposit of material ejected by the K/T impact. **C.** Locality map of the Leg 207 sites on Demerara Rise. The water depth for each site is indicated.

Figure F10. Paleogene biostratigraphic summary of the western sites (Sites 1258, 1260, and 1261) and eastern sites (Sites 1259 and 1257), which are in order by present-day relative water depth. Foram = foraminifers, Nanno = nannofossils, Rad = radiolarians.

Figure F11. Summary of Paleogene stratigraphy and lithologic succession at ODP Leg 207. Lithology is plotted against time to show duration of periods of deposition and location of unconformities. Western sites (Sites 1258, 1260, and 1261) and eastern sites (Sites 1259 and 1257) are in order by present-day relative water depth. PETM = Paleocene/Eocene Thermal Maximum. K/T = Cretaceous/Tertiary

Figure F12. Cretaceous biostratigraphic summary of the western sites (Sites 1258, 1260, and 1261) and eastern sites (Sites 1259 and 1257), which are in order by present-day relative water depth. Foram = foraminifers, Nanno = nannofossils, Rad = radiolarians.

Figure F13. Summary of Cretaceous stratigraphy and lithologic succession at ODP Leg 207. Lithology is plotted against time to show duration of periods of deposition and locations of unconformities. The western sites (Sites 1258, 1260, and 1261) and eastern sites (Sites 1259 and 1257) are in order by present-day relative water depth. Forams = foraminifers, Nannos = nannofossils.

Figure F14. Late Maastrichtian–Danian record of the Leg 207 sites. Cretaceous and Paleogene planktonic foraminiferal zones are shown. Note the uncertainty in thickness of planktonic foraminiferal Zone Pα is derived from the spacing of shipboard samples.

Figure F15. **A.** Summary of linear sedimentation rates (LSRs), expressed in centimeters per thousand years to easily compare with mass accumulation rates (MARs), derived from age-depth models at each of the Leg 207 sites. **B.** Summary of MARs calculated from LSRs and average DBD at each of the Leg 207 sites. P/E = Paleocene/Eocene, K/T = Cretaceous/Tertiary.

Figure F16. Magnetic susceptibility profiles for Leg 207 sites. The yellow shading indicates sections for which splice sections were created. Gaps within the splices are indicted. P/E = Paleocene/Eocene, K/T = Cretaceous/Tertiary.

Figure F17. Magnetic susceptibility profiles for Leg 207 sites for the Paleocene–lower Eocene interval. The positions of zonal boundaries are tentative, pending postcruise biostratigraphic refinements. The profiles are aligned on the P/E boundary. A red bar along the left side of the log indicates an interval covered by a sampling splice. P/E = Paleocene/Eocene, K/T = Cretaceous/Tertiary.

Figure F18. Magnetic susceptibility profiles for Leg 207 sites for the Campanian–Maastrichtian interval. The positions of zonal boundaries are tentative, pending postcruise biostratigraphic refinements. The profiles are aligned on the K/T boundary. A red bar along the left side of the log indicates an interval covered by a sampling splice.

Figure F19. GRA bulk density profiles for Leg 207 sites through the Cretaceous black shale sequence. The positions of stage boundaries are tentative, pending postcruise biostratigraphic refinements. The profiles are aligned on the top of the laminated organic-rich claystone. A red bar along the left side of the log indicates an interval covered by a sampling splice.

Figure F20. Comparison of Rock-Eval pyrolysis hydrogen index and T_{max} values for black shale and underlying claystone units of the five sites cored during Leg 207 on Demerara Rise. Fields for Type I (waxy), Type II (algal microbial), and Type III (land plant/detrital) organic matter are shown. Compositions of the black shales are dominated by thermally immature, relatively well preserved algal-microbial organic matter.

Figure F21. Comparison of total organic carbon (TOC) concentrations and C_{org}/N_{total} values of black shales (defined as >1% TOC) for black shale units of the five sites drilled during Leg 207 on Demerara Rise. Increasing C/N values with higher TOC concentrations probably reflect preservational conditions that favored burial of carbon and recycling of the nitrogenous components of marine organic matter.

Figure F22. Profiles of chemical constituents in IWs for Leg 207.

Figure F23. Velocity and porosity profiles for Leg 207. Velocity measurements, acquired using the Hamilton Frame on split cores, are uncorrected for in situ temperature and pressure. Porosity was determined along with wet bulk density, grain density, and water content on discrete samples.

Figure F24. Stratigraphy of the black shale interval revealed by FMS images and wireline measured physical properties from Hole 1261B.

Figure F25. Seismic traveltime vs. depth for each site. The relationships were derived from best fits with the synthetic seismograms. Note that Sites 1257, 1258, and 1260 have very similar curves and Sites 1259 and 1261 have similar shaped curves.

Figure F26. Depth-migrated seismic profile of line GeoB220 correlated with the lithologic summary for Site 1257.

Figure F27. Depth-migrated seismic profile of line GeoB221 correlated with the lithologic summary for Site 1258.

Figure F28. Depth-migrated seismic profile of line GeoB219 correlated with the lithologic summary for Site 1259.

Figure F29. Depth-migrated seismic profile of line GeoB215 correlated with the lithologic summary for Site 1260.

Figure F30. Depth-migrated seismic profile of line GeoB213 correlated with the lithologic summary for Site 1261.

Figure F31. Horizon C surface map. Depths were calculated assuming velocities of 1495 m/s for the water column and an average velocity of 2000 m/s for the sediment column.

Table T1. Operations summary, Leg 207.

Hole	Latitude	Longitude	Water depth (mbsl)	Number of cores	Interval cored (m)	Core recovered (m)	Total recovered (%)	Interval drilled (m)	Total penetration (mbsf)	Time on site (hr)	Time on site (days)
1257A	9°27.230′N	54°20.518′W	2951.0	31	284.7	216.1	75.9	0.0	284.7	104.2	4.3
1257B	9°27.218′N	54°20.508′W	2951.0	27	187.3	116.2	62.1	40.0	227.3	38.6	1.6
1257C	9°27.206′N	54°20.495′W	2951.0	16	153.9	96.6	62.8	82.0	235.9	26.2	1.1
		Site 1257 totals:		74	625.9	428.9	68.5	122	747.9	169.0	7.0
1258A	9°26.000′N	54°43.999′W	3192.2	50	447.5	375.5	83.9	0.0	447.5	63.9	2.7
1258B	9°26.000′N	54°43.982′W	3192.2	57	453.9	346.1	76.3	7.0	460.9	72.0	3.0
1258C	9°26.000′N	54°43.966′W	3192.2	34	215.2	161.1	74.9	269.8	485.0	93.7	3.9
		Site 1258 totals:		141	1116.6	882.7	79.0	276.8	1393.4	229.6	9.6
1259A	9°17.999′N	54°11.998′W	2353.8	60	558.8	372.1	66.6	0.0	558.8	62.9	2.6
1259B	9°18.048′N	54°11.945′W	2353.8	25	222.2	153.8	69.2	334.0	556.2	42.6	1.8
1259C	9°18.024′N	54°11.969′W	2355.8	19	148.6	118.9	80.0	405.1	553.7	39.7	1.7
		Site 1259 totals:		104	929.6	644.9	69.4	739.1	1668.7	145.2	6.1
1260A	9°15.948′N	54°32.633′W	2548.8	54	491.9	391.6	79.6	0.0	491.9	51.1	2.1
1260B	9°15.931′N	54°32.652′W	2548.8	46	370.3	326.5	88.2	138.7	509.0	88.4	3.7
		Site 1260 totals:		100	862.2	718.1	83.3	138.7	1000.9	139.5	5.8
1261A	9°2.917′N	54°19.038′W	1899.7	51	484.0	355.4	73.4	185.5	669.5	67.9	2.8
1261B	9°2.918′N	54°19.049′W	1899.7	16	148.8	92.5	62.2	525.3	674.1	84.9	3.5
		Site 1261 totals:		67	632.8	447.9	70.8	710.8	1343.6	152.8	6.3
		Leg 207 totals:		486	4167.1	3122.4	74.9	1987.4	6154.5	836.1	34.8

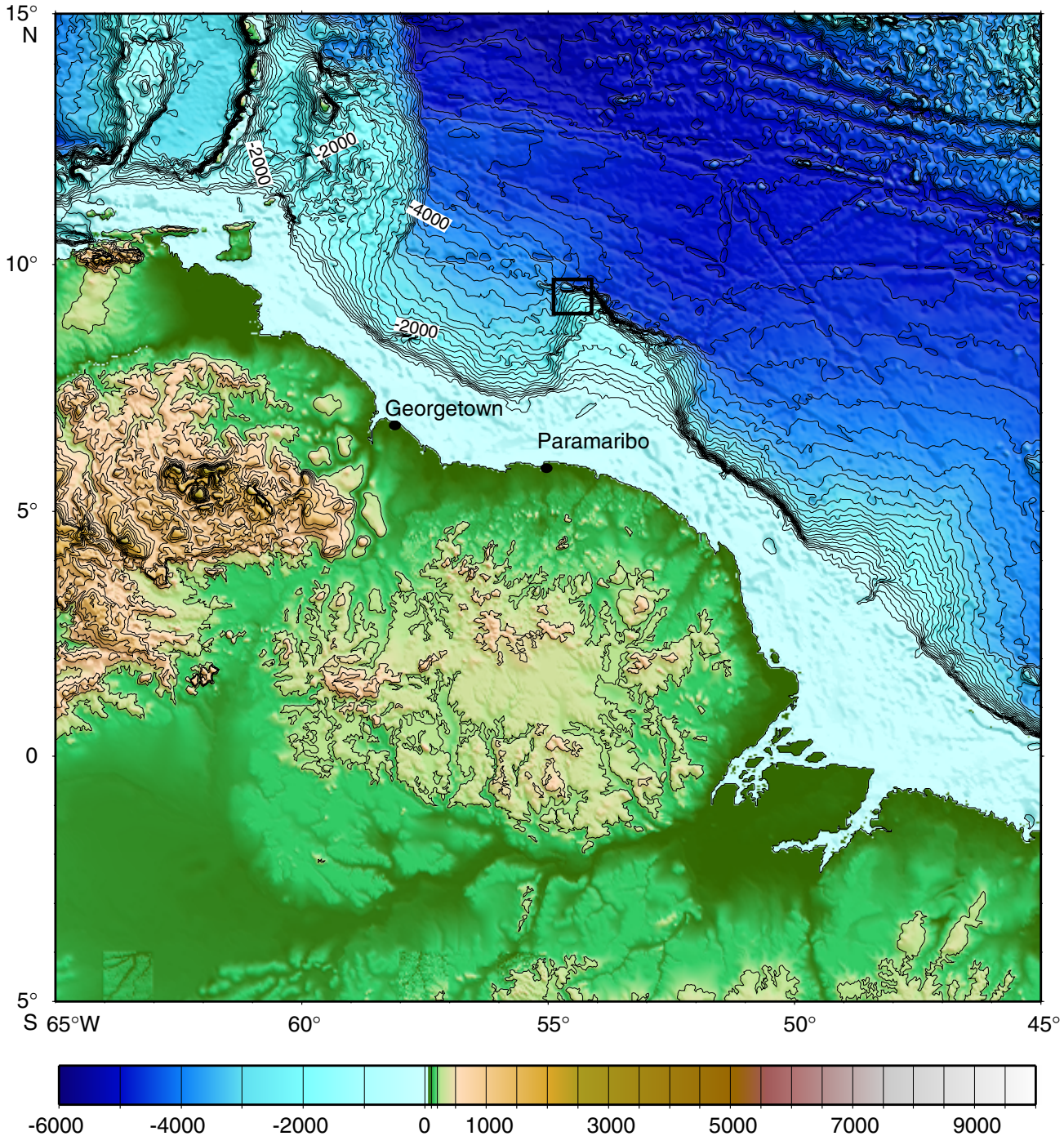
15° N
10°
5°
0
5° S
65°W
60°
55°
50°
45°
-2000
-2000
-4000
-2000
Georgetown
Paramaribo
-6000
-4000
-2000
0
1000
3000
5000
7000
9000

Figure F1

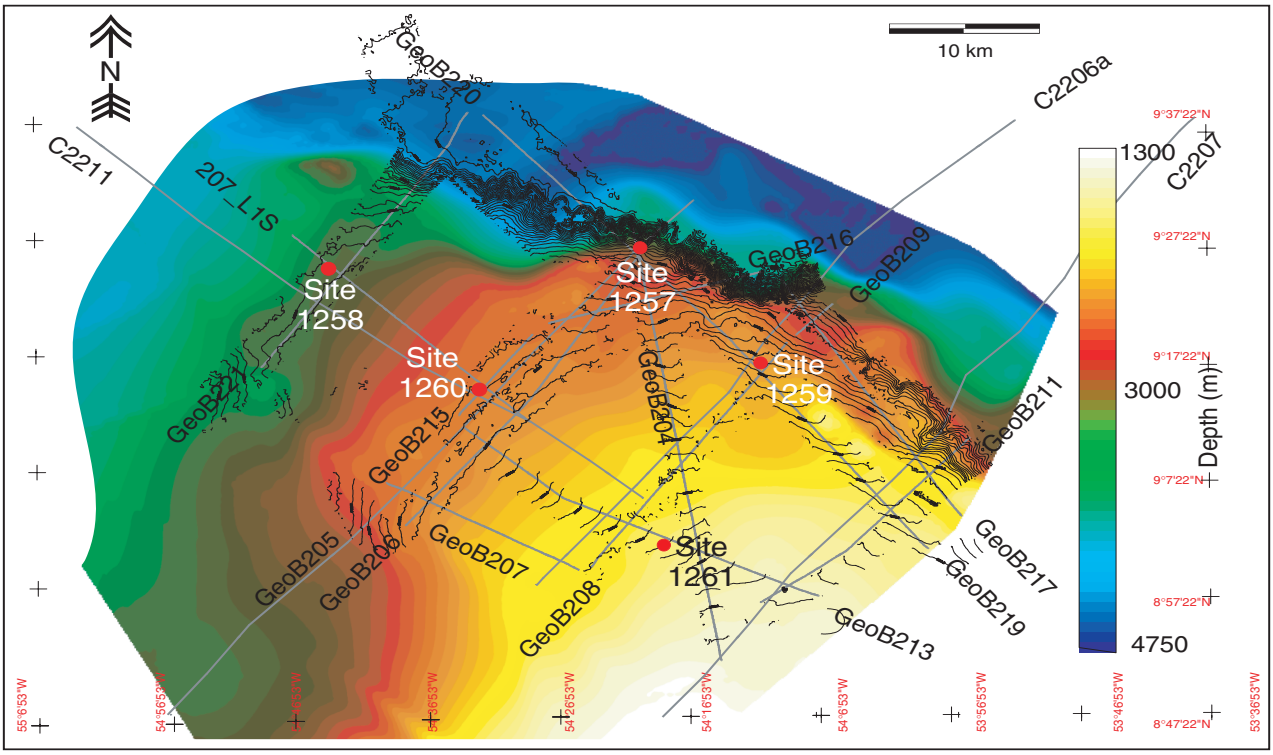
N
10 km
C2211
207_L1S
GeoB220
C2206a
C2207
GeoB216
GeoB209
Site 1257
Site 1258
Site 1260
Site 1259
Site 1261
GeoB227
GeoB215
GeoB204
GeoB211
GeoB205
GeoB206
GeoB207
GeoB208
GeoB217
GeoB219
GeoB213
1300
3000
4750
Depth (m)
9°37'22"N
9°27'22"N
9°17'22"N
9°7'22"N
8°57'22"N
8°47'22"N
55°6'53"W
54°56'53"W
54°46'53"W
54°36'53"W
54°26'53"W
54°16'53"W
54°6'53"W
53°56'53"W
53°46'53"W
53°36'53"W

Figure F2

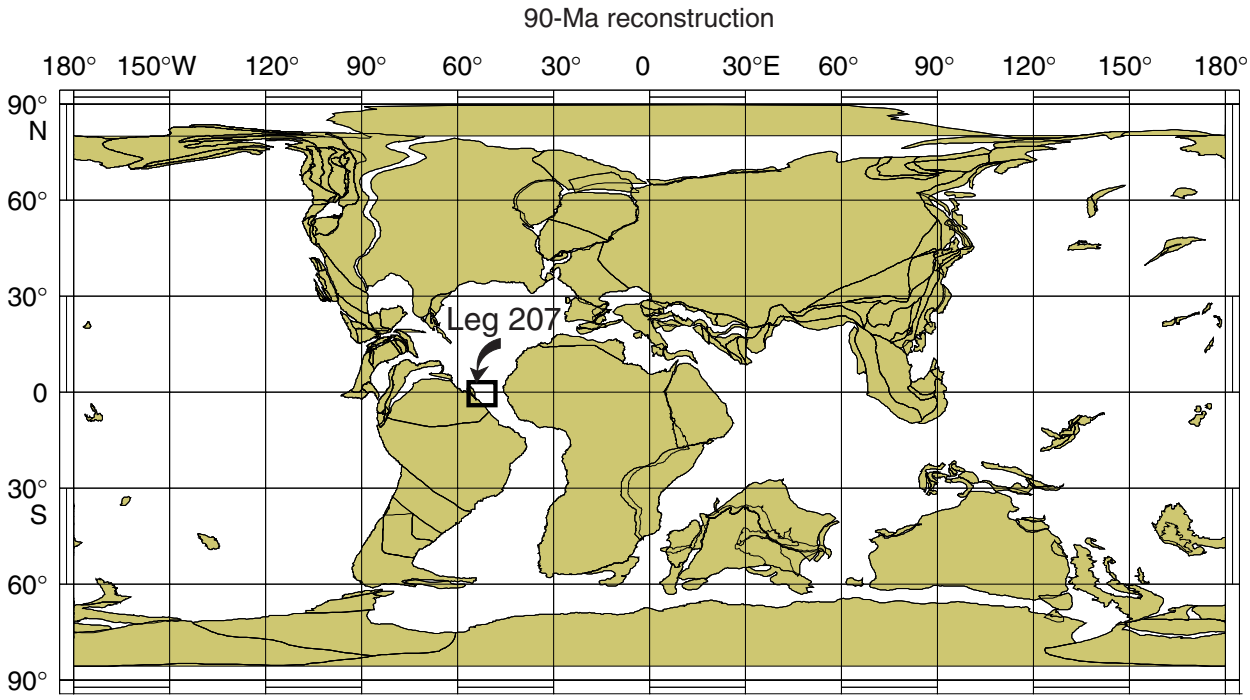
90-Ma reconstruction
180° 150°W 120° 90° 60° 30° 0 30°E 60° 90° 120° 150° 180°
90° N
60°
30°
0
30° S
60°
90°
Leg 207

Figure F3

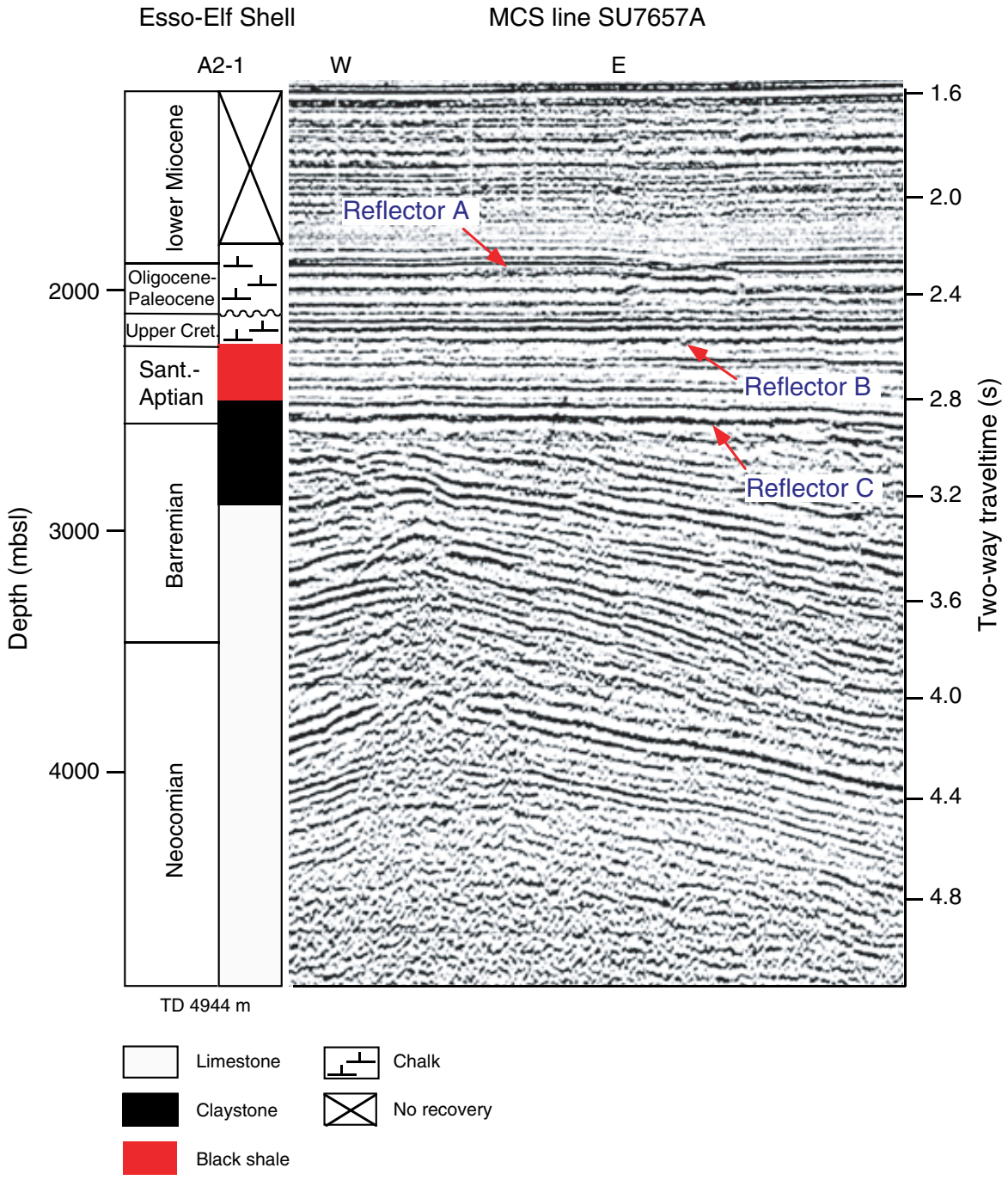
Esso-Elf Shell
MCS line SU7657A
A2-1
W
E
lower Miocene
Oligocene-Paleocene
Upper Cret.
Sant.-Aptian
Barremian
Neocomian
2000
3000
4000
Depth (mbsl)
Reflector A
Reflector B
Reflector C
1.6
2.0
2.4
2.8
3.2
3.6
4.0
4.4
4.8
Two-way traveltime (s)
TD 4944 m
Limestone
Chalk
Claystone
No recovery
Black shale

Figure F4

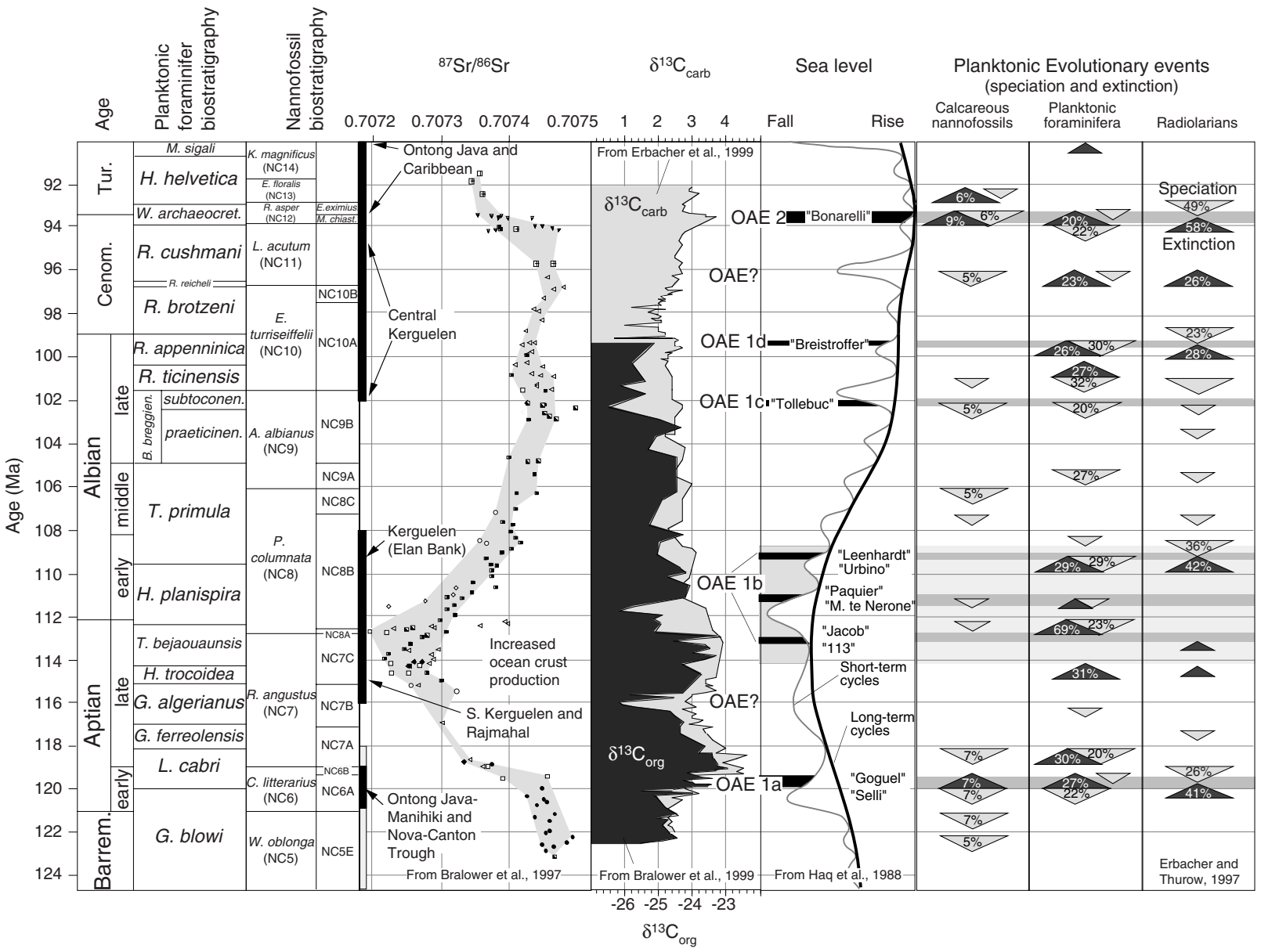
Age
Planktonic foraminifer biostratigraphy
Nannofossil biostratigraphy
87Sr/86Sr
δ13Ccarb
Sea level
Planktonic Evolutionary events (speciation and extinction)
Calcareous nannofossils
Planktonic foraminifera
Radiolarians
Fall
Rise
Age (Ma)
Tur.
Cenom.
Albian
Aptian
Barrem.
late
middle
early
M. sigali
H. helvetica
W. archaeocret.
R. cushmani
R. reicheli
R. brotzeni
R. appenninica
R. ticinensis
subtoconen.
praeticinen.
B. breggien.
T. primula
H. planispira
T. bejaouaunsis
H. trocoidea
G. algerianus
G. ferreolensis
L. cabri
G. blowi
K. magnificus (NC14)
E. floralis (NC13)
R. asper (NC12)
L. acutum (NC11)
E. turriseiffelii (NC10)
A. albianus (NC9)
P. columnata (NC8)
R. angustus (NC7)
C. litterarius (NC6)
W. oblonga (NC5)
E.eximius
M. chiast.
NC10B
NC10A
NC9B
NC9A
NC8C
NC8B
NC8A
NC7C
NC7B
NC7A
NC6B
NC6A
NC5E
0.7072 0.7073 0.7074 0.7075
1 2 3 4
Ontong Java and Caribbean
Central Kerguelen
Kerguelen (Elan Bank)
Increased ocean crust production
S. Kerguelen and Rajmahal
Ontong Java-Manihiki and Nova-Canton Trough
From Bralower et al., 1997
From Erbacher et al., 1999
δ13Ccarb
δ13Corg
From Bralower et al., 1999
OAE 2
"Bonarelli"
OAE?
OAE 1d
"Breistroffer"
OAE 1c
"Tollebuc"
OAE 1b
"Leenhardt"
"Urbino"
"Paquier"
"M. te Nerone"
"Jacob"
"113"
Short-term cycles
OAE?
Long-term cycles
OAE 1a
"Goguel"
"Selli"
From Haq et al., 1988
-26 -25 -24 -23
δ13Corg
Speciation
Extinction
Erbacher and Thurow, 1997

Figure F5

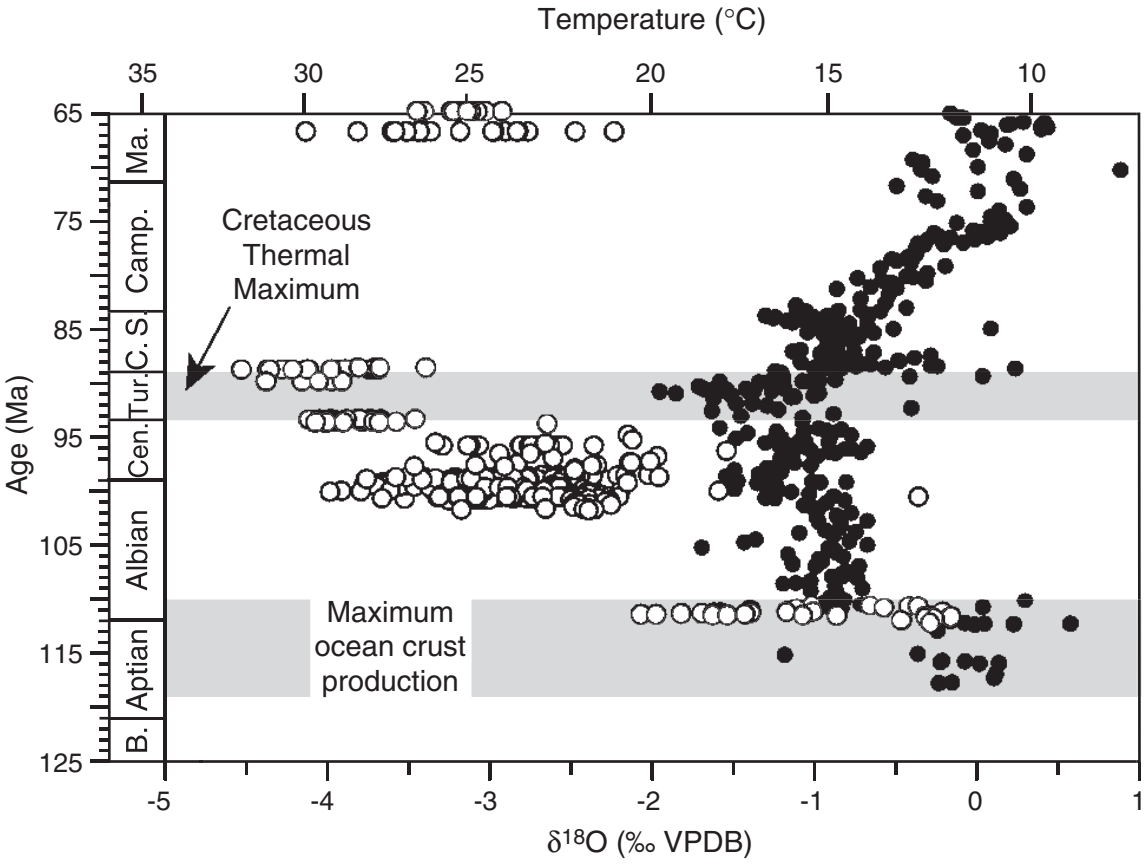
Temperature (°C)
35
30
25
20
15
10
65
75
85
95
105
115
125
Age (Ma)
Ma.
Camp.
C. S.
Tur.
Cen.
Albian
Aptian
B.
Cretaceous
Thermal
Maximum
Maximum
ocean crust
production
-5
-4
-3
-2
-1
0
1
δ18O (‰ VPDB)

Figure F6

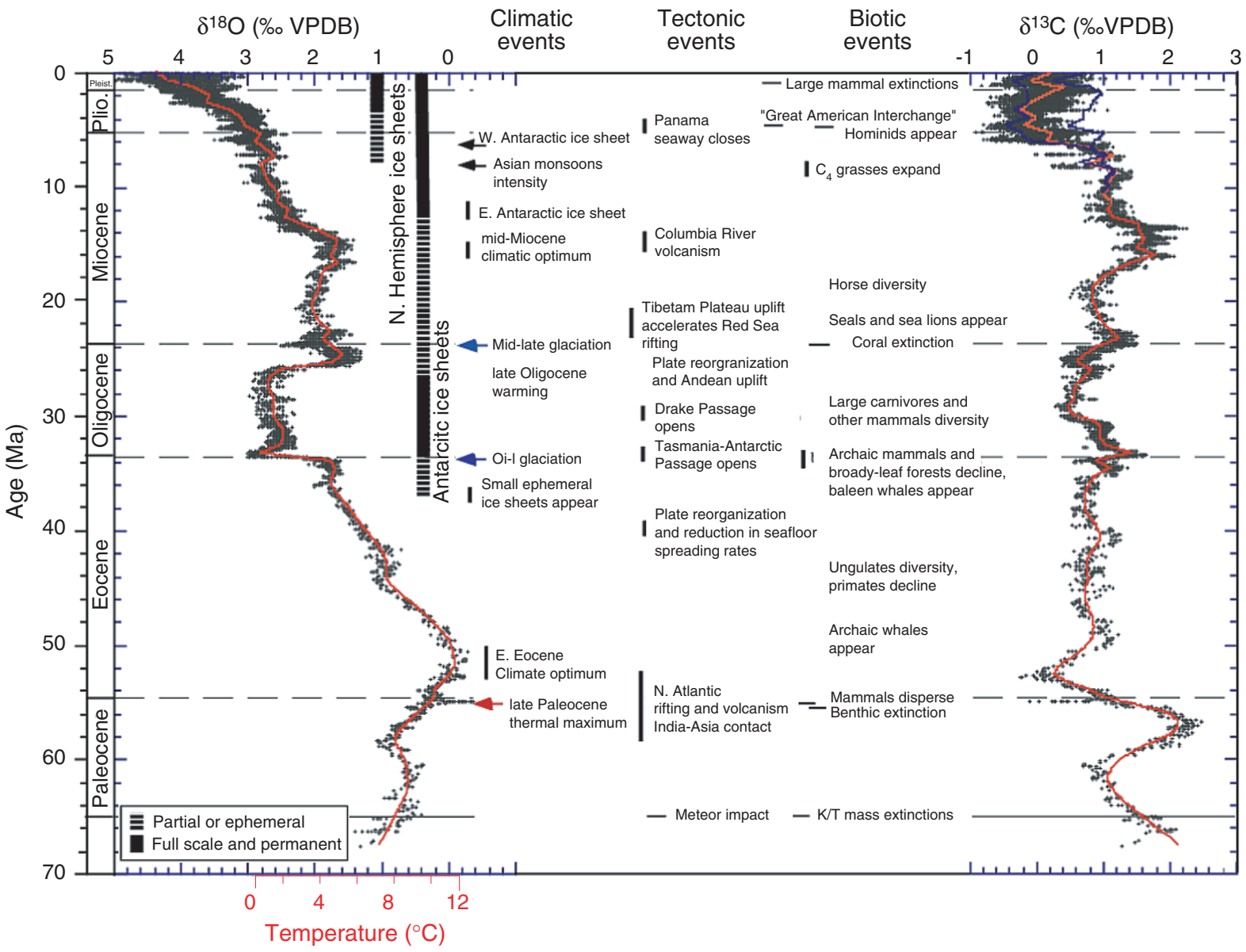
δ18O (‰ VPDB)
Climatic events
Tectonic events
Biotic events
δ13C (‰VPDB)
Age (Ma)
Pleist.
Plio.
Miocene
Oligocene
Eocene
Paleocene
N. Hemisphere ice sheets
Antarcitc ice sheets
W. Antarctic ice sheet
Asian monsoons intensity
E. Antarctic ice sheet
mid-Miocene climatic optimum
Mid-late glaciation
late Oligocene warming
Oi-I glaciation
Small ephemeral ice sheets appear
E. Eocene Climate optimum
late Paleocene thermal maximum
Panama seaway closes
Columbia River volcanism
Tibetam Plateau uplift accelerates Red Sea rifting
Plate reorgranization and Andean uplift
Drake Passage opens
Tasmania-Antarctic Passage opens
Plate reorganization and reduction in seafloor spreading rates
N. Atlantic rifting and volcanism India-Asia contact
Meteor impact
Large mammal extinctions
"Great American Interchange"
Hominids appear
C4 grasses expand
Horse diversity
Seals and sea lions appear
Coral extinction
Large carnivores and other mammals diversity
Archaic mammals and broady-leaf forests decline, baleen whales appear
Ungulates diversity, primates decline
Archaic whales appear
Mammals disperse
Benthic extinction
K/T mass extinctions
Partial or ephemeral
Full scale and permanent
Temperature (°C)

Figure F7

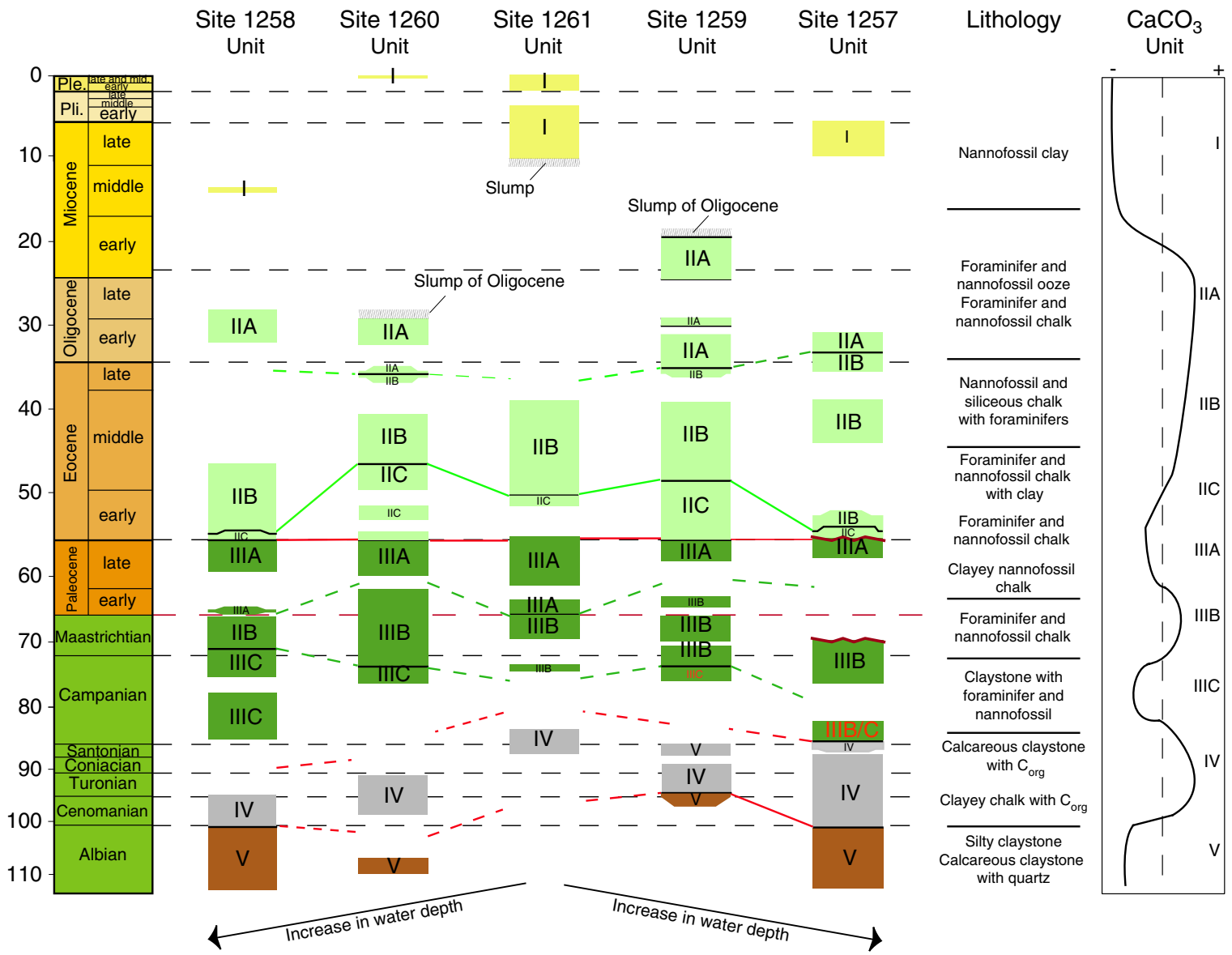
Site 1258
Unit
Site 1260
Unit
Site 1261
Unit
Site 1259
Unit
Site 1257
Unit
Lithology
CaCO3
Unit
Ple.
Pli.
Miocene
Oligocene
Eocene
Paleocene
Maastrichtian
Campanian
Santonian
Coniacian
Turonian
Cenomanian
Albian
Slump
Slump of Oligocene
Slump of Oligocene
Nannofossil clay
Foraminifer and nannofossil ooze
Foraminifer and nannofossil chalk
Nannofossil and siliceous chalk with foraminifers
Foraminifer and nannofossil chalk with clay
Foraminifer and nannofossil chalk
Clayey nannofossil chalk
Foraminifer and nannofossil chalk
Claystone with foraminifer and nannofossil
Calcareous claystone with Corg
Clayey chalk with Corg
Silty claystone
Calcareous claystone with quartz
Increase in water depth
Increase in water depth

Figure F8

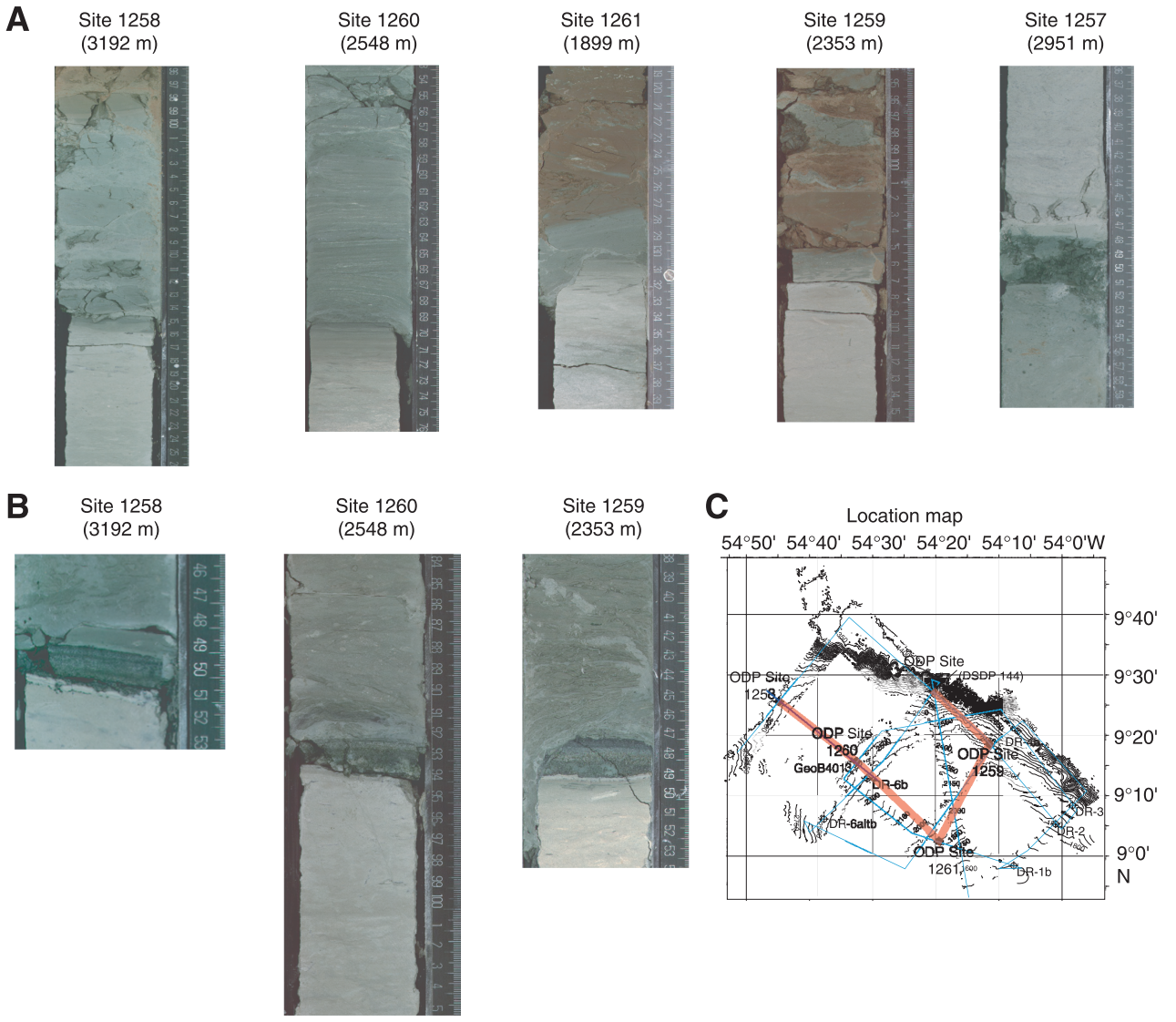
A
Site 1258
(3192 m)
Site 1260
(2548 m)
Site 1261
(1899 m)
Site 1259
(2353 m)
Site 1257
(2951 m)
B
Site 1258
(3192 m)
Site 1260
(2548 m)
Site 1259
(2353 m)
C
Location map
54°50' 54°40' 54°30' 54°20' 54°10' 54°0'W
9°40'
9°30'
9°20'
9°10'
9°0'
N
ODP Site
(DSDP 144)
ODP Site
1258
ODP Site
1260
GeoB4013
ODP Site
1259
DR-6b
DR-6altb
DR-3
DR-2
ODP Site
1261
DR-1b

Figure F9

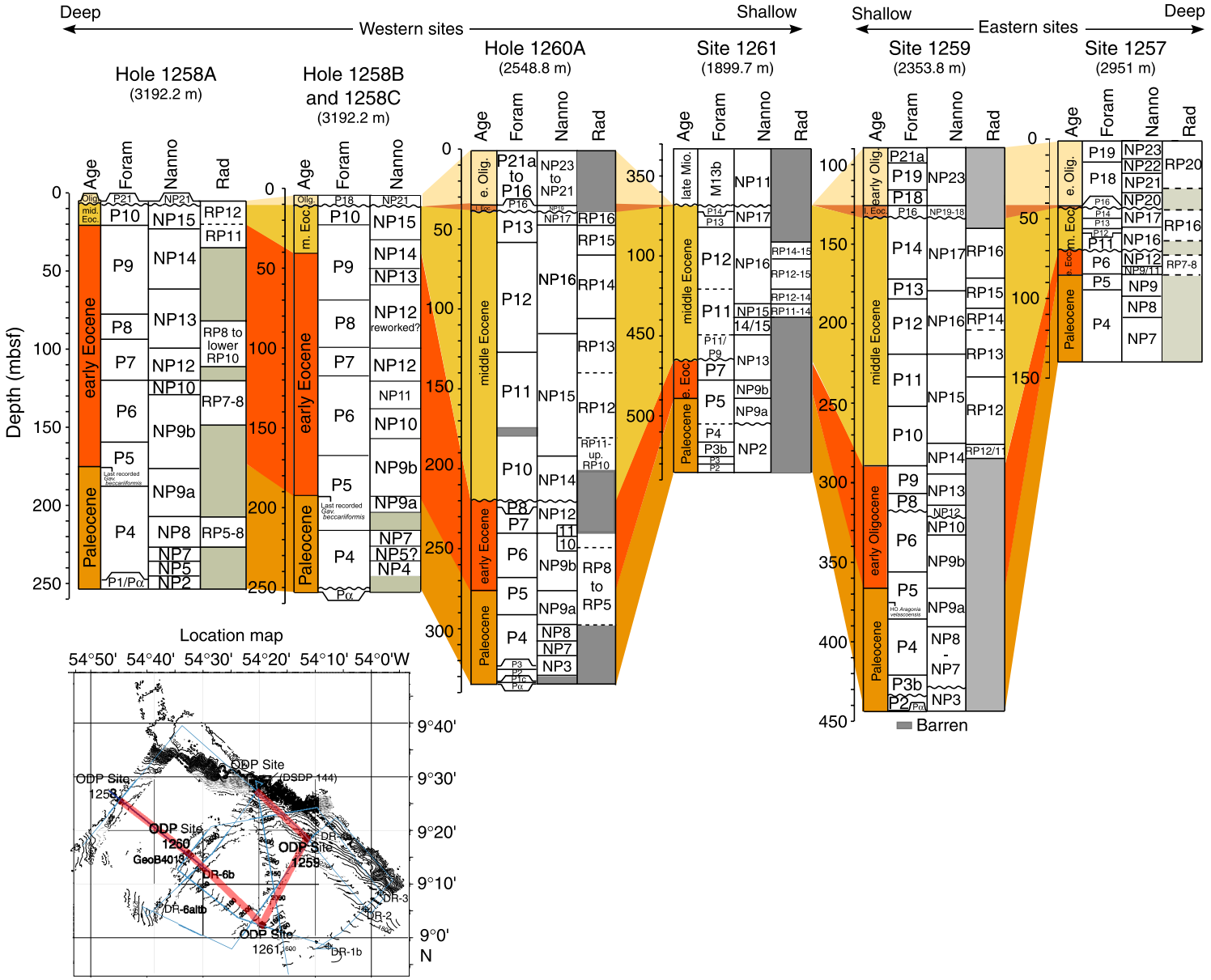
Deep
Western sites
Shallow
Shallow
Eastern sites
Deep
Hole 1258A
(3192.2 m)
Hole 1258B
and 1258C
(3192.2 m)
Hole 1260A
(2548.8 m)
Site 1261
(1899.7 m)
Site 1259
(2353.8 m)
Site 1257
(2951 m)
Depth (mbsf)
Age
Foram
Nanno
Rad
Location map
54°50' 54°40' 54°30' 54°20' 54°10' 54°0'W
9°40'
9°30'
9°20'
9°10'
9°0'
N
ODP Site 1258
ODP Site 1260
GeoB4013
ODP Site 1259
(DSDP 144)
ODP Site 1261
DR-6b
DR-6alt
DR-3
DR-2
DR-1b
Barren

Figure F10

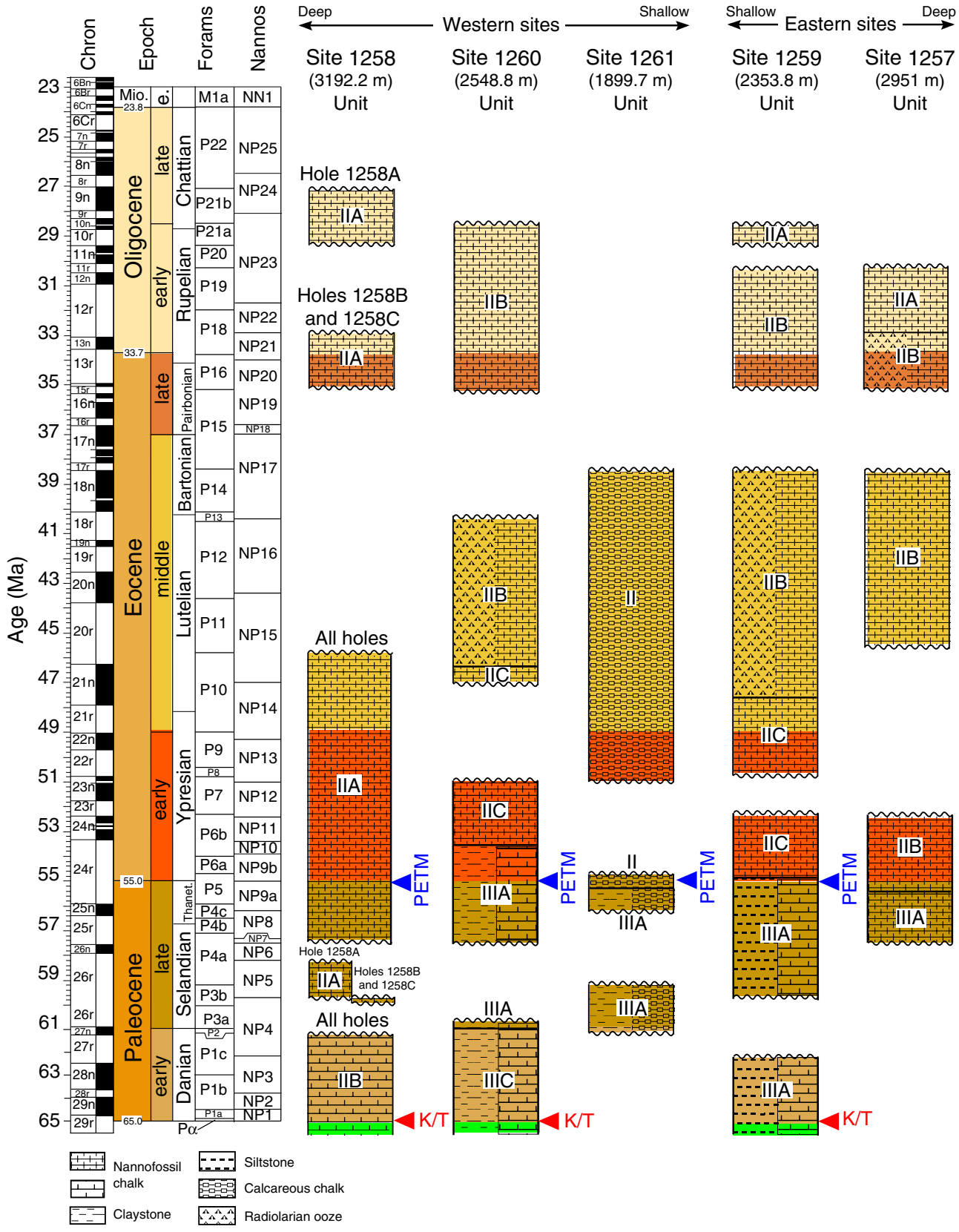
Chron
Epoch
Forams
Nannos
Age (Ma)
Deep
Western sites
Shallow
Shallow
Eastern sites
Deep
Site 1258
(3192.2 m)
Unit
Site 1260
(2548.8 m)
Unit
Site 1261
(1899.7 m)
Unit
Site 1259
(2353.8 m)
Unit
Site 1257
(2951 m)
Unit
Oligocene
Eocene
Paleocene
late
early
middle
Chattian
Rupelian
Pairbonian
Bartonian
Lutelian
Ypresian
Thanet.
Selandian
Danian
Hole 1258A
Holes 1258B
and 1258C
All holes
PETM
K/T
Nannofossil
chalk
Claystone
Siltstone
Calcareous chalk
Radiolarian ooze

Figure F11

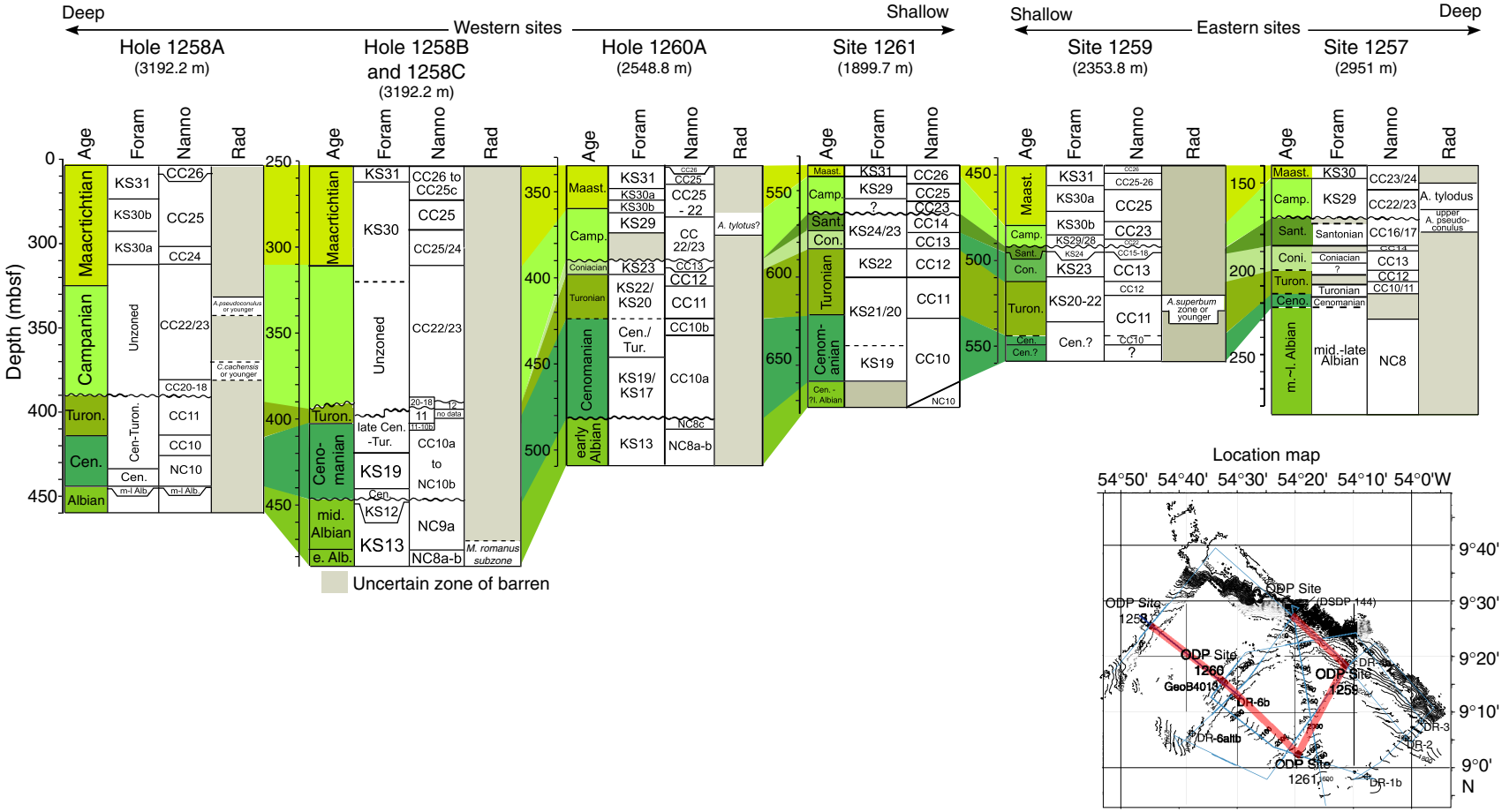
Deep
Western sites
Shallow
Shallow
Eastern sites
Deep
Hole 1258A
(3192.2 m)
Hole 1258B
and 1258C
(3192.2 m)
Hole 1260A
(2548.8 m)
Site 1261
(1899.7 m)
Site 1259
(2353.8 m)
Site 1257
(2951 m)
Age
Foram
Nanno
Rad
Depth (mbsf)
Maastrichtian
Campanian
Turon.
Cen.
Albian
Maast.
Camp.
Sant.
Con.
Coniacian
Turonian
Cenomanian
early Albian
Ceno-manian
mid. Albian
e. Alb.
Cen.-Turon.
late Cen.-Tur.
Cen./ Tur.
Cen.-?l. Albian
Cen.?
mid.-late Albian
m.-l. Albian
Coni.
Ceno.
Uncertain zone of barren
Location map
54°50'
54°40'
54°30'
54°20'
54°10'
54°0'W
9°40'
9°30'
9°20'
9°10'
9°0'
N
ODP Site 1258
ODP Site 1260
ODP Site 1259
ODP Site 1261
(DSDP 144)
GeoB4014
DR-6b
DR-6alt b
DR-1b
DR-2
DR-3

Figure F12

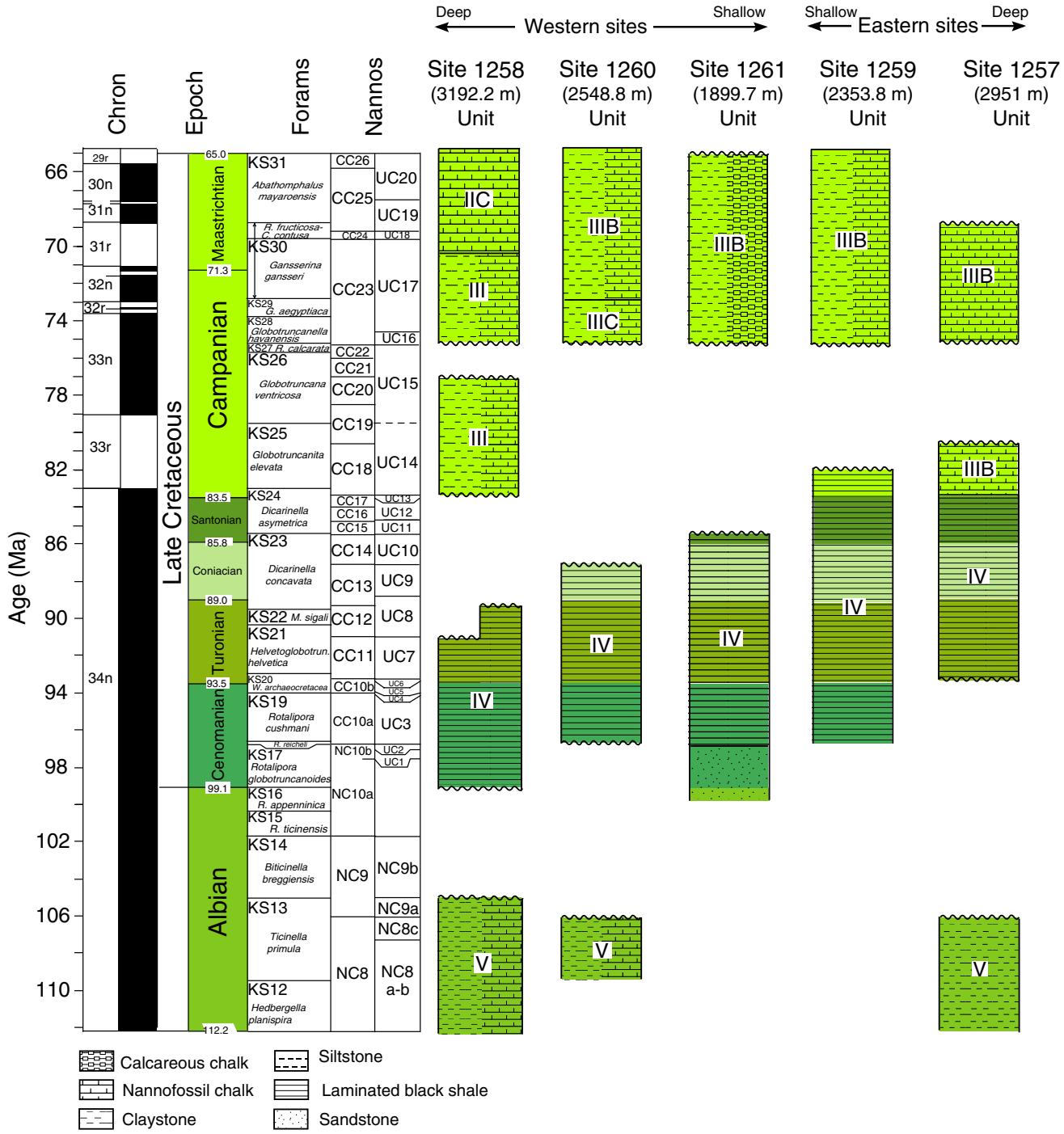
Deep
Western sites
Shallow
Shallow
Eastern sites
Deep
Chron
Epoch
Forams
Nannos
Site 1258 (3192.2 m) Unit
Site 1260 (2548.8 m) Unit
Site 1261 (1899.7 m) Unit
Site 1259 (2353.8 m) Unit
Site 1257 (2951 m) Unit
Age (Ma)
Late Cretaceous
Maastrichtian
Campanian
Santonian
Coniacian
Turonian
Cenomanian
Albian
KS31 Abathomphalus mayaroensis
KS30 Gansserina gansseri
KS29 G. aegyptiaca
KS28 Globotruncanella havanensis
KS27 R. calcarata
KS26 Globotruncana ventricosa
KS25 Globotruncanita elevata
KS24 Dicarinella asymetrica
KS23 Dicarinella concavata
KS22 M. sigali
KS21 Helvetoglobotrun. helvetica
KS20 W. archaeocretacea
KS19 Rotalipora cushmani
KS17 Rotalipora globotruncanoides
KS16 R. appenninica
KS15 R. ticinensis
KS14 Biticinella breggiensis
KS13 Ticinella primula
KS12 Hedbergella planispira
Calcareous chalk
Nannofossil chalk
Claystone
Siltstone
Laminated black shale
Sandstone

Figure F13

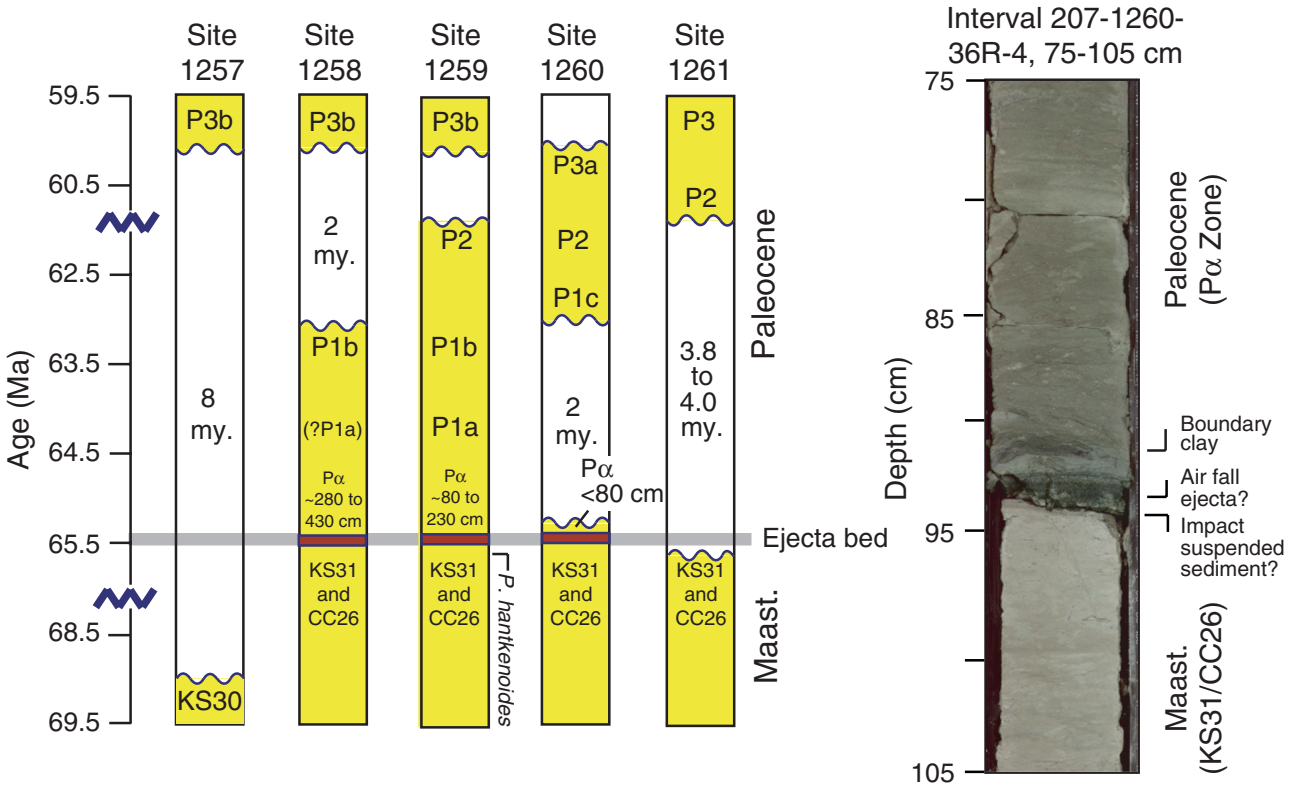
Site 1257
Site 1258
Site 1259
Site 1260
Site 1261
Age (Ma)
59.5
60.5
62.5
63.5
64.5
65.5
68.5
69.5
P3b
8 my.
KS30
P3b
2 my.
P1b
(?P1a)
Pα ~280 to 430 cm
KS31 and CC26
P3b
P2
P1b
P1a
Pα ~80 to 230 cm
KS31 and CC26
P. hantkenoides
P3a
P2
P1c
2 my.
Pα <80 cm
KS31 and CC26
P3
P2
3.8 to 4.0 my.
KS31 and CC26
Paleocene
Maast.
Ejecta bed
Interval 207-1260-36R-4, 75-105 cm
Depth (cm)
75
85
95
105
Paleocene (Pα Zone)
Boundary clay
Air fall ejecta?
Impact suspended sediment?
Maast. (KS31/CC26)

Figure F14

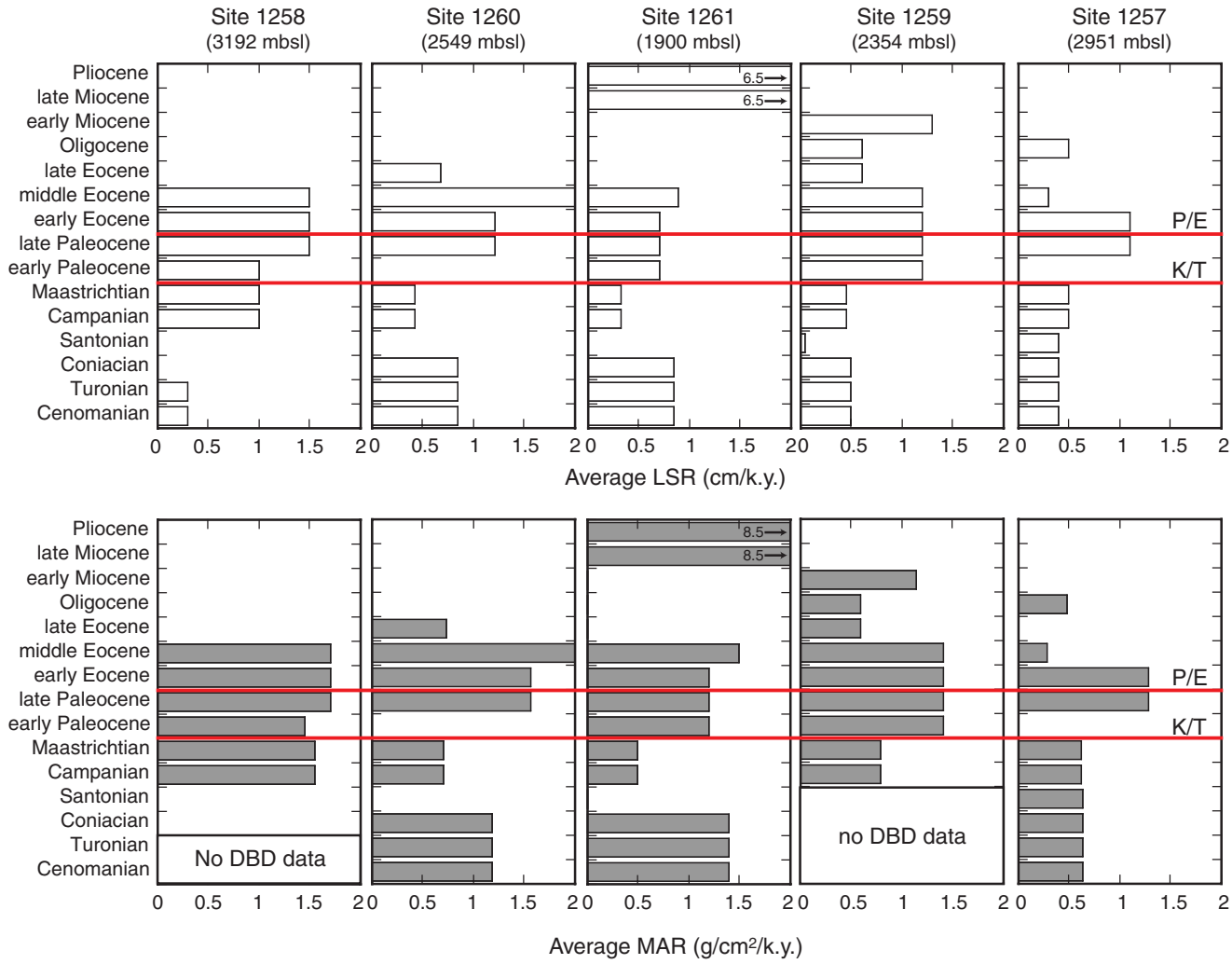
Site 1258
(3192 mbsl)
Site 1260
(2549 mbsl)
Site 1261
(1900 mbsl)
Site 1259
(2354 mbsl)
Site 1257
(2951 mbsl)
Pliocene
late Miocene
early Miocene
Oligocene
late Eocene
middle Eocene
early Eocene
late Paleocene
early Paleocene
Maastrichtian
Campanian
Santonian
Coniacian
Turonian
Cenomanian
6.5
6.5
P/E
K/T
0 0.5 1 1.5 2
Average LSR (cm/k.y.)
8.5
8.5
No DBD data
no DBD data
Average MAR (g/cm²/k.y.)

Figure F15

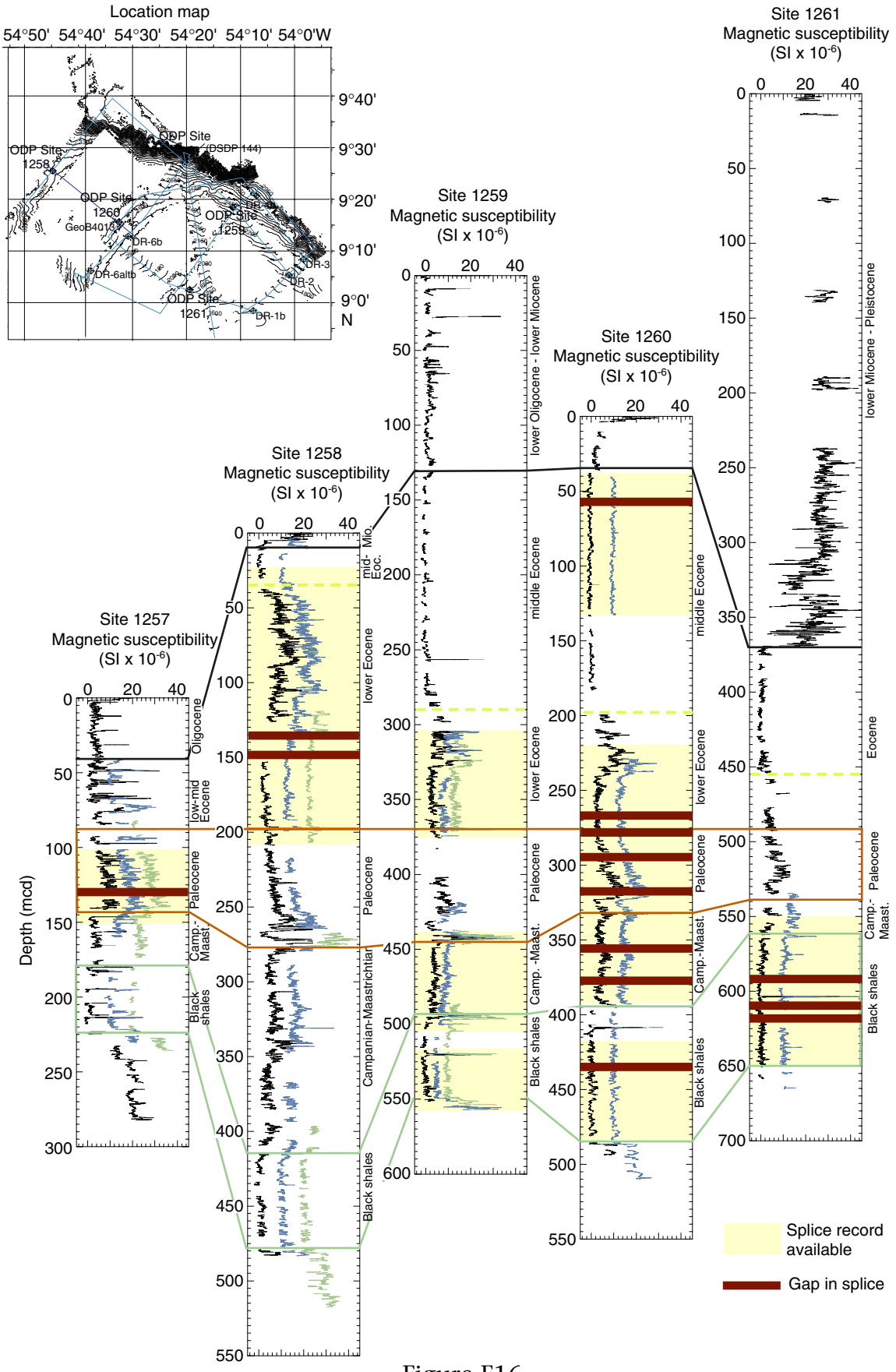
Location map
54°50' 54°40' 54°30' 54°20' 54°10' 54°0'W
9°40'
9°30'
9°20'
9°10'
9°0'
N
ODP Site 1258
ODP Site (DSDP 144)
ODP Site 1260
GeoB4013-1
ODP Site 1259
ODP Site 1261
DR-6b
DR-6altb
DR-3
DR-2
DR-1b
Site 1257
Magnetic susceptibility
(SI x 10-6)
Site 1258
Magnetic susceptibility
(SI x 10-6)
Site 1259
Magnetic susceptibility
(SI x 10-6)
Site 1260
Magnetic susceptibility
(SI x 10-6)
Site 1261
Magnetic susceptibility
(SI x 10-6)
Depth (mcd)
Oligocene
low-mid Eocene
Paleocene
Camp.-Maast.
Black shales
mid-Mio. Eoc.
lower Eocene
Paleocene
Campanian-Maastrichtian
Black shales
lower Oligocene - lower Miocene
middle Eocene
lower Eocene
Paleocene
Camp.-Maast.
Black shales
middle Eocene
lower Eocene
Paleocene
Camp.-Maast.
Black shales
lower Miocene - Pleistocene
Eocene
Paleocene
Camp.-Maast.
Black shales
Splice record available
Gap in splice

Figure F16

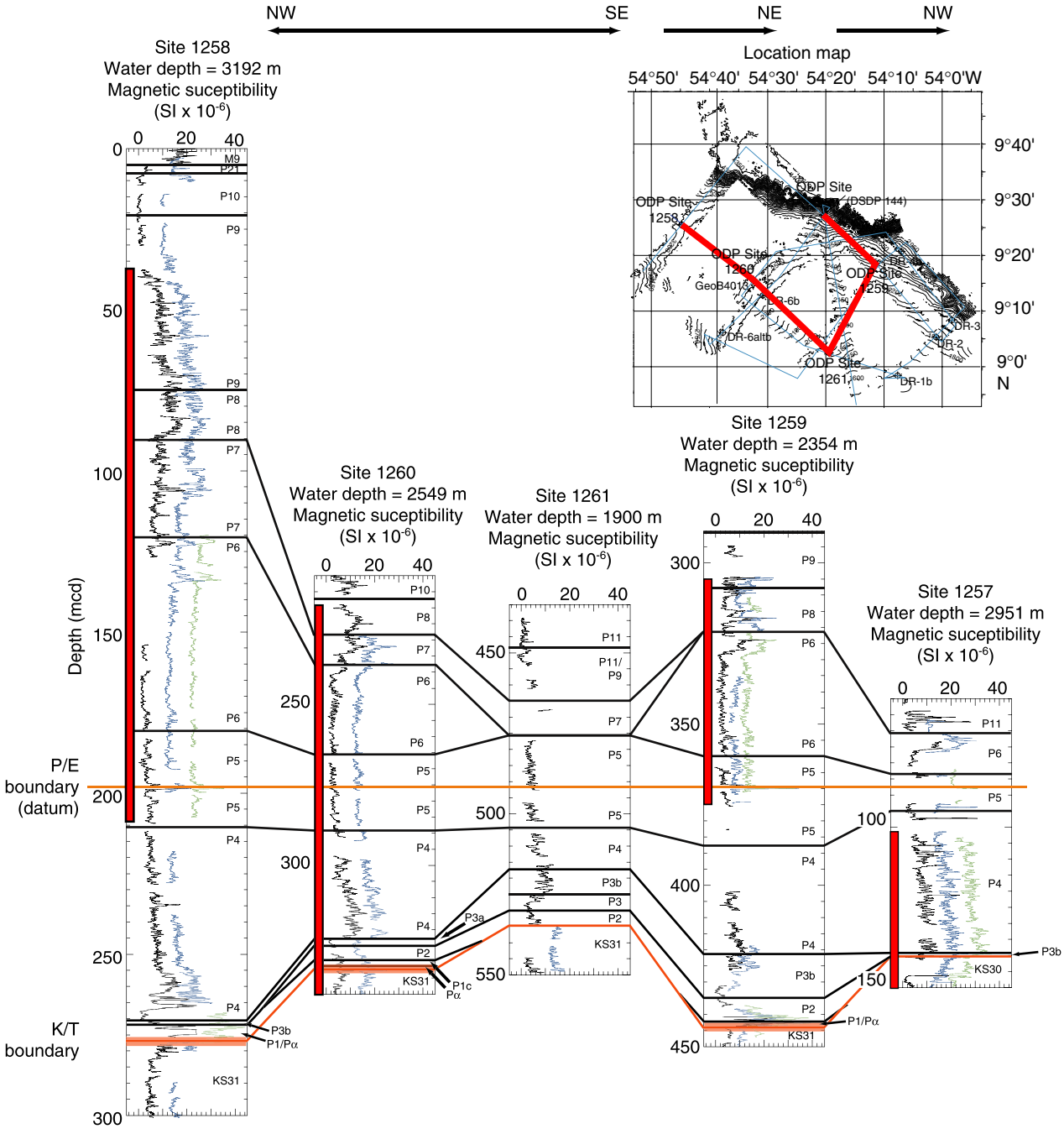
NW
SE
NE
NW
Location map
54°50' 54°40' 54°30' 54°20' 54°10' 54°0'W
9°40'
9°30'
9°20'
9°10'
9°0'
N
ODP Site 1258
ODP Site (DSDP 144)
ODP Site 1260
ODP Site 1259
ODP Site 1261
GeoB4013-4
DR-6b
DR-6altb
DR-3
DR-2
DR-1b
Site 1258
Water depth = 3192 m
Magnetic suceptibility
(SI x 10-6)
Site 1260
Water depth = 2549 m
Magnetic suceptibility
(SI x 10-6)
Site 1261
Water depth = 1900 m
Magnetic suceptibility
(SI x 10-6)
Site 1259
Water depth = 2354 m
Magnetic suceptibility
(SI x 10-6)
Site 1257
Water depth = 2951 m
Magnetic suceptibility
(SI x 10-6)
Depth (mcd)
P/E boundary (datum)
K/T boundary
M9
P21
P10
P9
P8
P7
P6
P5
P4
P3b
P3
P3a
P2
P1c
Pα
P1/Pα
KS31
KS30
P11
P11/P9

Figure F17

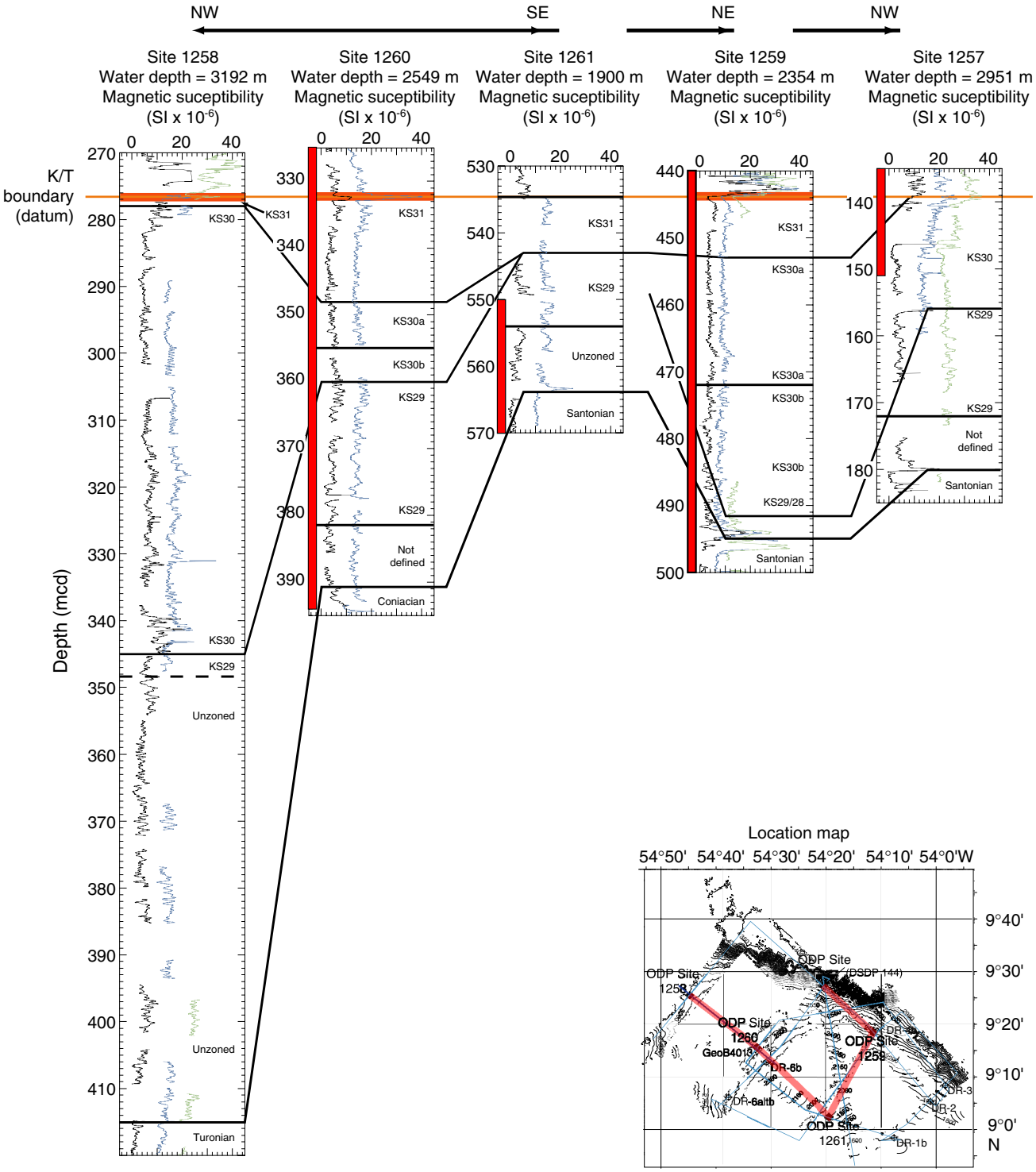
NW
SE
NE
NW
Site 1258
Water depth = 3192 m
Magnetic suceptibility
(SI x 10-6)
Site 1260
Water depth = 2549 m
Magnetic suceptibility
(SI x 10-6)
Site 1261
Water depth = 1900 m
Magnetic suceptibility
(SI x 10-6)
Site 1259
Water depth = 2354 m
Magnetic suceptibility
(SI x 10-6)
Site 1257
Water depth = 2951 m
Magnetic suceptibility
(SI x 10-6)
K/T boundary (datum)
Depth (mcd)
KS31
KS30
KS30a
KS30b
KS29
KS29/28
Unzoned
Not defined
Santonian
Coniacian
Turonian
Location map
54°50' 54°40' 54°30' 54°20' 54°10' 54°0'W
9°40'
9°30'
9°20'
9°10'
9°0' N
ODP Site 1258
ODP Site 1260
ODP Site 1261
ODP Site 1259
(DSDP 144)
GeoB4018
DR-6b
DR-6altb
DR-3
DR-2
DR-1b

Figure F18

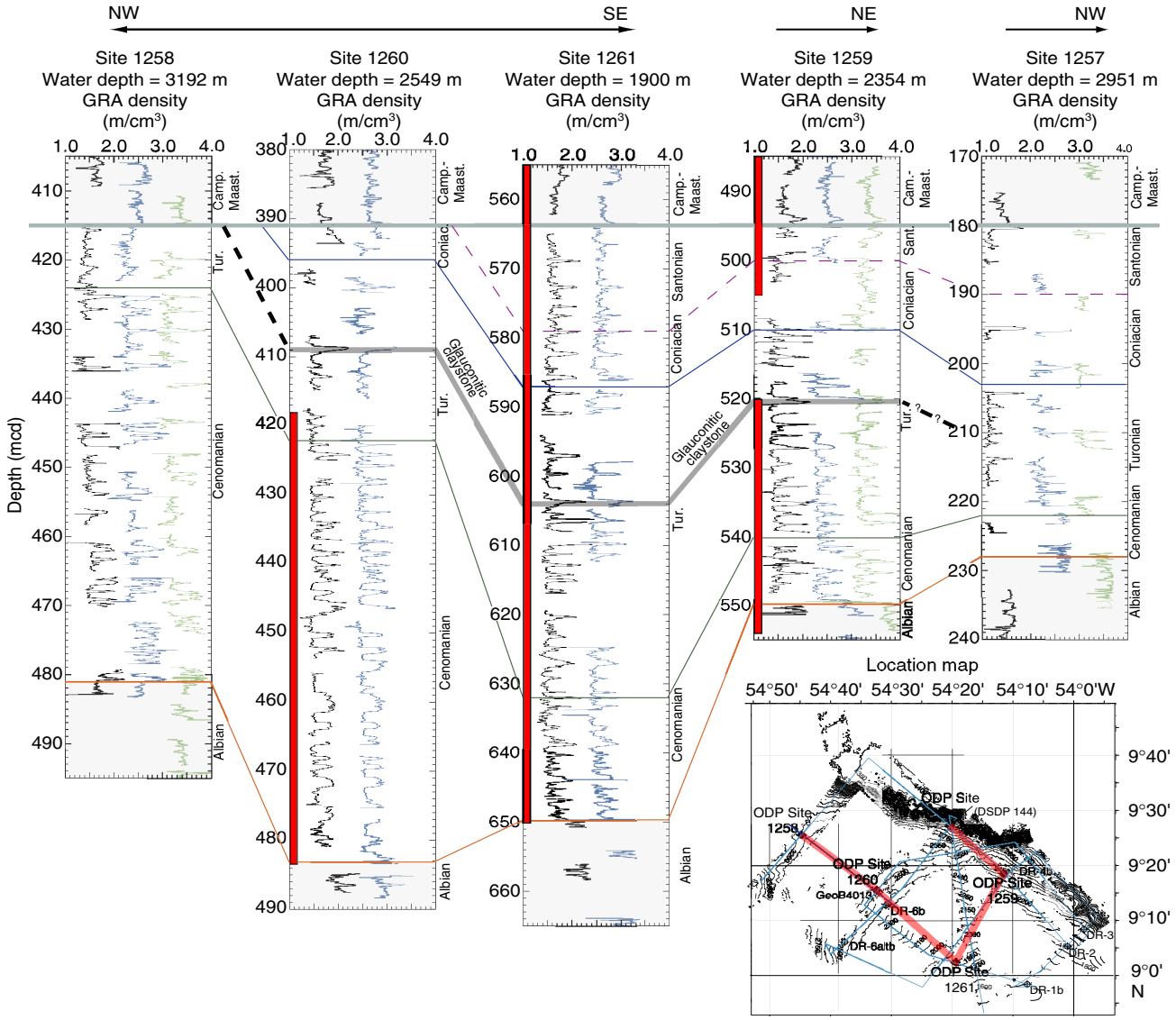

Figure SUM-19

Figure F19

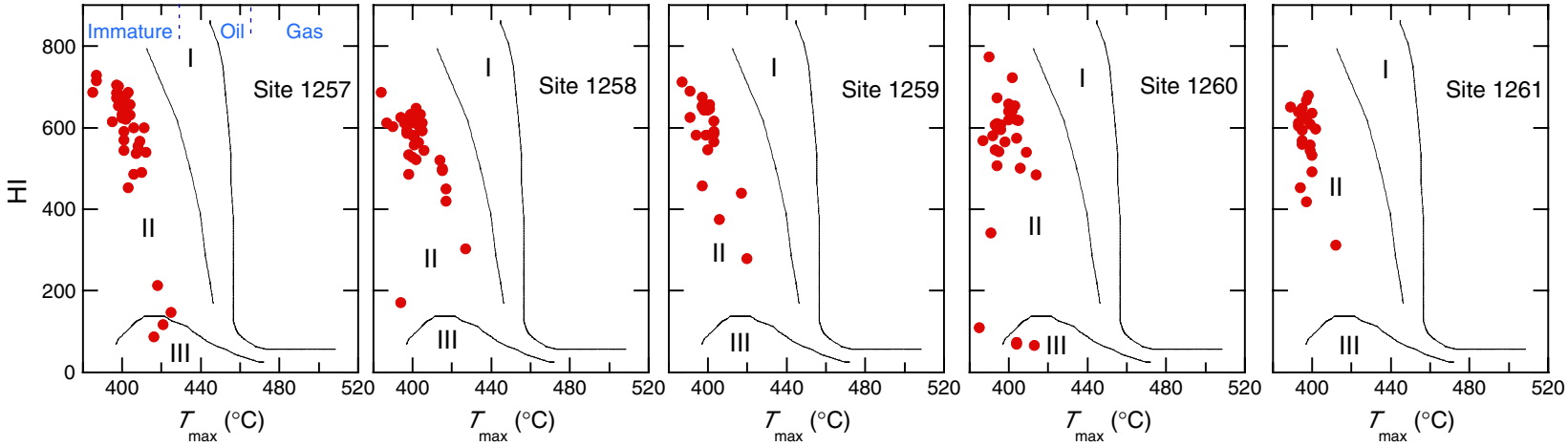
Immature
Oil
Gas
Site 1257
Site 1258
Site 1259
Site 1260
Site 1261
I
II
III
HI
0
200
400
600
800
400
440
480
520
T_{max} (°C)

Figure F20

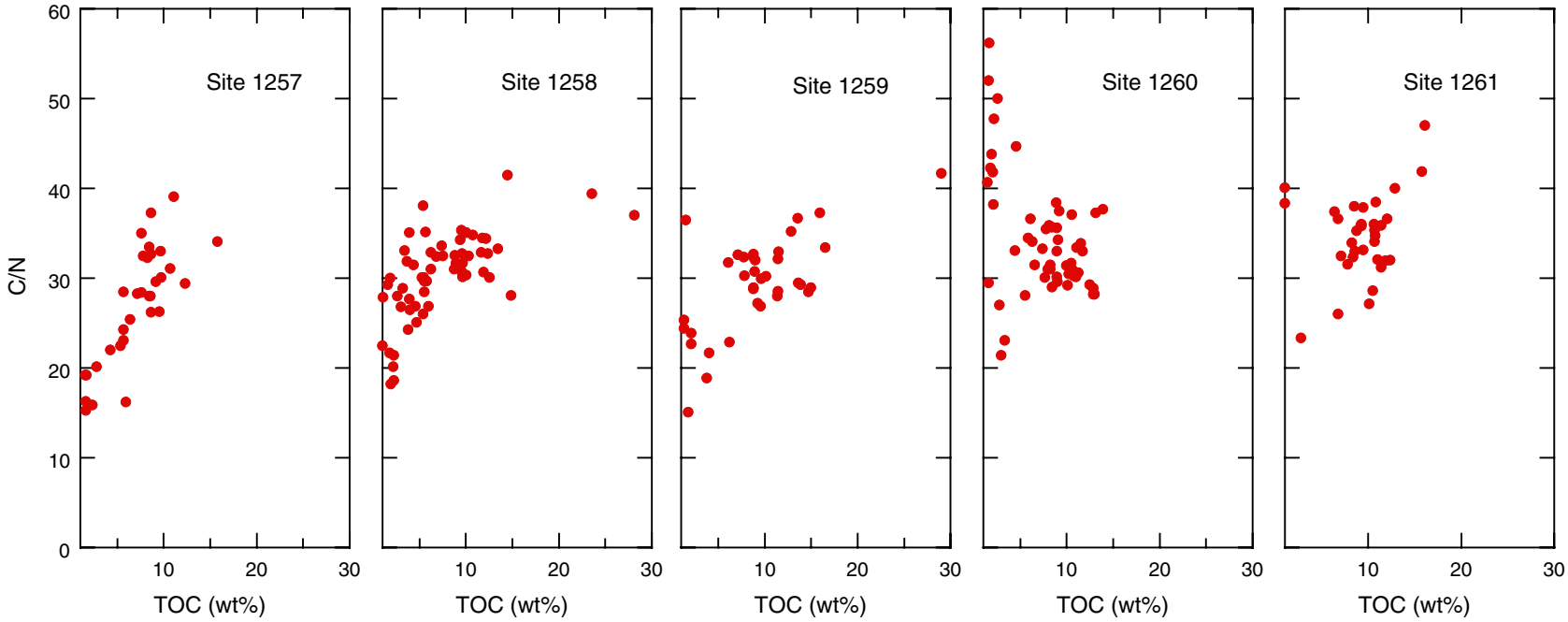
C/N
0
10
20
30
40
50
60
Site 1257
Site 1258
Site 1259
Site 1260
Site 1261
10
20
30
TOC (wt%)

Figure F21

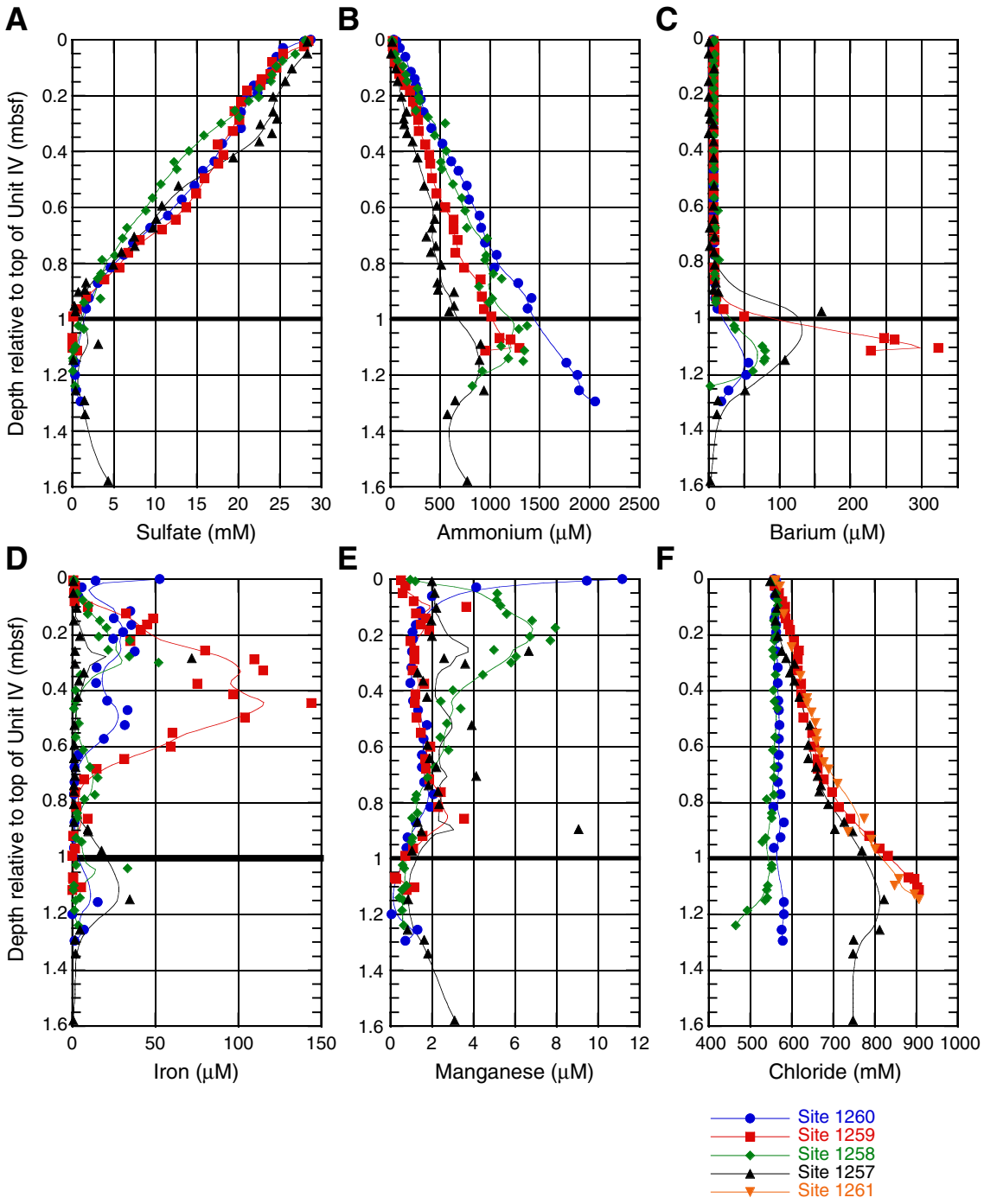
A
B
C
D
E
F
Depth relative to top of Unit IV (mbsf)
Sulfate (mM)
Ammonium (µM)
Barium (µM)
Iron (µM)
Manganese (µM)
Chloride (mM)
Site 1260
Site 1259
Site 1258
Site 1257
Site 1261

Figure F22

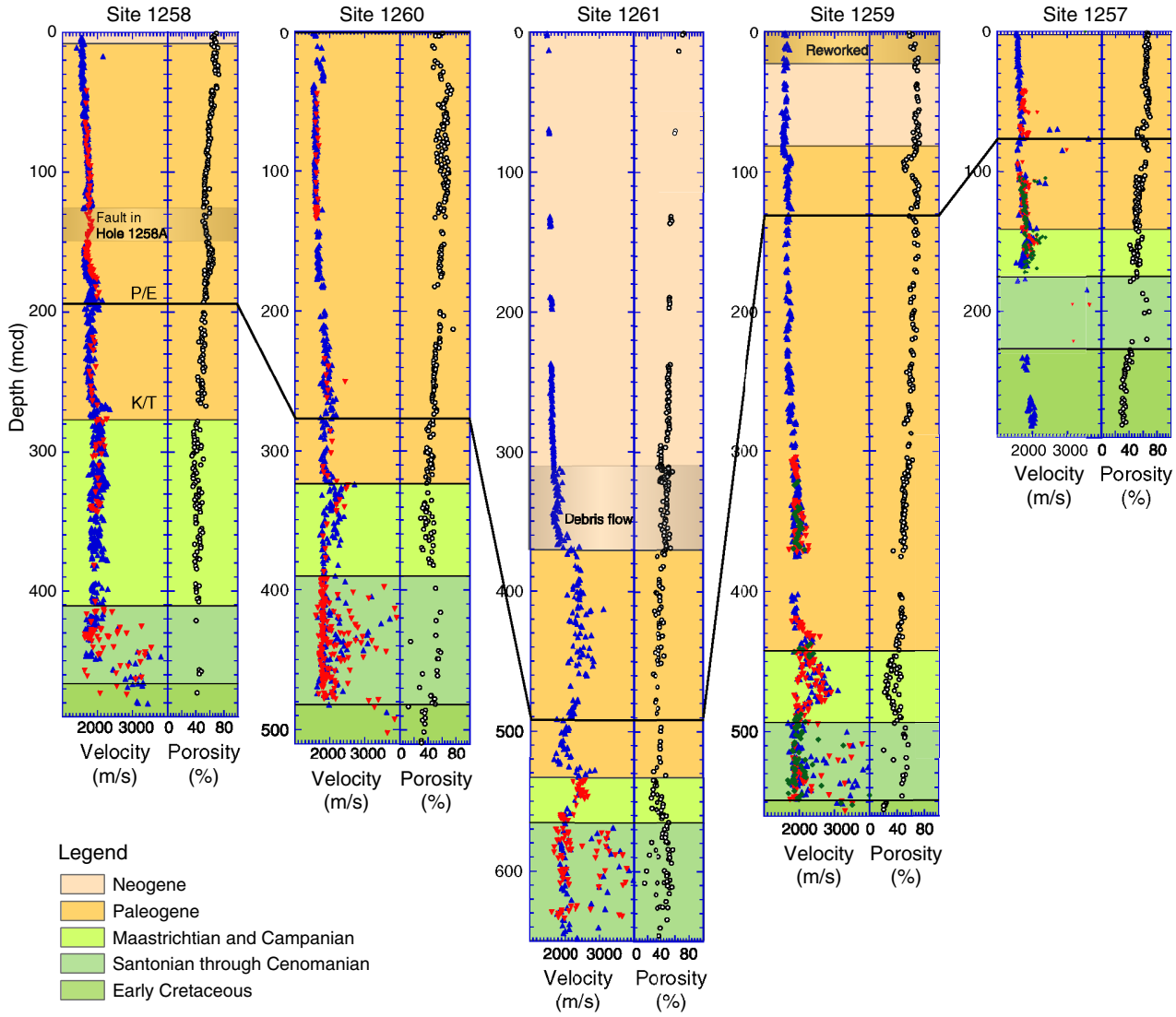
Site 1258
Site 1260
Site 1261
Site 1259
Site 1257
Depth (mcd)
Fault in Hole 1258A
P/E
K/T
Debris flow
Reworked
Velocity (m/s)
Porosity (%)
Legend
Neogene
Paleogene
Maastrichtian and Campanian
Santonian through Cenomanian
Early Cretaceous

Figure F23

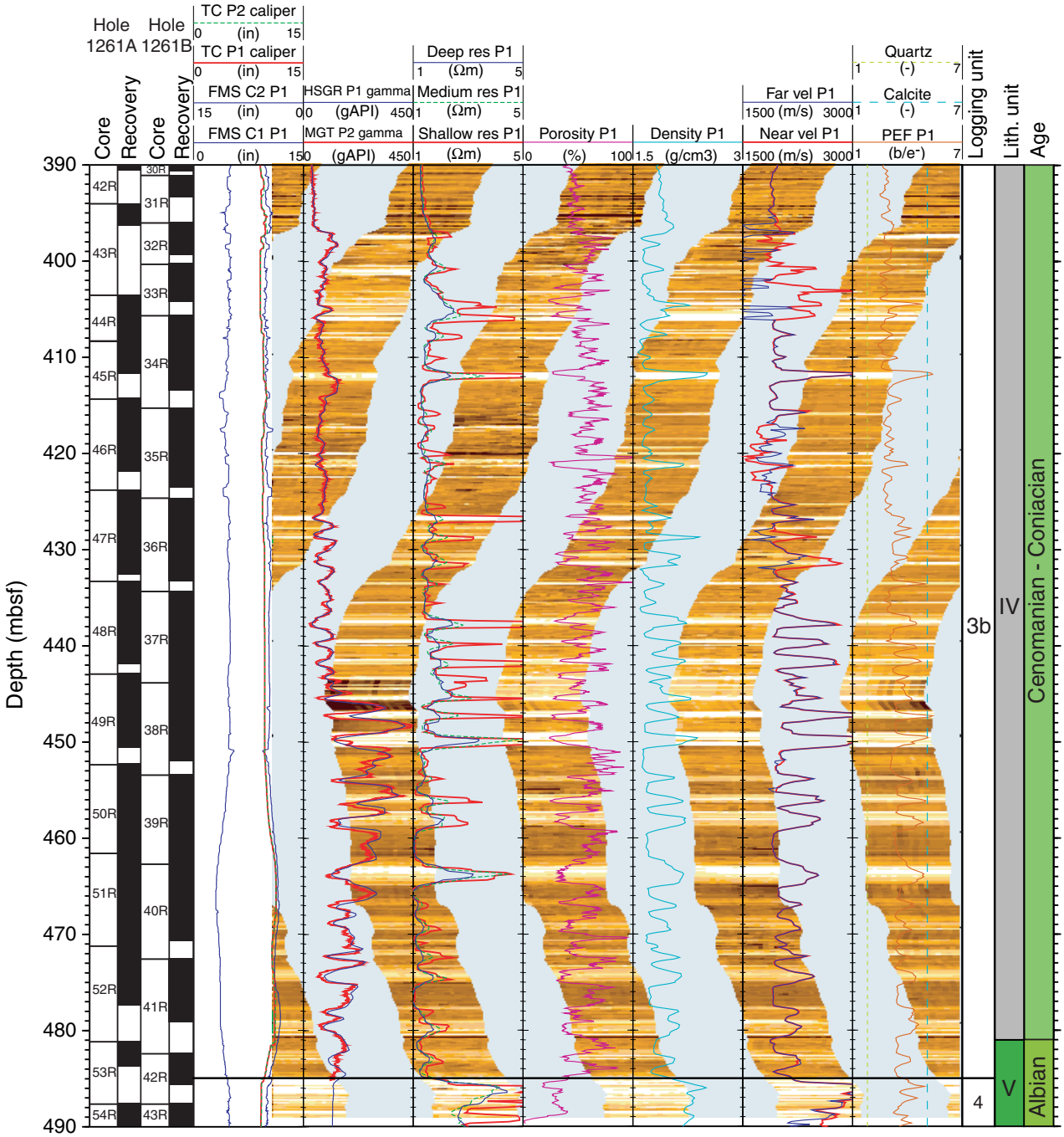
Hole 1261A
Hole 1261B
Core Recovery
Core Recovery
TC P2 caliper
0 (in) 15
TC P1 caliper
0 (in) 15
FMS C2 P1
15 (in) 0
FMS C1 P1
0 (in) 15
HSGR P1 gamma
0 (gAPI) 450
MGT P2 gamma
0 (gAPI) 450
Deep res P1
1 (Ωm) 5
Medium res P1
1 (Ωm) 5
Shallow res P1
1 (Ωm) 5
Porosity P1
0 (%) 100
Density P1
1.5 (g/cm3) 3
Far vel P1
1500 (m/s) 3000
Near vel P1
1500 (m/s) 3000
Quartz
1 (-) 7
Calcite
1 (-) 7
PEF P1
1 (b/e⁻) 7
Logging unit
Lith. unit
Age
Depth (mbsf)
390
400
410
420
430
440
450
460
470
480
490
42R
43R
44R
45R
46R
47R
48R
49R
50R
51R
52R
53R
54R
30R
31R
32R
33R
34R
35R
36R
37R
38R
39R
40R
41R
42R
43R
3b
4
IV
V
Cenomanian - Coniacian
Albian

Figure F24

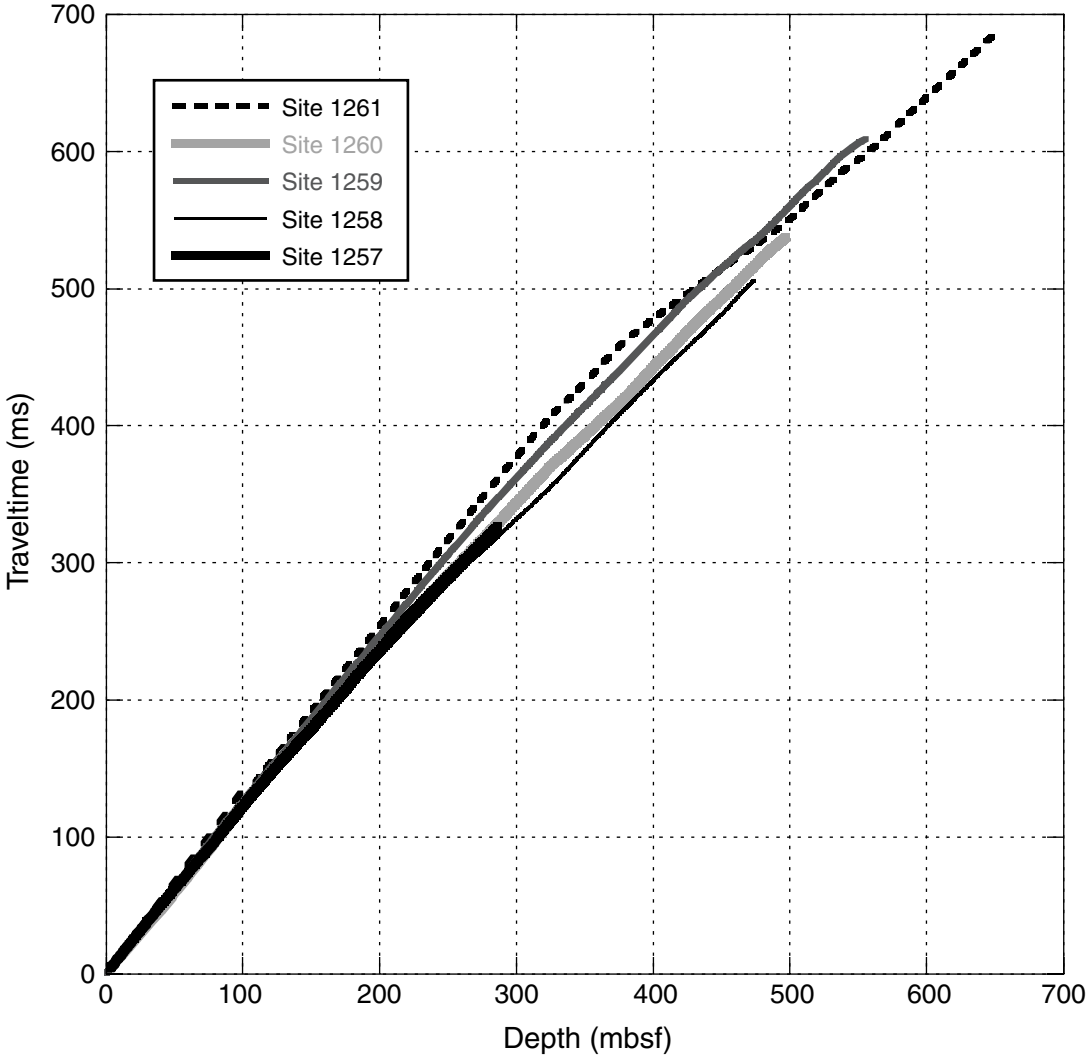
Site 1261
Site 1260
Site 1259
Site 1258
Site 1257
Traveltime (ms)
Depth (mbsf)
0
100
200
300
400
500
600
700

Figure F25

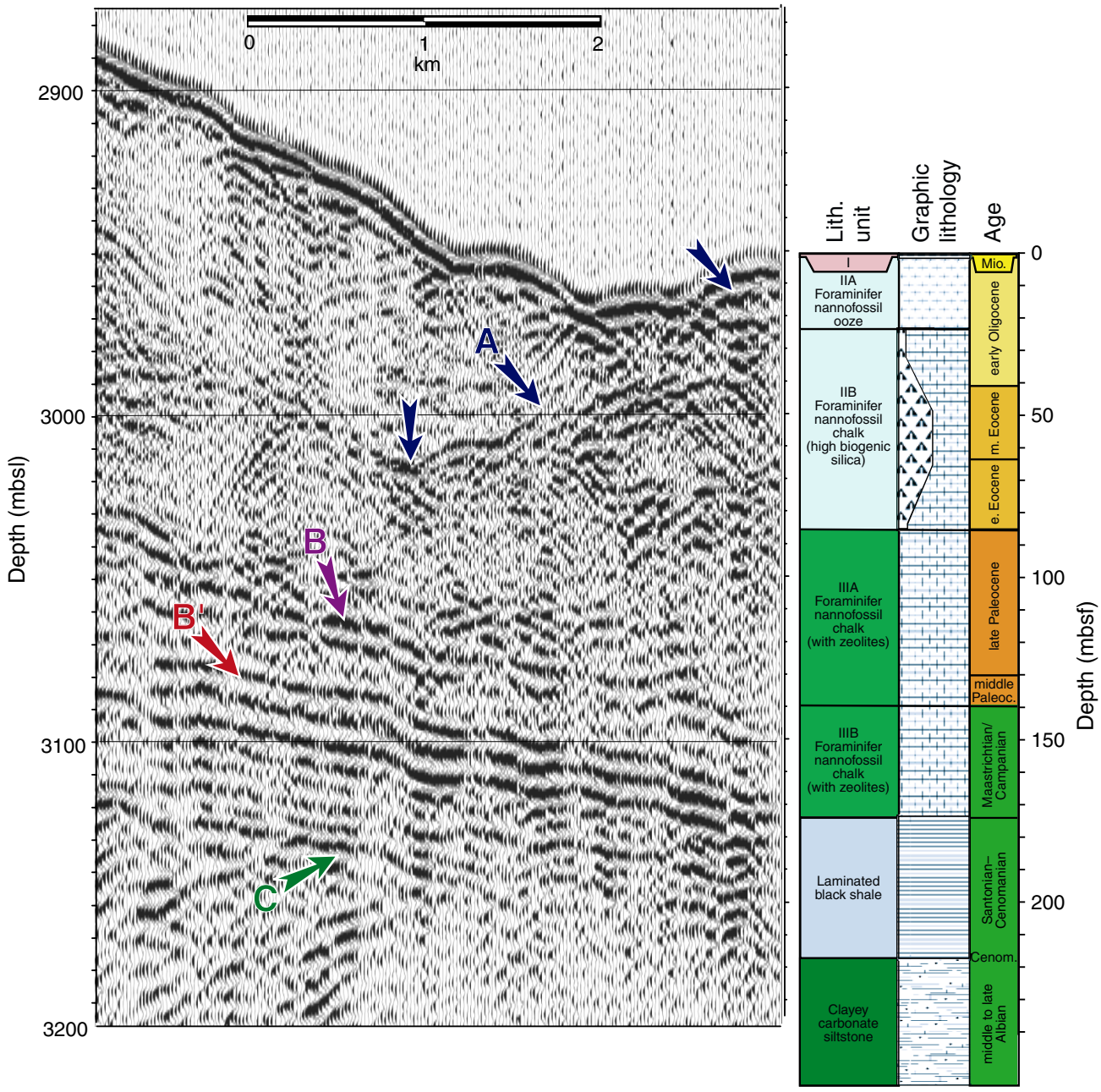
0
1
km
2
2900
3000
3100
3200
Depth (mbsl)
A
B
B'
C
Lith. unit
Graphic lithology
Age
I
IIA Foraminifer nannofossil ooze
IIB Foraminifer nannofossil chalk (high biogenic silica)
IIIA Foraminifer nannofossil chalk (with zeolites)
IIIB Foraminifer nannofossil chalk (with zeolites)
Laminated black shale
Clayey carbonate siltstone
Mio.
early Oligocene
m. Eocene
e. Eocene
late Paleocene
middle Paleoc.
Maastrichtian/ Campanian
Santonian–Cenomanian
Cenom.
middle to late Albian
0
50
100
150
200
Depth (mbsf)

Figure F26

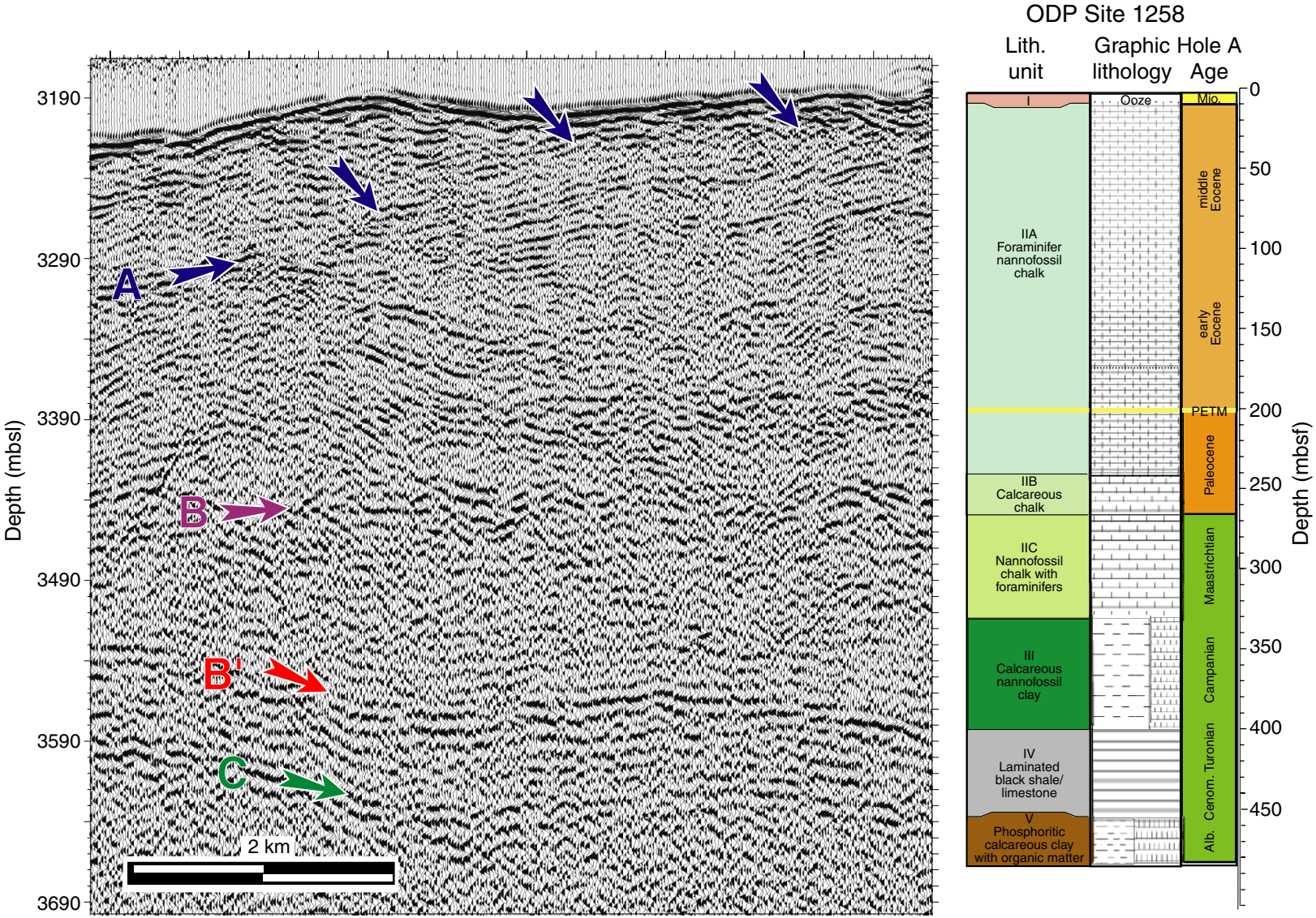
Depth (mbsl)
3190
3290
3390
3490
3590
3690
A
B
B'
C
2 km
ODP Site 1258
Lith. unit
Graphic lithology
Hole A Age
I
IIA Foraminifer nannofossil chalk
IIB Calcareous chalk
IIC Nannofossil chalk with foraminifers
III Calcareous nannofossil clay
IV Laminated black shale/ limestone
V Phosphoritic calcareous clay with organic matter
Ooze
Mio.
middle Eocene
early Eocene
PETM
Paleocene
Maastrichtian
Campanian
Cenom. Turonian
Alb.
0
50
100
150
200
250
300
350
400
450
Depth (mbsf)

Figure F27

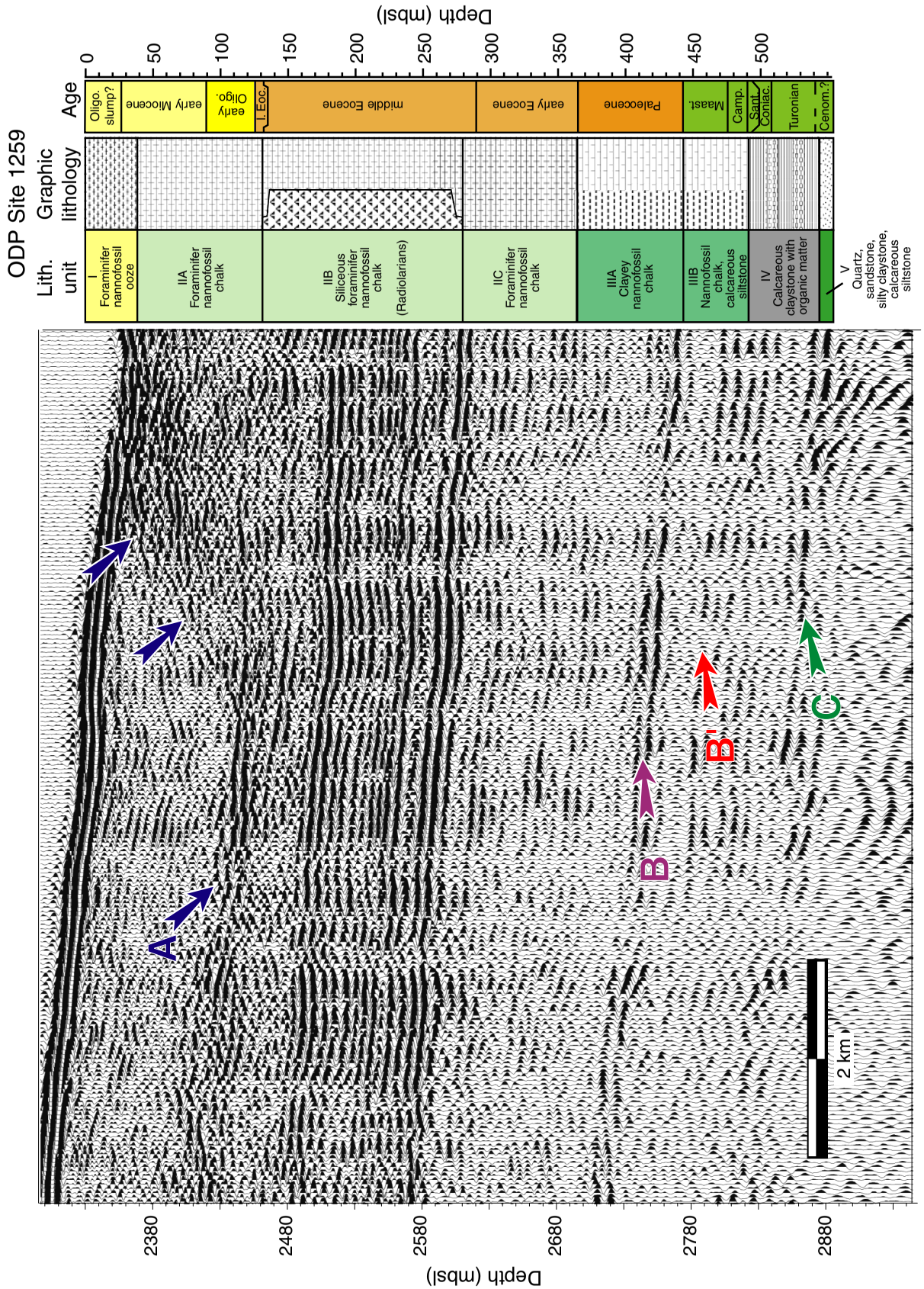
ODP Site 1259
Lith. unit
Graphic lithology
Age
Depth (mbsl)
I Foraminifer nannofossil ooze
IIA Foraminifer nannofossil chalk
IIB Siliceous foraminifer nannofossil chalk (Radiolarians)
IIC Foraminifer nannofossil chalk
IIIA Clayey nannofossil chalk
IIIB Nannofossil chalk, calcareous siltstone
IV Calcareous claystone with organic matter
V Quartz, sandstone, silty claystone, calcareous siltstone
Oligo. slump?
early Miocene
early Oligo.
L. Eoc.
middle Eocene
early Eocene
Paleocene
Maast.
Camp.
Sant./ Coniac.
Turonian
Cenom.?
0
50
100
150
200
250
300
350
400
450
500
2380
2480
2580
2680
2780
2880
A
B
B
C
2 km

Figure F28

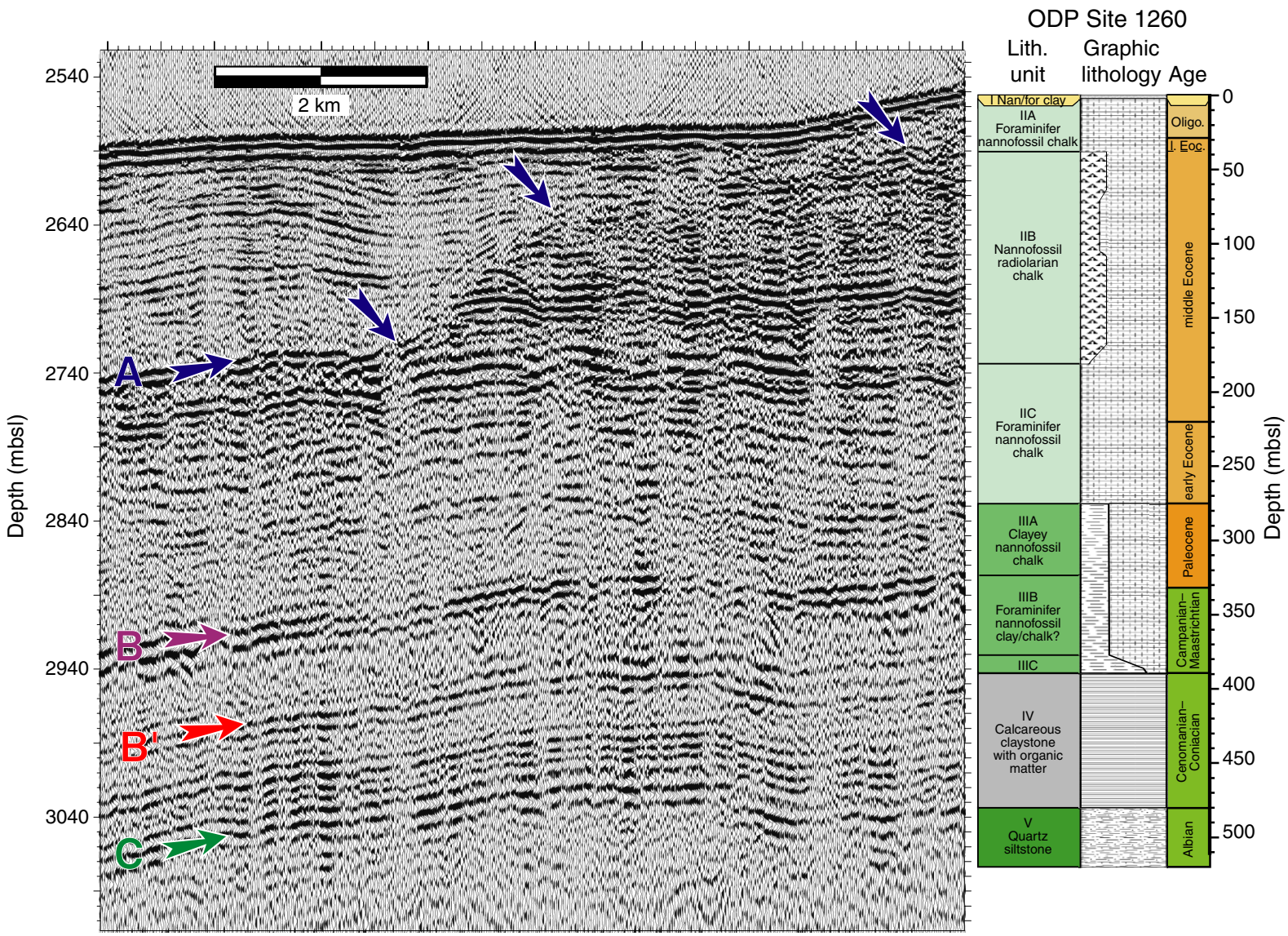
2 km
2540
2640
2740
2840
2940
3040
Depth (mbsl)
A
B
B'
C
ODP Site 1260
Lith. unit
Graphic lithology
Age
I Nan/for clay
IIA Foraminifer nannofossil chalk
IIB Nannofossil radiolarian chalk
IIC Foraminifer nannofossil chalk
IIIA Clayey nannofossil chalk
IIIB Foraminifer nannofossil clay/chalk?
IIIC
IV Calcareous claystone with organic matter
V Quartz siltstone
Oligo.
L. Eoc.
middle Eocene
early Eocene
Paleocene
Campanian–Maastrichtian
Cenomanian–Coniacian
Albian
0
50
100
150
200
250
300
350
400
450
500
Depth (mbsl)

Figure F29

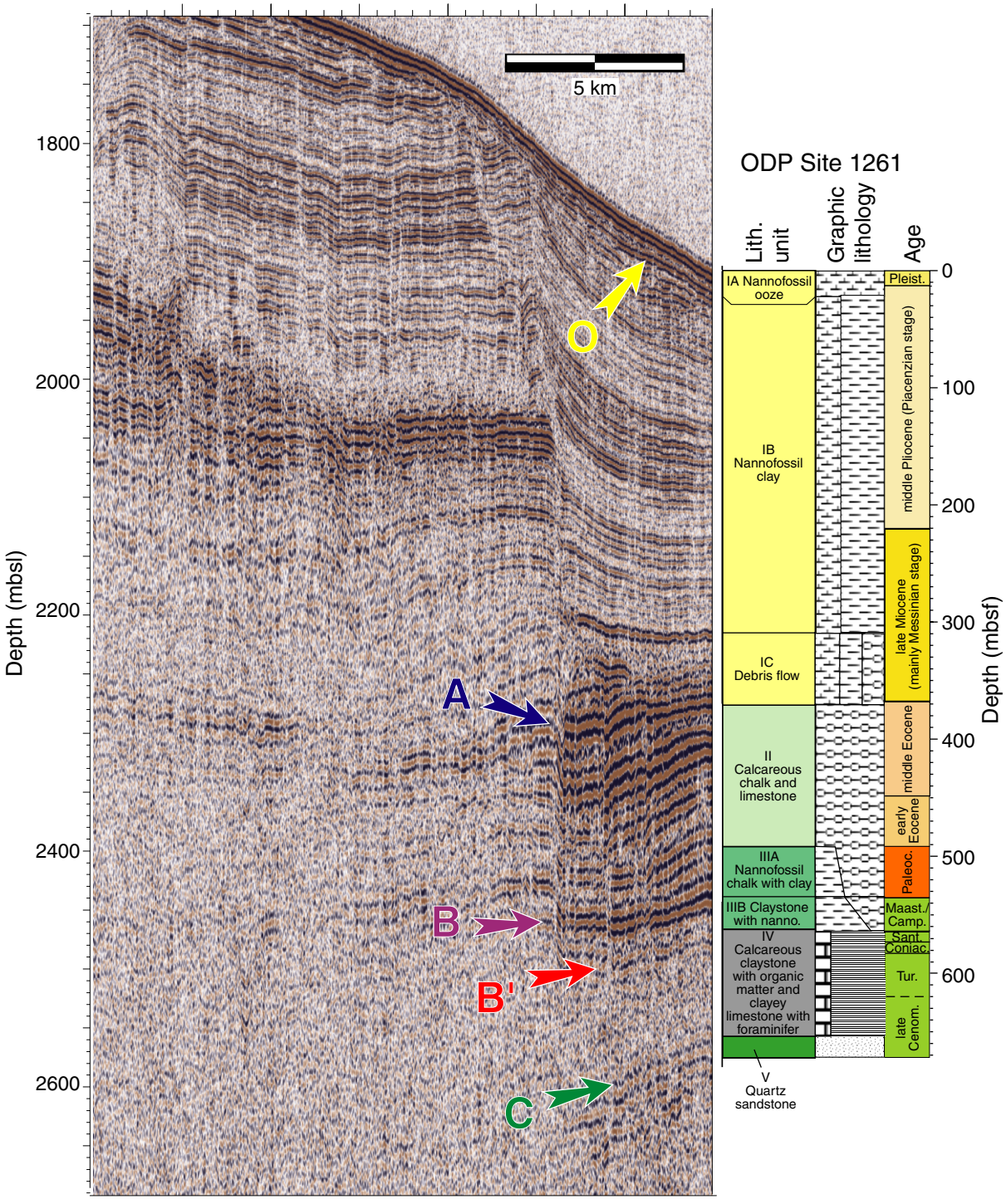
5 km
1800
2000
2200
2400
2600
Depth (mbsl)
O
A
B
B'
C
ODP Site 1261
Lith. unit
Graphic lithology
Age
IA Nannofossil ooze
IB Nannofossil clay
IC Debris flow
II Calcareous chalk and limestone
IIIA Nannofossil chalk with clay
IIIB Claystone with nanno.
IV Calcareous claystone with organic matter and clayey limestone with foraminifer
V Quartz sandstone
Pleist.
middle Pliocene (Piacenzian stage)
late Miocene (mainly Messinian stage)
middle Eocene
early Eocene
Paleoc.
Maast./ Camp.
Sant. Coniac.
Tur.
late Cenom.
0
100
200
300
400
500
600
Depth (mbsf)

Figure F30

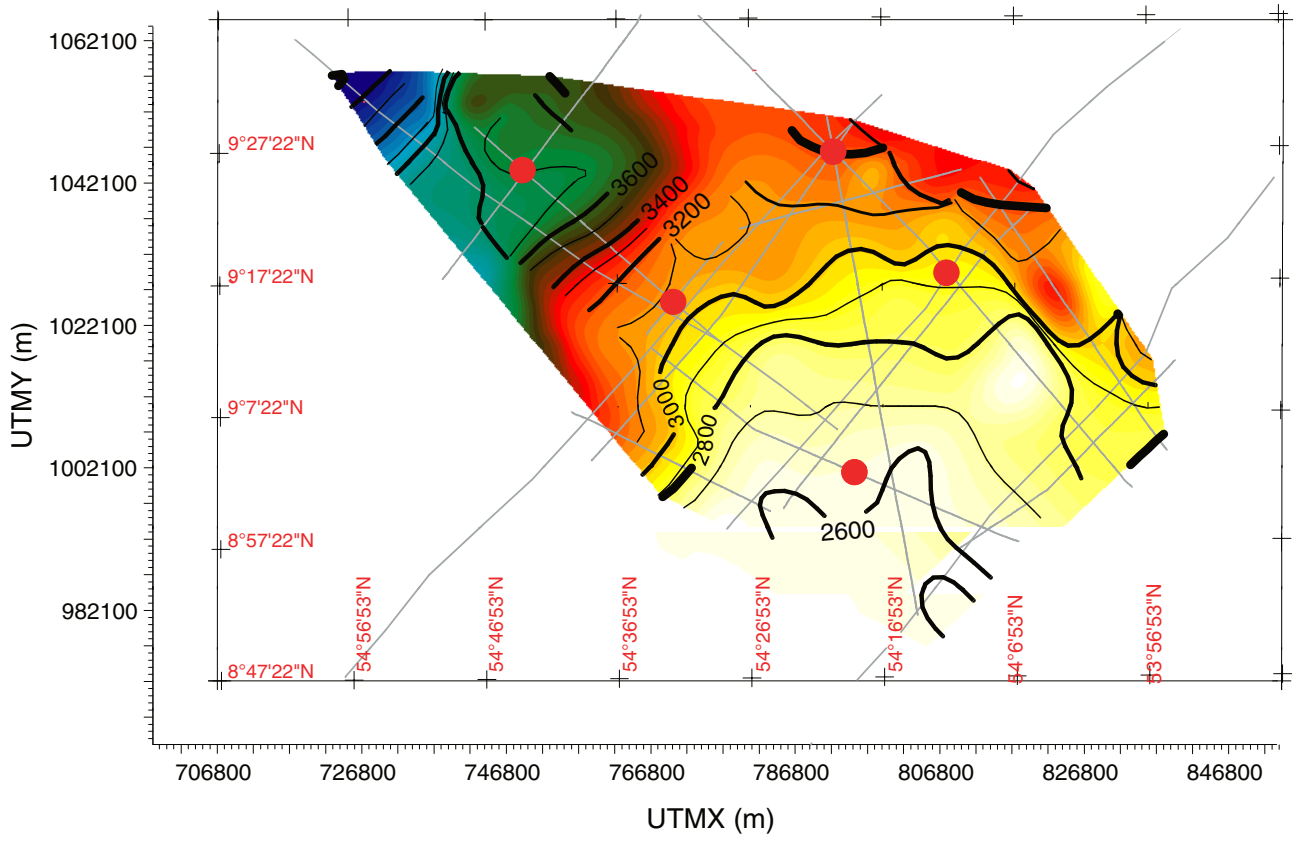
1062100
1042100
1022100
1002100
982100
UTMY (m)
9°27'22"N
9°17'22"N
9°7'22"N
8°57'22"N
8°47'22"N
3600
3400
3200
3000
2800
2600
54°56'53"N
54°46'53"N
54°36'53"N
54°26'53"N
54°16'53"N
54°6'53"N
53°56'53"N
706800
726800
746800
766800
786800
806800
826800
846800
UTMX (m)

Figure F31